Investigation of the main chain orientation in side-chain liquid crystalline polymers by natural abundance ^{13}C NMR

Dissertation

Zur Erlandung des akademischen Grades doctor rerum naturalium

(Dr. rer. nat.)

vorgelegt der

Mathematisch-Naturwissenschaftlich-Technischen Fakultät

der Martin-Luther-Universität Halle-Wittenberg

von Frau Albena Dimitrova

geb. am: 16. 08. 1970 in Silistra, Bulgarien

Gutachter:

1. Prof. Dr. Horst Schneider
2. Prof. Dr. Dieter Geschke
3. PD Dr. Claudia Schmidt

Halle (Saale), 04. 07. 2000

Zusammenfassung

Untersuchung der Hauptketten-Orientierung von flüssigkristallinen Seitenketten-Polymeren mittels NMR an ^{13}C-Kernen in natürlicher Häufigkeit

Von Albena Dimitrova

Flüssigkristalline Seitenkettenpolymere zählen zur Gruppe der flüssigkristallinen Polymere. Zur Untersuchung von deren Struktur und Eigenschaften sind bisher eine große Zahl von theoretischen und experimentellen Arbeiten veröffentlicht worden. Die makroskopischen Eigenschaften polymerer Materialien werden stark durch die molekulare Orientierung beeinflusst. Diese wurde im Falle flüssigkristalliner Seitenkettenpolymerer mit verschiedenen Methoden (NMR, Röntgenstreuung, DSC, Neutronenstreuung, IR-Dichroismus) untersucht, meist jedoch hinsichtlich der mesogenen Seitenketten. Dagegen ist über die Struktur der *Hauptkette* recht wenig bekannt, obwohl diese bedeutsam ist für solche Eigenschaften wie Viskosität, Festigkeit, mechanische Moduli und Glasübergang.

Eine Anzahl experimenteller Untersuchungen der Hauptkettenkonformation von Polysiloxanen und Poly(meth)acrylaten wurden mittels Neutronen-Kleinwinkelstreuung (SANS) ausgeführt. Deren Ergebnisse führten zu dem allgemeinen Schluss, dass die Hauptkette in der smektischen Phase eine oblate Form hat, während ihre Form im Nematischen von der Existenz einer smektischen Tieftemperaturphase abhängt: Wenn es eine solche gibt, ist die Hauptkette leicht oblat; wenn nicht, hat sie eine prolate Form mit teilweise beträchtlicher Anisotropie.

Der hohe Aufwand sowohl für die notwendige Deuterierung der Substanzen als auch für die Neutronenstreu-Experimente selbst wirft die Frage nach alternativen Methoden auf. Röntgenstreuuntersuchungen sind in der smektischen Phase sehr erfolgreich; in der mehr ungeordneten nematischen Phase jedoch ergeben sich meist nur sehr diffuse Reflexe, die kaum auswertbar sind. Weitere Möglichkeiten bestehen in der Anwendung verschiedener NMR-Verfahren. Aus der Literatur sind Arbeiten bekannt, in denen mittels ^{2}H-NMR die Orientierung von Molekülsegmenten bestimmt wurde, so auch die von Haupt- und Seitenketten sowie Spacergrup-

pen flüssigkristalliner Seitenkettenpolymerer. Allerdings ist auch für solche Experimente eine selektive Deuterierung notwendig.

Im Rahmen dieser Arbeit wurden NMR-Verfahren benutzt, die diesen zusätzlichen Aufwand nicht benötigen und stattdessen die in natürlicher Häufigkeit vorhandenen Kerne benutzen. Dabei dient die *Anisotropie der chemischen Verschiebung* dazu, den Orientierungszustand im Spektrum sichtbar zu machen. Das Ziel der quantitativen Auswertung der Spektren ist die *Orientierungsverteilungsfunktion*, hier repräsentiert durch *Orientierungsgrade* (Koeffizienten der Entwicklung in Legendresche Polynome).

Statische ^{13}C-Spektren gaben Hinweise darauf, dass zwei verschiedene Polyester eine unterschiedliche Anordnung von Haupt- und Seitenketten aufweisen. Eine quantitative Auswertung war jedoch unmöglich, da sich wegen der größeren Anzahl von chemisch nichtäquivalenten ^{13}C-Kernen in den Molekülen mehrere Resonanzen im Spektrum überlagern. Dies erfordert eine Erhöhung der Spektrenauflösung mittels **MAS**. Um jedoch die Information über den Orientierungszustand dabei nicht zu verlieren, sind zeitaufwendige zwei- und dreidimensionale Verfahren (Harbison-Vogt-Spiess-Verfahren [71], ORDER [84, 69], PASS [92]) verwendet worden.

Für die Datenanalysen wurden die Tensoren der chemischen Verschiebung benötigt. Diese wurden ebenfalls im Rahmen dieser Arbeit bestimmt (2D-ORDER-Experiment, Analyse nach Herzfeld und Berger):

PMA-OCH$_3$ σ_{iso} = 177,7 ppm, σ_{11} = 114 ppm, σ_{22} = 149 ppm, σ_{33} = 269 ppm
6PBAy σ_{iso} = 168,5 ppm, σ_{11} = 97 ppm, σ_{22} = 183 ppm, σ_{33} = 220 ppm

Einige Orientierungsgrade $\langle P_L \rangle$ $(L = 2;4;6)$ der Probe PMA-OCH$_3$ (COO, quarternäres ^{13}C, Phenyl-^{13}C) wurden mit dem 3D-ORDER-Verfahren gewonnen. Die Datenanalyse wurde dabei anders vorgenommen als aus der Literatur bekannt: Anstelle einer als Gaußfunktion angesetzten Orientierungsverteilungsfunktion wurden die drei niedrigsten Orientierungsgrade unabhängig voneinander mit einem mehrdimensionalen Regressionsverfahren ermittelt. Dabei wurde der Einfluss wichtiger Parameter untersucht, die Auswirkungen auf das Ergebnis haben könnten, wie Zahl der berücksichtigten Rotationsseitenbänder, Genauigkeit der Seitenbandintensitäten und Genauigkeit der zuvor ermittelten Tensorwerte.

Für die Karboxylgruppe der genannten Polymethacrylatprobe ergab sich $\langle P_2 \rangle_S = 0.13$. Der recht kleine Wert bedeutet, dass diese Atomgruppe nur geringfügig geordnet ist, was wegen ihrer Lage zwischen Spacer und Hauptkette nicht überrascht. Die Vorzugsorientierung liegt dabei *parallel* zum Seitenkettendirektor. Auch für das direkt in der Hauptkette befindliche quarternäre Kohlenstoffatom ergab sich eine geringfügige Ordnung. Da jedoch für dieses Atom nichts über die Ausrichtung des Tensors der chemischen Verschiebung innerhalb des Moleküles bekannt ist, kann keine weitergehende Information über die Hauptkettenorientierung gewonnen werden.

Es lagen zwei weitere Proben vor, deren Hauptketten unterschiedlich lange Alkyl-Spacer zwischen den Seitenketten-Verknüpfungspunkten enthalten. Die hier direkt in den Hauptketten befindlichen COO-Gruppen konnten genutzt werden, um Orientierungsgrade für die entsprechenden Segmente mittels 2D-PASS zu erhalten (Die letzte Zahl innerhalb der Probenbezeichnung gibt Auskunft über die Zahl der Methylengruppen im Hauptkettenspacer):

6PBA8 : $\langle P_2 \rangle_S = -0.23$, das negative Vorzeichen bedeutet, dass die Segmente vorzugsweise *senkrecht* zum Seitenkettenspacer orientiert sind;
6PBA13: $\langle P_2 \rangle_S = 0.14$, hier ist trotz größerer Unordnung eine vorzugsweise *parallele* Anordnung von Haupt- und Seitenketten zu vermerken.
Dies bestätigt die qualitativen Schlussfolgerungen aus den statischen Experimenten. Weiterhin stimmt dieses Ergebnis mit Vermutungen überein, die sich aus früheren Röntgenstreuexperimenten an diesen Proben ergaben.

Abstract

Investigation of the main chain orientation in side-chain liquid crystalline polymers by natural abundance ^{13}C NMR

By Albena Dimitrova

Side-chain liquid crystal polymers belong to the large family of high molecular weight materials called liquid crystal polymers. The necessity of knowledge about the properties and behaviour of such materials under different conditions have given rise to a lot of investigations in theoretical, experimental and applied physics. The macroscopic properties of all polymers materials, and especially of liquid crystalline substances depend significantly on their molecular orientation distributions. . The molecular order of such systems has been the subject of different physical studies (NMR, EPR, X-ray, DSC, SANS, IR dichroism) but most of them concentrate on the behaviour of mesogenic groups. Very little is known about the ordering of the *main chain*. The structure of the main chain influences strongly the mechanical and thermodynamical properties of the polymer like viscosity, strength, moduli and glass transition.

A number of experimental investigations of the backbone conformation of polysiloxanes and poly(meth)acrylates were based on small-angle neutron scattering (SANS). A general result of these studies for side-end fixed LCP (liquid crystalline polymers) was that in the smectic phases the backbone has a flat oblate conformation, whereas the backbone shape in the nematic phase depends on the existence of a low temperature smectic phase. If there is such a phase, the backbone takes a slightly oblate shape, presumably because of smectic fluctuations; otherwise the backbone will be prolate with an appreciable magnitude of anisotropy.

The high effort for both the synthesis of the deuterium labelled substances and for the neutron scattering experiments requires looking for alternative methods. X-ray studies are very successful in the smectic phases. In the nematic phase, however, because of the higher disorder in the system information about main chain obtained from diffraction patterns is relatively scarce.

In the investigation presented in this dissertation some NMR techniques based on the chemical shift interaction of the natural abundance ^{13}C are used. The advantage of this

interaction is that the anisotropy of the chemical shift interaction reveals the orientation information in the spectrum. The aim of this investigation was to get quantitative information about the (*orientation distribution function*) ODF, presented in the spectrum with its *order parameters* for some liquid crystalline side chain polymers.

Static ^{13}C spectra gave a hint that, two different Polyester samples show different mutual orientation between the main and the side chain. However a quantitative estimation of the ODF was not possible from this spectra, as the number of distinct ^{13}C sites in the chemical structure is big and many resonances overlap. As a further step increasing of the spectral resolution by **MAS** was needed. For the sake to keep the fool information about the orientation some MAS 2D and 3D methods (Harbison-Vogt-Spiess [71], ORDER [84, 69] and PASS [92]) were applied.

Chemical shift values for COO nuclei were required for the extraction of the data. They were evaluated (2D ORDER experiment, analysis of the Herzfeld-Berger) as follows:
for PMA-OCH$_3$ σ_{iso} = 177,7 ppm, σ_{11} = 114 ppm, σ_{22} = 149 ppm, σ_{33} = 269 ppm
for 6PBAy σ_{iso} = 168,5 ppm, σ_{11} = 97 ppm, σ_{22} = 183 ppm, σ_{33} = 220 ppm

The **3D ORDER method** introduced by Titman *et al.* was applied for extracting of $\langle P_L \rangle$ ($L = 2, 4, 6$) for PMA-OCH$_3$. As an alternative for former investigations [69, 71] where for the data evaluation, mostly the Gaussian fitting procedure was used, here $\langle P_L \rangle$ were calculated independently one from another by a linear regression least square fitting. The results are compared with the result of Titman *et al.* for PA-OCH$_3$. The influence of some factors, like the error of the measured line intensities, exactness of the chemical shift tensor values and number sidebands included in the system on the stability of the solution for order parameters was studied.

The order parameters of ODF of some different ^{13}C sites (namely OCO, quaternary and phenyl ^{13}C) for oriented PMA-OCH$_3$ were extracted. For COO group $\langle P_2 \rangle_S = 0.13$ was obtained. This is a very small value and it means that there is a high disorder and it can be concluded that there are more segments aligned parallel to the magnetic field and the side chain director ***N***. Part of the main chain is a quaternary ^{13}C . There is an evidence that this group is also slightly oriented but no further conclusions about the preferable direction of segment orientation can be done, as there is no information for the orientation of the tensor with respect to the local chain.

The orientation distribution of the chemical shift tensor of the ester COO group located in the main chain in some similar liquid crystalline side chain polymers with different length of the spacer unit was monitored by 2D PASS NMR method and the order parameters were extracted by linear regression procedure from the line intensities of the 2D PASS spectra.

For 6PBAy samples the estimation of $\langle P_2 \rangle_S$ for COO group, which is a part of the main chain for this substances gives the following results:
6PBA8: $\langle P_2 \rangle_S = -0.23$, the negative sign is an indication of preferable orientation of the main chain perpendicular to the side chain;
6PBA13: $\langle P_2 \rangle_S = 0.14$, or in opposite to the other sample here the main chain is estimated to orient parallel to the side chain despite of the high disorder.

This results confirm the indications which were obtained from the angle dependent static ^{13}C NMR measurements. Moreover these results are in agreement with suppositions done from the earlier X-ray measurements with the same substances.

Contents

1. Introduction

Determining the structure of a material is a basic goal of physical science. The means one uses to determine the structure depend on the nature of the material. For crystalline solids, scattering of X-rays or neutrons by single crystal yields detailed diffraction patterns, from which the structure can be derived in terms of atomic coordinates within the unit cell. If the material of interest is disordered however, diffraction methods become progressively less useful because with decreasing order the diffraction patterns smear out resulting in diffuse arcs and halos [1]. The disorder may be macroscopic in nature, e.g., failure to obtain a single crystal of a crystalline solid, or microscopic, e.g., loss of the periodicity in an amorphous solid. Many interesting materials, including glassy synthetic or liquid crystalline polymers, and many biopolymers fall into this category. Side-chain liquid crystal polymers belong to the large family of high molecular weight materials called liquid crystal polymers which are very widely used in the industry for liquid-crystalline displays. The necessity of knowledge about the properties and behaviour of such materials under different conditions have given rise to a lot of investigations in theoretical, experimental and applied physics [2, 3]. The term ‘side chain’ indicates that mesogenic units are attached to the linear chain which is usually a non-mesogenic polymer (such as polymethacrylate, polysiloxanes etc.), always via a spacer. These polymers may exhibit a phase sequence similar to that of thermotropic liquid crystals: isotropic, nematic, smectic and glassy or crystalline. The molecular order of such systems has been the subject of different physical studies (NMR, EPR, X-ray, DSC, SANS, IR dichroism) [4, 5] but most of them concentrate on the behaviour of mesogenic groups. Very little is known about the ordering of the main chain. Typical polymer behaviour for such long chain is to tend to the maximum of entropy by forming a random coil. This property of the main chain is in contradiction to the tendency of the mesogenic units to form an considerably ordered structure. The flexible spacer in this system is like a mediator: it is decoupling the two units to enable mesophase and also helps for avoiding the complete

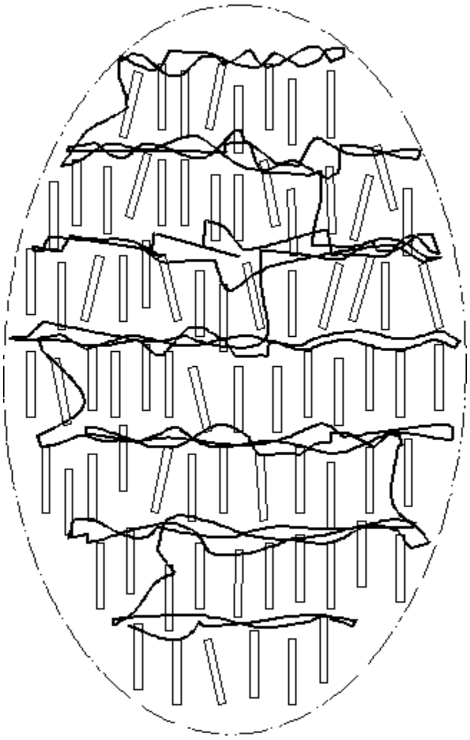

Fig. 1.1. Scheme of the LC molecule

segregation and the average backbone shape is deformed to an ellipsoid. The structure of the main chain influences strongly the mechanical and thermodynamical properties of the polymer like viscosity, strength, moduli and glass transition. For example, the theory of Brochard [6] predicts the influence of the shape anisotropy of the macromolecules on some viscosity parameters in a mixture of polymer and liquid crystal.

One question one tries to answer is what is the conformation of the backbone in the different liquid crystal phases, how does it depend on some parameters like spacer length, type of the mesogenic group and how does this conformation influences the stability of the mesophase.

There are some theoretical approaches to this problem. Vasilenko et al [7] used a lattice model, which is based on the athermal parameters and can therefore hardly be brought into accordance with the temperature dependent experimental results. Wang and Warner [8] developed a theory based on the model of worm-like chains; the segment-segment, segment-mesogen, and mesogen-segment interactions are described by Maier-Saupe potentials. They predict three different phases for nematic liquid-crystalline side-group polymers. Two of them are important for our systems: N_I – which contains main chains which are perpendicular to the director and N_{III} which is characterized by a mesogen-parallel arrangement of the main chain. Parameters governing the phase diagram are magnitude and sign of the main chain – side group interaction as well as the volume fraction of mesogens. It must be stated that for realistic values of the volume fraction, only perpendicular conformation is predicted.

A number of experimental investigations of the backbone conformation of polysiloxanes and poly(meth)acrylates were based on small-angle neutron scattering; reviews are given in [9,10]. The mesogen-induced backbone anisotropy is expressed by the gyration radii R_{II} and $R_{\perp}$ parallel and perpendicular to the director filed respectively. A general result of these studies for side-end fixed LCP (liquid crystalline polymers) was that in the smectic phases the backbone has a flat oblate conformation, whereas the backbone shape in the nematic phase depends on the existence of a low temperature smectic phase. If there is such a phase, the backbone takes a slightly oblate shape, presumably because of smectic fluctuations; otherwise the backbone will be prolate with an appreciable magnitude of anisotropy. The high effort for both the synthesis of the deuterium labelled substances and for the neutron scattering experiments requires looking for alternative methods. X-ray studies are very successful in the smectic phases [11]. In the nematic phase, however, because of the higher disorder in the system, information about main chain obtained from diffraction patterns is relatively scarce.

Nuclear magnetic resonance (NMR) seems to be an ideal way to charaterize such kind of partially ordered solids [12-15] since the interactions of nuclear spins with their surroundings are anisotropic and the scale one can monitor with NMR can resolve the contribution of individual groups. The big drawback of all other experimental techniques is that they measure a bulk property of the material and one can not reach high resolution. Characterization of such systems with NMR involves specifying an orientation distribution function (ODF) which describes the deviation of a molecular-fixed coordinate system from some preferential macroscopic set of axes. A variety of methods exist for probing the microscopic ODF [14, 16, 17, 18, 19, 20, 21, 22]. Most of the NMR methods mentioned above are based on the chemical-shift interaction and are able to do a high resolution analysis of the ODF only if the number of distinct sites in the chemical structure is small, and from the other site they are static experiments that means a relatively poor sensitivity. For some substances like polysiloxanes with ^{29}Si NMR it is quite easy to determine the main chain orientation even from a normal static cross-polarization spectrum because the spectrum consists of only one resonance [21]. Like an alternative for the chemical shift interaction in some cases [23] deuteron quadrupolar interaction has been used to measure the ODF in several selectively labelled systems. The big advantage of ^{2}H NMR technique is the very good signal-to-noise ratio. These experiments gave information that in particular polyacrylate the main chain and also the spacer are parallel to the side groups; the corresponding polymethacrylate shows a perpendicular structure. Although for commercially produced synthetic polymers and naturally occurring biopolymers, this NMR method is less useful because like in the case of SANS the necessity of selective deuteron labelling which is difficult and sometimes possible only with extreme effort task for chemists.

The aim of the investigation presented in this thesis is to extract the orientation distribution function and information about backbone conformation in liquid crystalline side chain polymers via any other natural abundance ^{13}C NMR method, which does not need any special sample treatment like selective deuteration.

As a basis for the following considerations in the next chapter the literature survey is presented, describing the current state of the problem of studying the main chain orientation of side chain liquid crystalline polymers by different techniques: SANS, X-ray, ^{29}Si and ^{2}H NMR. In Chapter 3 proper static ^{13}C NMR measurements with 6PBAy samples are shown. Chapters 4, 5, 6 show the methodical basis for the quantitative analysis and extraction of ODF by 2D and 3D NMR techniques and own application and results obtained by these methods.

2 Knowledge about molecular order of main chain in polymeric side chain liquid crystals from the literature

2.1 Structure and chain conformation of side chain liquid crystal polymers as revealed by SANS

Backbone anisotropy and the structure of mesophases of a series of side-chain liquid crystal polymers have been studied in the bulk by neutron scattering. These polymers involve an acrylate, a methacrylate or a siloxane backbone (see Table 2.1).

Table 2.1 List of the polymers studied for the main chain orientation by SANS

Polymer	Name	Reference Nr.	Backbone	Spacer	Rigid core	End of the mesogenic group
Polymethacrylates	PMA-OC_4H_9	[24,25,26, 27,28]	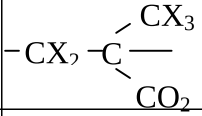 $-CX_2-C(CX_3)(CO_2)-$	$(CH_2)_6$	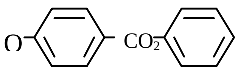	OC_4H_9
	PMA-CN	[24]	id	id	id	CN
	PMA-OCH_3	[29,27,30]	id	id	id	OCH_3
	PMA-$(CH_2)_5CH_3$	[29]	id	id	id	$(CH_2)_5CH_3$
Polyacrylates	PA-OCH_3	[31]	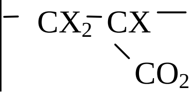 $-CX_2-CX(CO_2)-$	id	id	OCH_3
	PA_6-CN	[32,31]	id	id	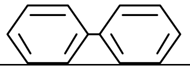	CN
		[33]	id	$(CH_2)_4$	id	CN
	PA_4-C_4H_9	[31]	id	id	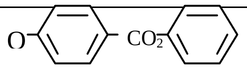	C_4H_9
	PA_5-OCH_3	[34]	id	$(CH_2)_5$	id	OCH_3
Polymethasiloxane	PMS	[35,33]	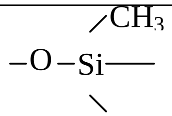 $-O-Si(CH_3)-$	$(CH_2)_4$ or $(CH_2)_3$-CX_2	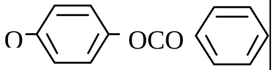	OCX_3

Small angle neutron scattering is due to fluctuations of concentration in the medium. An artificial way to create such fluctuations in bulk (and hence the signal at small angles) is to mix hydrogenous polymers with deuterated polymers. The bulk samples are mixtures of fully protonated and partially deuterated polymers in equal parts. Deuterium can be on the backbone or in the terminal group (in the case of polymethacrylates) in the position given as

X in the Table 2.1. It has been demonstrated [36] that the neutron scattered by a mixture of hydrogenated and deuterated polymers produces a small angle neutron scattering associated to interference between pairs of scatterers belonging to the same chain. In the configuration where the magnetic field and the scattering plane are placed perpendicular to the incident beam, one may measure the scattering intensity in the planes containing the directions parallel and perpendicular to the magnetic field. The obtained intensity is proportional to the form factor $P(q)$, q is the module of the scattering vector of the backbone which is deuterated part of the polymers. By calling R_{II} and $R_{\perp}$ the components of the radius of gyration of the backbone in the directions parallel (II) and perpendicular (⊥) to the magnetic field one has [27]

$$\begin{aligned} P^{-1}(q_{II}) &= P^{-1}(0).(1+q_{II}^{2}\bullet R_{II}^{2}) \\ P^{-1}(q_{\perp}) &= P^{-1}(0).(1+q_{\perp}^{2}\bullet R_{\perp}^{2}) \end{aligned} . \tag{2.1}$$

From the SANS study all these side-chain liquid crystal polymers the following general features can be drawn. In the nematic phase, whatever the polymer backbone is (polyacrylate, polymethacrylate or polysiloxane) two backbone conformations can be obtained: oblate and prolate. It appears that all the polymers giving rise to a smectic phase on decreasing the temperature have in the nematic phase an oblate shape in which polymer backbone is more or less perpendicular to the orientation of the mesogenic units. Smectic fluctuations, which are associated with the coming smectic phase and are present in the nematic phase have correlation lengths of the same order or higher than the size of the polymer backbone in nematic phase. The smectic fluctuations induce an oblate conformation, which is the characteristic conformation of the backbone in the smectic phase. In opposite to this, purely nematic polymers induce prolate conformation.

For the first polymer in the table, PMA-OC_4H_9 , in the nematic phase the values of R_{II} and $R_{\perp}$ (60 ± 3 Å, and 65 ± 3 Å, respectively) indicate that the polymer backbone adopts a slightly oblate shape (since $R_{II} < R_{\perp}$). In the smectic phase there is an increase in $R_{\perp}$ and a simultaneous decrease in R_{II} when the temperature decreases. These changes occur over a range of 10°C below the nematic-smectic phase transition, beyond R_{II} and $R_{\perp}$ keep constant values.

The second polymer, PMA-OCH_3 differs from the first one only in the terminal group, and this difference produces a 35°C broadening in the nematic temperature range. At lower temperature a smectic phase appear, although it has not always been identified in the literature [29]. The layer thickness is 25 ± 1 Å which is also the length of the mesogenic group in its extended form (S_{A1}). In the nematic phase R_{II} becomes smaller than in the isotropic phase, whereas $R_{\perp}$ keeps similar value. This oblate deformation remains slight over the entire nematic range. In the smectic phase the increase in $R_{\perp}$ and the decrease in R_{II} are similar to those obtained in the case of PMA-OC_4H_9 when the temperature decreases but the anisotropy remains less strong than in the first case.

For the third polymer PA-OCH_3 in the nematic phase the global size of the backbone decreases, since R_{II} decreases markedly, while $R_{\perp}$ remains close to the value adopted in the isotropic phase. This again corresponds to the oblate shape. In the smectic phase one has the same anisotropy ($R_{II} < R_{\perp}$), but the evolution of R_{II} and $R_{\perp}$ differs from that observed in the case of PMA-OC_4H_9 and PMA-OCH_3. The parallel component R_{II} is extremely small and does not vary, whereas $R_{\perp}$ increases from 21 to 27 Å over the same range of temperature.

The PMA-CN differs from PMA-OC_4H_9 and PMA-OCH_3 in having in the end of the mesogenic unit a cyano group. CN group enhances the polarity of the mesogenic groups and this changes the molecular organization of the smectic phase. In this case it corresponds to a partially bilayered smectic phase (S_{Ad}) since the layer thickness d = 35 Å is larger than the length of the extended mesogenic group (23 Å), but smaller than twice this length (46 Å). In the nematic phase the anisotropy is weak and of the oblate type $R_{\perp} > R_{II}$. In the smectic phase, the difference between R_{II} and $R_{\perp}$ increases with failing temperature, but in contrast to the previous polymers, $R_{\perp}$ does not increase and maintains values close to those obtained from the isotropic phase, whereas R_{II} becomes smaller than in the isotropic phase.

PA_6-CN has a polyacrylate backbone and the rigid core of the side group is constituted by a cyanobiphenyl group, which is therefore different from that in all preceding polymers. The extended length of the mesogenic group is 23 Å and the smectic larger thickness is 34 Å. In the high temperature nematic phase, the anisotropy corresponds to a weak oblate shape, $R_{\perp}$ >

R_{II}. In the smectic phase, R_{II} decreases as the temperature decreases, whereas $R_{\perp}$ keeps a value close to that of the isotropic phase (52 ± 2 Å). The polymer presents than a behaviour similar to that of PMA-CN in the smectic phase. In the re-entrant nematic phase, a striking result is obtained: there is an inversion of the backbone anisotropy which becomes prolate ($R_{II} > R_{\perp}$). Therefore the same polymer can present two types of anisotropy (oblate and prolate) dependent upon the temperature.

The next polymer: PA_5-OCH_3 is unlike the other polymers in that it possesses only a wide range of nematic phase I-N-T_g. In the nematic phase the backbone clearly adopts a prolate shape like PA_6-CN in the re-entrant nematic phase. Should be noted that the deformation of the backbone begins with an increase of R_{II} whereas $R_{\perp}$ keeps nearly the same value as in the isotropic phase. The anisotropy and its variation are inverted compared to that for the polymers presenting a smectic phase ($R_{\perp}$ always increases and R_{II} sometimes decreases).

PA_4-CN differs from polymer PA_6-CN by its spacer length of four (CH_2) instead of six (CH_2). In agreement with Gubina *et al.* [37] this polymer gives only a nematic phase on cooling the isotropic phase. The polymer backbone adopts only a prolate shape over all nematic range. However, the prolate anisotropy remains weak for about 10°C below I-N transition and then develops.

The liquid crystal polymethasiloxanes called PMS differ from the preceding polymers in their backbone, their shorter spacer $(CH_2)_4$ directly drafted to the Si atom and the inversion of the carbonyl group localised between the two phenyl rings. There are some specific problems, which cause the uncertainty about the values of the gyration radii and the type of anisotropy (prolate or oblate) can not be surely determined. And these problems can be essential for the comparison of SANS to other methods. From the measurements of the PMS deuterated in the last methylene group of the spacer, connected to the rigid core is concluded that the backbone conformation is also oblate in nematic phase. Because the polysiloxane is deuterated at different position in the side group the shape obtained from SANS is not necessarily that of the backbone. One way for correction is shown in ref. [38]; the apparent molecular shape was estimated for different label distances to the backbone and extrapolated to zero distance. Another possibility for correction was given in [33]. There is also studied another possible problem: segregation into deuterated and hydrogenated phase could occur in some cases.

Empirical interpretation of the conformation in the nematic phase based on SANS. Five oblate shapes and three prolate shapes have been determined. All the polymers presenting an oblate shape form a smectic phase on decreasing the temperature from nematic phase. Moreover strong smectic fluctuations [34, 39] or correlation lengths larger or comparable to $R_{\perp}$ are always detected in nematic phase. It is then concluded that the oblate backbone conformation could be simply the result of the smectic fluctuations.

In this way, the 'natural' conformation adopted by the backbone of a side-chain polymer in a pure nematic phase is a prolate shape. This agrees with the structure of the nematic phase which is made of rod-like mesogenic moieties and which sterically favours (if the spacer enables it) a packing of the backbone in the direction parallel to the rod-like units. This prolate shape is relatively independent of the spacer length, since PA_6-CN, PA_4-CN, PA-OCH_3 and PA_5-OCH_3 possesses different spacers. The spacer is not short and rigid enough to hold the backbone perpendicular to the liquid-crystal part. The same prolate anisotropy has been found for a 'diluted' side-chain polymer where the mesogenic units are statistically distributed along a polyacrylate-copolymer [40]. This seems to indicate that the drafting ratio (frequency of mesogenic unit repetition along the backbone) does not influence the anisotropy type. Interesting is that side-chain liquid-crystal polysiloxanes too exhibit a prolate shape in nematic solutions [41]. The prolate shape appears than to be a shape relatively independent of the medium for the nematic phase. This excepts the case of stretched polymers, for which different backbone conformations have been found, depending on the odd or even number of (CH_2) segments in the spacer [42]. However in this investigation only the case where a magnetic field is applied is considered and one cannot compare the mechanism involved in the case of stretched chain with those for alignment of the side-chain parts by a magnetic field.

For the smectic phase it appears from the small angle neutron scattering data that the global backbone conformation is oblate ($R_{II} < R_{\perp}$) and becomes more and more oblate when the temperature decreases. The component parallel to the magnetic field R_{II} can reach the spectacularly low value of 7 ± 2Å in the case of PA-OCH_3. The value of R_{II} is smaller than the smectic layer thickness of 25 ± 1Å [43] (and even half of the layer thickness); the extension of the backbone is not on average sufficient to fill all the thickness of the smectic layer. Since the smectic phase comes from the segregation of the aromatic parts from the aliphatic parts, it is deduced that the polymer backbone is mostly located between two successive mesogenic layers. The periodic backbone confinement is also confirmed by the distribution profiles of the backbone which have been determined for a smectic polymer PMA-OC_6H_{13} [44] and also for PMA-OC_4H_9 [28]. The case of PA-OCH_3 demonstrates that the backbones, taken as sandwiched between the liquid crystal layers can be confined quasi-bidimensionally (that is to say on average without crossing though the mesophase layer) between two successive mesogenic layers. The other polymers of higher molecular weight do not present such a confinement, since the R_{II} value indicates that the backbone crosses the layers. Therefore, it seems that the polymerisation degree plays an important role in the strong anisotropy of PA-OCH_3. All the polymers except PMA-OCH_3 show values of R_{II} similar to or larger than the half of the layer thickness, which implies that on average the backbone does in these cases cross the mesogenic layer.

It has been shown by X-ray [45] and by neutron scattering [31] that the strong anisotropy of PMA-OC_4H_9 coincides with a high density of the mesogenic groups inside the layers (strong 001 Bragg peak intensity) and a better localisation of these groups inside the layers (multiplicity of the Bragg orders). It is remarkable to see that such a small change in extremity length of the liquid crystal group induces such a strong difference in the backbone anisotropy, despite keeping the structure of the smectic phase the same - S_{A1}.

The type of the smectic phase (S_{A1}, S_{Ad}) has also a strong influence on the backbone behaviour. In the case of partially billiard smectic phase, S_{Ad}, the polymer backbone (PMA-CN, PA_6-CN) does not extend itself in the direction perpendicular to the mesogenic units, keeping the $R_\perp$ value of the isotropic phase ($R_\perp \approx R_{iso}$). This is in contrast to the strong increase in $R_\perp$ always observed for polymers giving a monolayered smectic phase S_{A1} (PMA-OCH_3, PA-OCH_3, PMA-OC_4H_9). The difference could be interpreted by the weak compactness of the S_{Ad} phase which reduces sterically the constraints on the backbone which is more or less localised between the mesophase layers.

Finally it should be noted that the small angle scattering, from which R_{II} and $R_\perp$ are extracted is obtained with a mixture of hydrogenous and deuterated polymers. This mixture is assumed to be ideal. This seems correct in the case of deuterated backbones, but this is no longer the case when the extremities of the mesogenic units are deuterated. The H/D separation clearly appears as soon as smectic phase occurs; this shows how sensitive this phase is to local interactions, in particular between the mesogenic tails, and how much the deuteration affects the physical (liquid-crystal) properties of the liquid crystal polymers. It is certain that many other studies have to be done to clarify the problem with the orientation and conformation of the backbone in liquid-crystal polymers.

2.2 Theoretical models existing for nematic phase

The lattice model for side-chain polymers (Vasilenko *et al.* [7]). This model considers that each macromolecule is a succession of n repetitive blocks. The lattice is formed by a set of N polymers. The partition function Z corresponding to the number of different polymer arrangements in the lattice is calculated, taking into account the fact that the backbone and the spacer are more flexible than the mesogenic group and that they form an angle between them. The minimization of the free energy $\triangle F = -NkT \ln Z$ gives different relations between the parameters from which phase diagrams are deduced. There result three oblate conformations. The oblate tendency is more or less important depending on the volume ratio of the backbone sites and the mesogenic unit sites. In the case of polyacrylates or polymethacrylates studied here, this ratio would be 0.1. Following this theoretical model, the strongest oblate conformation should be obtained when the backbone remains perpendicular to the nematic axes. This model does not fit to the experimental results obtained from SANS; moreover it can not take into account the conformation change with temperature, since model is build on athermal parameters.

A worm-like chain model. Wang and Warner [8] treat side-chain polymer systems by a mean-field model, which combines the usual Maier-Saupe theory for the liquid crystal part and the model of worm-like chain for the polymer part. The backbone is considered as a continuous chain where, at each point, a tangent unit vector **u** is defined. **u** wanders over the surface of a sphere and is attracted to or repulsed from the poles with a potential U. U contains all the parameters necessary for the description of side chain polymer systems. Five coupling parameters between mesogenic group, spacer and backbone and two order parameters S_A and S_B are so defined. The last two correspond, respectively to the usual

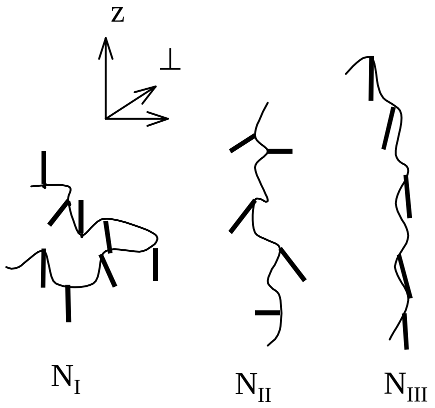

Figure 2.1 Schematic presentation of the three backbone conformation as defined by Wang and Warner

orientation parameter of the liquid crystal and a backbone order parameter, which gives the type of anisotropy ($S_B>0$ in the prolate case and $S_B<0$ for oblate shape). Three backbone conformations called N_I, N_{II} and N_{III} are deduced, corresponding to different values of the coupling parameters and to the ratio χ of the volume fraction of mesogenic group on the backbone, and also as a function of temperature. These three types of nematic phases differ in the relative preferred direction of main chains and side groups. If these different directors tend to be parallel (N_{III}) then the corresponding backbone conformation results in a prolate shape of the polymer. This situation is expected to occur when the spacers are flexible, so that the coupling between the director of the backbones and that of the side-group dominates. In the reverse case of relatively stiff spacers the backbones tends to be oriented in planes perpendicular to the side groups (N_I phase). In that case the overall shape of the polymer is oblate. For the investigated liquid crystal the value of χ was evaluated to $\chi>0.9$. Such a high frequency of mesogenic group repetition along the chain should produce, in all cases an oblate conformation (N_I phase). This theory cannot explain the prolate shape obtained for PA_6-CN, PA_4-CN and PA_5-OCH_3. Weaker values of χ can account for the two backbone conformations, oblate and prolate, with realistic values of coupling parameters. A nematic-nematic re-entrance is even predicted [46] for which the polymer backbone adopts an oblate shape at high temperature and becomes prolate when the temperature decreases. This could correspond to what is observed for PA_6-CN, but no smectic phase is predicted between the two nematic phases. Moreover the NI-III re-entrance is theoretically based on a strong backbone mesogenic group coupling, which has no physical basis, since the aromatic part of the liquid crystal has no affinity with for the aliphatic part of the backbone.

2.3 X-ray studies of backbone conformation of liquid-crystal polymer

The levels of alignment of the mesogenic units and polymer backbone trajectory for polyacrylate based [40, 47] side chain liquid-crystal polymers, elastomers and polymethasiloxane [41] were evaluated by using X-ray procedure.

The object of [47] is to study the backbone conformation of PA_6-CN using high resolution X-ray diffraction and to compare the result with the former SANS observations [32, 31]. According to Noirez *et al.* The backbone conformation in PA_6-CN is perpendicular to the side groups in the nematic (N) and S_{Ad} phase and parallel in the nematic re-entrant (N_r) phase. This transition from an N_I –like to an N_{III} –like local structure would mean that the backbone conformation undergoes a giant change at the N_r - S_{Ad} phase transition. The possibility should be considered that the variations in the mosaicity in the smectic phase are a signature of the backbone conformation already changing in the smectic phase. The observed difference in mosaicity upon heating and cooling should indicate that the backbone conformation in the smectic phase depend on the temperature history of the sample. This seems rather unlikely, since upon heating and cooling, neither differences in the ratio in the intensities of the first and the second harmonic of the Bragg peak nor in the layer thickness have been found. The variations in the mosaicity are of the similar magnitude to those that also occur in monomeric liquid crystals upon changing the temperature over ten’s of degrees in the smectic phase. In combination with the possibility of aligning the new N_r phase, it seems most likely that the transition from an oblate backbone conformation to a prolate backbone conformation happens in the N_r phase during the pretransitional effects associated with the phase transition to S_{Ad}. Then the N_r phase can indeed be identified as an N_{III} phase, while in contrast, the smectic fluctuations have the perpendicular N_I –like backbone conformation. In that case, the change of the backbone conformation from N_{III} to N_I –like occurs with the growth of the smectic fluctuations. From the packing point of view, it seems intuitively difficult to impose a smectic density modulation upon a N_{III} –like structure, which could provide the driving force for the change in backbone conformation. The conclusion from this investigation is that the change in the backbone conformation from N_{III} to N_I –like occurs in the N_r phase parallel to the growth of the S_{Ad} fluctuations.

In [42] the focus of the study is to examine directly the shape and dimension of the polymer chain trajectory in the elastomers obtained from side-chain liquid crystals (polyacrylates) by introducing a moderate of chemical crosslinking as a function of temperature and. The X-ray scattering measurements show that substantial levels of preferred orientation of mesogenic units can be introduced through magnetic field and through mechanical extension. The order parameter $<P_2>_n$ was been evaluated in the nematic phase for the mesogenic units and it was found that it is of the same order like in the case of uncrosslinked polymer. Small angle neutron scattering measurements show that for highly aligned samples an anisotropic polymer backbone trajectory is observed in which the envelope is slightly extended by ≈ 10 % n the direction parallel to the axes of alignment of the mesogenic units like for the uncrosslinked polymer. The level of anisotropy is similar to that in neutron scattering studies of other nematic forming liquid crystal polymers based on both methacrylates [24, 25, 26, 27, 28, 29, 30] and acrylates [31, 32, 33, 34] but the sense of anisotropy is opposite to that seen in other materials. In polyacrylates studied here the polymer chain aligns preferentially parallel to the mesogenic units. This type of arrangement was labelled N_{III} by Warner [8].

In [41] the conformation of the side chain poly-(methylsiloxanes) as a function of spacer length and degree of polymerisation in nematic solutions was determined by X-ray scattering. It is shown that the macromolecules are conformationally anisotropic. The macromolecule sizes in the directions $\perp$ and II to the mean field director ($\vec{\mathbf{n}}_0$) are effectively different. Hence the hypothesis of conformational anisotropy in ordered media (in nematic phase N) is useful for understanding these systems. The present measurements complete that hypothesis by providing the form of the anisotropy and its magnitude as follows:

$$R_{II} > R_{\perp} \text{ and } \quad R_{II} / R_{\perp} \approx 1.3 - 1.6$$

The difference between these two sizes is larger than the experimental uncertainties. The characteristic sizes R_{II} and $R_{\perp}$ in the nematic phase do not evolve in a strong temperature dependent manner except within a range close enough to the clearing point. The magnitude of the anisotropy is also very weakly dependent on the spacer length. The chain dimensions in the disordered isotropic phase R_i are large compared to conventional chains with a similar degree of polymerization. For instance a poly(dimethilsiloxane) (PDMS) chain Gaussian coil, with degree of polymerization N = 100 and a statistical segment $b \approx 5.4$ Å [48] would give $R_G \approx 18.5$ Å to be compared to $R_i \approx 45$ Å. The measured dimensions for the nematic solutions are consistent; they obey the volume conservation condition and $R_\perp < R_i < R_{II}$. The isotropic sizes R_i are large compared to an ordinary polymer with the same degree of polymerisation. From these result a conclusion is done about the effect of the polymer concentration of the absolute size of polymer chains in ordered solutions but not on the form of the anisotropy or its magnitude. The results are consistent with an independent viscoelastic study [49] reported on this materials.

From all the X-ray studies found in the literature one can resume that it is quite hard to use this method for investigation of the backbone. The X-ray pattern from the backbone was not possible to obtain in the case of [40], in [47] was possible only in the more ordered state of the material – in the smectic phase, and in [41] the measurement was taken in solution where the special problem is to find appropriate solvent, which has the electron density close to the monomers of phenyl benzoate and the polymethasiloxane.

2.4 ^{29}Si NMR investigations of the main chain orientation in side chain polysiloxanes

The orientation of the main-chain segments of some polysiloxanes containing mesogenic side groups was estimated in [21] by ^{29}Si NMR under high power decoupling. A further question is the connection between backbone conformation and stability of the mesophase. The latter can be varied by changing the mesogen [50]. The polymerization-caused mesophase stabilization expressed by the difference between the isotropization temperatures of polymer and monomer, respectively, depends on the degree of steric hindrance between mesogen and main chain. In this paper is shown that different amounts of steric hindrance between side and main chain can lead to different backbone orientations, i. e. phases N_I or N_{III}.

The proton decoupled ^{29}Si spectra of non-oriented polysiloxane samples exhibit a line shape which is characteristic of an axialsymmetric chemical shift tensor (Fig. 2.2). The main values of the chemical shift tensor σ $(\sigma_{11}, \sigma_{22}, \sigma_{33})$ appear in the spectrum as singularities of the

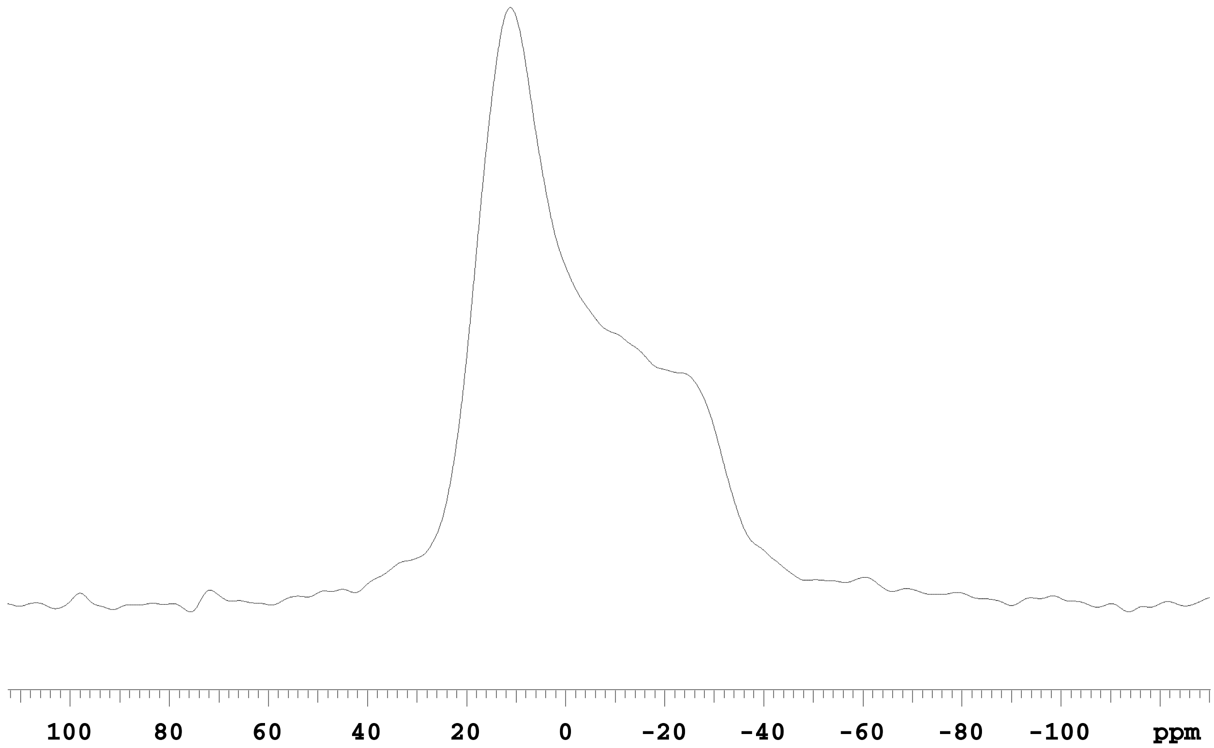

Figure 2.2 ^{29}Si NMR spectrum of isotropic polysiloxane sample adopted from [21]

characteristic shape [51]. For polysiloxane chains is observed that the chemical shift tensor is axialsymmetric, i.e. two of its three main values have equal shift value $\sigma_\perp$ with respect to the isotropic average σ_{iso}. The consequence of this anisotropy is that every ^{29}Si nucleus has its own individual chemical shift $\sigma(\theta)$ which is dependent upon the angle θ between the direction of the static magnetic field $\mathbf{B_0}$ and the tensor symmetry axis

$$\sigma(\theta) = \sigma_{II}\cos^2\theta + \sigma_\perp \sin^2\theta = \sigma_{iso} + \frac{2}{3}\vartriangle\sigma \bullet P_2(\cos\theta)\,. \tag{2.2}$$

The normalized line shape function $S(\sigma)$ resulting from the superposition of the contributions of all individual spins depends on the distribution of the angles θ. For a non-oriented sample when all the orientations of the spin tensors are equally distributed in the space [51]:

$$S(\sigma) = \begin{cases} \dfrac{1}{2\sqrt{\vartriangle\sigma}\sqrt{\sigma - \sigma_\perp}} & if\, \sigma_{II} \le \sigma \le \sigma_\perp \\ 0 & otherwise \end{cases} \tag{2.3}$$

In an oriented sample, certain orientations σ are more abundant than in the non-oriented case. This leads to the variation of the abundance of the chemical shifts of the individual nuclei and the result is a deformation of the line-shape function. The spectrum depends also on the angle

δ between the sample director and $\mathbf{B_0}$. This is because the following: during rotation of the sample by an increment $\Delta\delta$, the angle θ of a certain tensor symmetry axis is with respect to $\mathbf{B_0}$ is also changed. Maxima of the θ distribution are shifted to different angles. This change of the θ distribution also has a consequence for the σ distribution, i.e. the line shape $S(\sigma)$, because of Eq. (2.2).

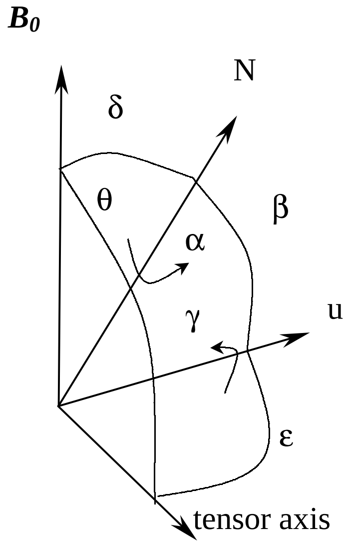

Figure 2.3 Angles used for description of ODF in the case of axialsymmetric tensor

In this particular case we are interested in a distribution of orientations of the main-chain segments. The orientation of one segment is expressed by the segment vector **u** (Fig. 2.3) which is defined as the vector connecting the two oxygens neighbouring to a silicon atom in the main chain. As mentioned above, the ^{29}Si line shape contains only information about the distribution of the polar angle θ, which is denoted as $U(\cos\theta)$. The other two Eulerian angles corresponding to the azimuth of the tilting and to a rotation about the siloxane group around the tensor axis do not enter in the Eq. (2.2) because of the axialsymmetry. Thus from the spectra we can get only information about the one dimensional ODF $U(\cos\theta)$ of the chemical-shift axes.

For a description of the distribution of the segment orientations, however, a one-dimensional ODF is not sufficient. This two-dimensional ODF is denoted like $V(\cos\beta, \gamma)$. It should be mentioned that $V(\cos\beta, \gamma)$ (or some parametrical information about it) is the aim of the quantitative evaluation, whereas $U(\cos\theta)$ is only an intermediate result which can be obtained immediately from the spectrum analysis which is used to get the parameters needed for estimating the $V(\cos\beta, \gamma)$. Thus the data analysis consist of two parts:

- first, the calculation of data concerning the chemical shift tensor orientations;
- second, the estimation of parameters which characterise the segment orientation.

The following expansion of the ODF into a Legendre polynomials is in most of the cases used:

$$U(\cos\theta) = \sum_{n=0}^{\infty} u_n P_n(\cos\theta) \tag{2.4}$$

The orthogonality of P_n permits the calculation of the expansion coefficients:

$$\begin{aligned} u_n &= \frac{2n+1}{2}\int_{-1}^{1} U(\cos\theta) P_n(\cos\theta) d(\cos\theta) \\ &= \frac{2n+1}{2}\langle P_n \rangle_{CV} \end{aligned} \tag{2.5}$$

The integral $\langle P_n \rangle$ represents the average over the Legendre polynomial of the *n*-th order and gives a measure of the orientation. It is denoted as 'orientation degree of *n*-th order'. The index '$_{\mathrm{CV}}$' states that these parameters belong to the chemical shift tensor orientation (rather than the segment orientation. All the coefficients with odd *n* vanish because $\cos\theta$ enters in Eq. (2.2) only by its square which means that θ and $180°-\theta$, cannot be distinguished by this method and *U* is only the symmetric part of the real ODF.

In the case of ^{29}Si there are two possibilities for estimation of the $\langle P_n \rangle_{\mathrm{CV}}$ from the spectra of polysiloxane:

1. One can calculate the ODF corresponding to the division procedure [52]. Such analysis is very complicated when there are relatively strong rounding-off effects deforming the spectra. On the other hand, a quantification of the orientation by the whole function seems to be overestimated and not reasonable, so it would be enough to have only a single number which expresses the magnitude of orientation.
2. Calculation of $\langle P_n \rangle_{\mathrm{CV}}$ from the moments of the resonance line corresponding to the procedure developed by Hentschel, Sillescu and Spiess [14, 15].

The first procedure gives *U(cosθ)* by dividing the anisotropic spectrum by that of a non oriented sample. The $\langle P_n \rangle_{\mathrm{CV}}$ are then calculated by using (2.5).

The second method relies on the fact that the orientation is reflected in the *moments* M_n of the resonance line

$$M_n = \int (\sigma - \sigma_{iso})^n S(\sigma) d\sigma \,. \tag{2.6}$$

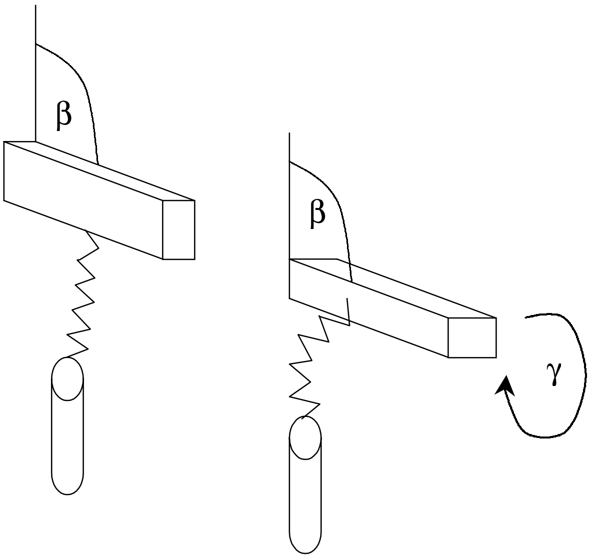

Figure 2.4 Sketch illustrating that different γ lead to different conformations even when tilt angles β are equal

As mentioned above after this steps of evaluation of the $\langle P_n \rangle_{\mathrm{CV}}$ one arrives at an intermediate state of the data analysis because the ODF of the main chain segments is of interest instead that of the tensor axes. A calculation of the latter is possible only if additional information about the distribution of the tensor axes in the planes perpendicular to **u** is available. In the formulae of Hentschel *et al.* [14] transverse isotropy is assumed; then an estimation of the segment orientation degrees $\langle P_n \rangle_{\mathrm{S}}$ will be possible immediately:

$$\langle P_n \rangle_{CV} = \langle P_n \rangle_S \cdot P_n(\cos\varepsilon) \tag{2.7}$$

where ε is the angle between tensor axis and **u**, in this case 90°.

For the backbone segments of side-group LCP, however, essential deviations from transverse isotropy are expected. For example, (Fig. 2.4) we can consider all monomer units of the sample where the mesogens are parallel to sample director **N** and the **u** (segment director) perpendicular to it. A rotation of the main-chain segment demands different conformations of the spacer and different excluded volumes, and thus there is a priori no equal probability for all γ. Therefore one must take into account a violation of transverse isotropy leading to some correction terms for Eq. (2.7). In extreme cases, this could mean not only a small quantitative correction, but also reverse of the sign of orientation degrees as shown below.

In the following, a transverse-anisotropy correction for Eq. (2.7) for $n = 2$ is presented:

$$\langle P_2 \rangle_{CV} = -\frac{1}{2}\langle P_2 \rangle_S + \frac{1}{2}\langle \cos 2\gamma \rangle - \frac{1}{2}\langle P_2(\cos\beta)\cos 2\gamma \rangle \qquad (2.8)$$

The last two terms of Eq. (2.8) represent the transverse-anisotropy correction for Eq. (2.7) for $\varepsilon = 90°$.

A summarized presentation about the orientation degrees obtained from the ^{29}Si spectra of PMS is given in Tab. 2 of [21]. The dependence of $\langle P_2 \rangle_{CV}$ on the varied structures (spacer length $m = 3$, 6 or 11, and different lengths of the terminal group of the mesogenic unit) is as follows:

- For short spacers, the enhanced depression of the clearing temperature connected to increased sterical hindrance because of increasing wing-group length is accompanied by significant decrease of $\langle P_2 \rangle_{CV}$.
- For the 11 membered spacer however, there is not such a clear dependence; $\langle P_2 \rangle_{CV}$ even seems to grow when the wing groups get longer. Obviously the extremely long spacer prevents conflicts between main chains and wings.

The calculation of $\langle P_2 \rangle_S$ corresponding to Eq. (2.8) is not possible without discussing the transverse part of the ODF. To get more insight into this problem, some particular cases will be discussed:

1. $\gamma = 0°$ for all segments. This means that all tensor axes are in the same plane as **N** and **u**. Then, $\langle P_2 \rangle_{CV} = 1/2 - \langle P_2 \rangle_S$. This case however is very unlikely because near $\beta = 0$ no γ dependence should occur.
2. $\gamma = 90°$ for all segments, i.e. all tensor axes are perpendicular to the plane spanned by **N** and **u**. Then $\langle P_2 \rangle_{CV} \equiv -1/2$. Like 1., this is only a theoretical limiting case.
3. Equal abundance for all γ: this is the case of transverse isotropy which gives Eq. (2.7) with $\varepsilon = 90°$.
4. The transversely anisotropic part of $V(\cos\beta, \gamma)$ can be factorized into a pure γ- dependent part:

$$V(\cos\beta,\gamma)=\frac{1}{2\pi}U_0(\cos\beta)+U_1(\cos\beta)\cdot g(\gamma) \tag{2.9}$$

Thereby $U_0(\cos\theta)$ is the transversely isotropic part of V defined by:

$$U_0(\cos\beta)=\int_0^{2\pi}V(\cos\beta,\gamma)d\gamma \tag{2.10}$$

$U_1(\cos\theta)$ represents the amplitude of the γ dependence. It should be zero for β = 90°. As a simple approach to this constraint, $U_1 = \sin\beta$ is used next. The transverse part of the product $g(\gamma)$ can be replaced by its Fourier series; because $g(\gamma)$ must have the plane spanned by **u** and **N** as its symmetry plane, no sinus terms appear in this expansion:

$$g(\gamma)=\sum_{n=1}^{\infty}g_n\cos n\gamma \tag{2.11}$$

The constant term (g_0) must vanish to fulfil Eq (2.10). Inserting this into Eq. (2.8) gives:

$$\left\langle P_2\right\rangle_{CV}\approx-\frac{1}{2}\left\langle P_2\right\rangle_S+\frac{9}{35}\pi^2\cdot g_2\approx-0.5\left\langle P_2\right\rangle_S+2.776\cdot g_2 \tag{2.12}$$

The two simplifications of the problem used in the derivation of Eq. (2.12) – possibility of factorization and transverse amplitude proportional to sinβ - seem to be reasonable and at least usable for a qualitative interpretation of the obtained values.

Certainly the question arises in which cases the transverse anisotropy correction term is essential and in which cases it can be neglected. Because of the lack of an appropriate model, we can discuss this topic only qualitatively. The main chain order degrees are quite small compared to those of mesogenic units. This means that the nematic field for the concrete case of [21] appears to be able to create a strong longitudinal ordering of the segments. This implies the conclusion that the mesogen-induced transverse order is also weak. The transversal order of those segments which lie perpendicular to **N** can be expected to have at maximum the same order of magnitude as the longitudinal order of the whole sample, which means $\langle P_2\rangle_S \sim \langle\cos 2\gamma\rangle$ for those segments. The transverse isotropy will be smaller for subgroup of segments, which are tilted by a smaller angle against **N**, and vanishes for those segments arranged parallel to **N**. Thus, the transverse anisotropy of the whole sample $\langle\cos 2\gamma\rangle$ is expected to be of the order of $(\langle P_2\rangle_S)^2$. This qualitative argument would lead to the conclusion that the influence of the correction term is more essential for well-ordered (with respect to the main chain) samples. An experimental estimation can not be made by these measurements; therefore experiments are necessary which are based on another interaction, the symmetry axis of which is not parallel to that of the chemical shift tensor. However from literature data some indications of quite strong transversal anisotropy are known: for example one of the samples of Titman *et al.* [50] yields a value of 0.35 for $\langle P_2\rangle_{CV}$, leading to the impossible value of –0.7 for $\langle P_2\rangle_S$ if one applies the transverse isotropy relation (2.8).

The conclusion is that one has to consider the values for $\langle P_2\rangle_S$ obtained under the assumption of transverse isotropy that they are uncertain in magnitude but correct in sign because the correction term should be of second order.

The resulting values of $\langle P_2\rangle_S$ neglecting the presumably small contribution of the transverse anisotropy for the investigated polymethasiloxanes have in almost all cases negative values, which means that also for these pure nematic side-group polymers the main-chain order is perpendicular to the director. This is in contradiction to the SANS results (Chapter 2.1.). For two of the substances differing in the spacer length and the terminating group for the mesogenic unit in exception the parallel arrangement of side and main chain is slightly more probable than the perpendicular one. This effect is caused from the hard conflict because of sterical hindrance. For short spacer lengths, the conflict is between long wing groups and main chain, which must overlap or make a bent structure to keep perpendicular orientation. This parallel arrangement seems to be connected with the sterically induced destabilization of the mesophase found by Jacobi *et al.* [53]. For polysiloxane samples investigated in [21] the more stable phases are connected with a perpendicular arrangement; a parallel structure means a destabilization. Additionally the wedge-like shape of the mesogens [54] must be taken into account for further discussions.

An explanation of the differences in some cases between NMR (^{29}Si and ^{2}H [23]) and SANS [33] can be found in the different length scales belonging to the methods. The conflict comes from the conclusion that a parallel arrangement of side and main chain means a prolate ellipsoid, and a perpendicular structure an oblate average shape of the molecule. This conclusion is justified if the model of a Gaussian chain is appropriate; in other words, the orientation probability of a segment is governed by the ODF alone and does not depend on the orientation of the neighbouring segment. If it is true the components l_{II}^2 and $l_{\perp}^2$ of the mean square end distance l^2 parallel and perpendicular to **N**, respectively, are proportional to the corresponding gyration radii and are connected to $\langle P_2\rangle_S$ as:

$$R_{II}^2 \propto l_{II}^2 = \frac{l^2}{3}(1+2\langle P_2\rangle_S); \qquad R_{\perp}^2 \propto l_{\perp}^2 = \frac{l^2}{3}(1-2\langle P_2\rangle_S) \tag{2.13}$$

If however, the independence of the orientation of neighbouring molecules is violated, the relations (2.13) are no longer valid. It is even possible that a main chain whose segments are mostly perpendicular to the director has a prolate shape. Than the largest part of the main chain is compressed between the mesogenic layers perpendicular to **N**; only a very few number of segments are members of the part of the chain which is crossing the layers. Than the ODF should clearly monitor this mostly perpendicular arrangement, even though the shape of that molecule is prolate.

A parallel arrangement of main and side groups does not necessarily mean a prolate shape of the macromolecule, and vice versa perpendicular main and side groups are not necessarily connected to oblate chain conformation. Another problem is the transverse anisotropy, which occurs at least in a few samples; its influence is generally expected to be small but nevertheless special cases may exist where this can lead to misinterpretations. Further information concerning these two problems can be obtained if another spin interaction is included into the experiments the symmetry axis of which is not parallel to the symmetry axis of the ^{29}Si chemical shift tensor.

2.5 Molecular order of spacer and main chain in side-groups liquid crystal investigated by ^{2}H NMR

In [23] ^{2}H NMR in combination with specific labelling has been used to get the molecular order via the orientation distribution function of individual C-H bond directions[15]. Two different systems were investigated with 4-hydroxibenzoate as the mesogenic unit - PMA-OCH$_3$ and PA-OCH$_3$ from Table 2.1, Chapter 2.1. The spacer consists of 6 methylene units and the backbone is build up from poly(acrylic acid - PA-OCH$_3$) and poly(methacrylic acid PMA-OCH$_3$).

The orientation of the systems is studied in the glassy state at room temperature where no chain motion has to be considered. The spectra are dominated by the quadrupole coupling of the I = 1 spin with the axially symmetric field gradient tensor in the C-^{2}H, and can be analysed to yield the orientation distribution function [14, 15]. The NMR line-shape can easy be calculated using an expansion of the ODF $P(\beta)$ in terms of Legendre polynomials. The total spectrum $S(\omega)$ is then obtained as a superposition of subspectra $S_l(\omega)$ corresponding to the order parameters $\langle P_l \rangle = \langle P_l(\cos\beta) \rangle$ for even l:

$$S(\omega) = \sum_{l=0,2,4,6...} (2l+1)\langle P_l \rangle S_l(\omega) P_l(\cos\beta_0) \tag{2.14}$$

β_0 is the angle between the director and the magnetic field. The $S_l(\omega)$ can be calculated analytically [14,15]. If the conformation of the macromolecule is not known in detail, the order parameters $\langle P_l \rangle$ are best referred to the C-^{2}H bond directions used as a labels in this experiment. For systems of transverse isotropy they can easily be converted into the order parameter of a different molecular direction $\langle P_l \rangle_{mol}$, e.g. a chain direction forming an angle θ with the C-^{2}H bond according to [14,15] and Eq. (2.7).

In low-molecular-weight liquid crystals the alkyl side chains take part in the liquid-crystalline order. The order parameters are position dependent [55] and decrease with increasing distance from mesogenic group. From earlier results on polymeric liquid crystals [56] in the mesophase it is known that the order parameters of the alkyl part is lower than for low-molecular weight systems. For the spacer deuterated sample there is a strong angular dependence observed even for this position (^{2}H in the spacer, most close to the main chain) that clearly shows a remarkable orientation. A line-shape analysis yields an ODF with $\langle P_2 \rangle_{C-H} = -0.26$ and $\langle P_4 \rangle_{C-H} = 0.07$.

For the main-chain deuterated samples there is also an angular dependence of the spectra observed, but not so strong like in the former case. The difference spectra $S_I - S_{II}$ for $\beta_0 = 0°$ and $\beta_0 = 90°$ clearly show that the chains are ordered, although much less than the spacer deuterated system. More important, main-chain ordering must be opposite in nature for both systems, because the differences of intensities at equivalent spectral regions are of opposite sign. To specify the nature of the order one can compare the order parameters with the values expected for *all-trans* chains aligned parallel or perpendicular to the director $\mathbf{n_0}$. For the former, the C-H bonds form a planar distribution [14,15] with an unique axis parallel to $\mathbf{n_0}$ and $\langle P_2 \rangle_{C-H} = -0.5$, $\langle P_4 \rangle_{C-H} = 0.38$. For the latter the C-H bonds form planar distribution, the unique axes of which are uniformly distributed in the plane perpendicular to the director and $\langle P_2 \rangle_{C-H} = 0.25$, $\langle P_4 \rangle_{C-H} = 0.14$. The signs of the order parameter for $l = 2$ observed clearly indicate that both the axes of the spacer and the main chain are preferentially aligned *parallel* to the director in the PA-OCH_3 but the main chain is oriented *perpendicular* to the director in the PMA-OCH_3. It should be noted that in the PMA-OCH_3 the order parameters $\langle P_2\rangle$ and $\langle P_4\rangle$ are equal in magnitude but opposite in sign.

The different nature and degree of orientation of main-chain order are discussed in relation to the liquid-crystalline mesophase involved (smectic for PA-OCH_3, nematic for PMA-OCH_3) and the chain stiffness, being higher for the latter. The major difference between these two systems is the sign of order parameter. These results are consistent with the molecular shape of the polymer chain as a rotational ellipsoid with its long axis parallel to the director for PA-OCH_3 and perpendicular to it for PMA-OCH_3. This is considered as an indication that the main-chain stiffness rather than differences in the mesophase is responsible for the opposite chain ordering. The result from the latter are in agreement with SANS studies for PMA-OCH_3 [29, 25] but in contradiction to the SANS reported on the PA-OCH_3 in [33]. Possible contradiction in the different SANS results can be the uncertainty of the determination of $R_{\perp}$ and R_{II} . Liquid crystalline elastomers based on polyacrylates and polymethacrylates show a similar behaviour [40]. Therefore it is concluded that the relative orientation of the polymer chain and mesogenic groups is strongly influenced by the stiffness of polymer chain. Chain stiffness has been considered to be a parameter in model calculation of Khokhlov [7] predicting much higher order parameters for the main chain than the observed one. It should be mentioned that the relative orientation of side groups and main chain may also depend on the spacer length as found in liquid-crystalline elastomers [57].

The mesogenic groups can induce significant orientation of the polymer chain only if both are linked chemically. In mixtures of low-molecular weight liquid crystal and polymers, e.g. polystyrene, no significant macroscopic alignment of the polymer is observed [58]. In comparison to main-chain liquid crystalline polymers, where a complete alignment requires high-order parameters in both the rigid mesogenic part and the flexible part of the molecule, the side group systems show a decrease in molecular order from the mesogenic unit via the spacer to the main chain. This nicely corroborates the model considerations [59, 60] on side group polymers that the different tendencies of orientation of the polymer main chain and the mesogenic units are decoupled by the spacer, which increases the conformational freedom of the system.

2.6 Summary of the literature survey

The studies of the orientation of the main chain in the side chain liquid crystalline polymers hold by four different techniques (SANS, X-ray, ^{29}Si NMR, ^{2}H NMR) give information about the backbone conformation by measuring very different by nature molecular properties of the material: in the case of the SANS, for example, the order of the main chain is demonstrated by the scattered beam of the deuterium atoms located in the main chain of the whole macromolecule, while in the case of NMR the order of the main chain is demonstrated by the orientation dependence of the correspondent tensor of interaction (chemical shift in the case of ^{29}Si , or quadrupolar interaction in the case of ^{2}H NMR). Different scales of different techniques (the length of the whole macromolecule for SANS and much smaller scale corresponding to the interatom distances for NMR) can be the reason for a certain contradiction between the results of the studies done on the same substances, like in the case of PA-OCH_3.

From the other side all the techniques reported here are applicable only for a certain type of substances: for SANS and ^{2}H NMR the condition is that the main chain must be deuterated, and ^{29}Si is applicable only for poylsiloxanes. This special conditions narrow very strong the possibilities for investigating the whole large variety of different liquid crystalline polymers. A very big group of such substances having ^{13}C in the main chain can not satisfy this conditions (if they are not isotopically labelled) and consequently can not be investigated by these techniques. They can be investigated by ^{13}C NMR techniques. The presence of very big number of different ^{13}C site in such polymer compounds makes big problems for the simple NMR techniques. In comparison to ^{29}Si NMR for poylsiloxanes and ^{2}H NMR the natural abundance ^{13}C has a very bad signal to noise ratio, and second spectrum is quite complicated with different and overlapping lines (sidebands in the case of MAS experiments). Therefore ^{13}C investigation should rely on pulse programs, which are much more complicated, and 2D or 3D NMR methods should be applied. This requires a very long measuring times.

3 Static ^{13}C NMR measurements

Some not standard side-chain liquid crystalline polyesters were synthesized in the Institute of Physical Chemistry of the Martin Luther University of Halle [61]. The structural formula was drawn on the Fig. 3.1. The substantial difference here, comparing to the standard substances shown in Table 2.1 is ***first*** in the mesogenic unit type, which consists of 3 aromatic rings connected with nitrogen bondings, and ***second***: in the main chain, which has in this case not only an aliphatic groups but also an typical ester –OOC- carboxylic group. In the case of NMR studies this fact gives good opportunity to study directly the main chain orientation without necessity to change the structure by selective deuteration because this group is localized only in the main chain, and no ester group exists in the mesogenic unit neither in the spacer.

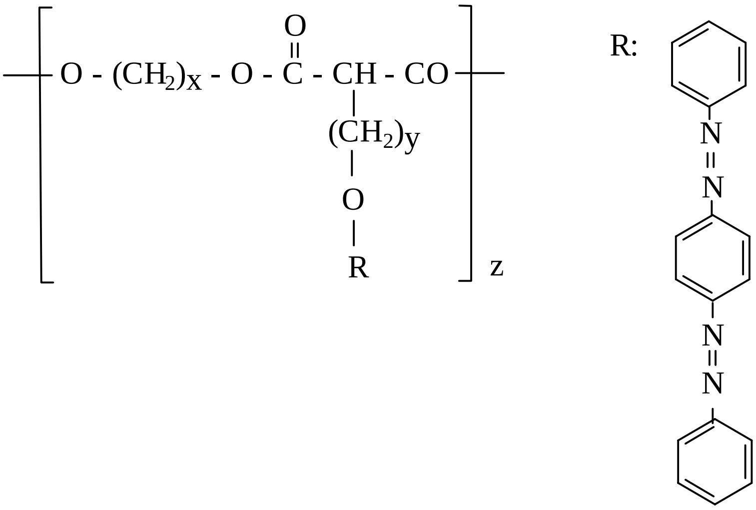

Figure 3. 1 Formula of the 6PBAy liquid crystalline substances

Table 3.1 Properties of the 6PBAy substances

6PBAy	Polym. Degree z	Mn (g/mol)	Phase properties (from polarization microscopy)
6PBA8	≈ 8	11 300	T_{Cr} 100 (S_X 87 S_C) S_C 110 N 119 I
6PBA12		18 200	T_{Cr} (N 109 I) 109 I
6PBA13		-	T_g 54 S_A 104 N 11 I

In Table 3.1 some data are presented about the samples which can be generally denoted like: ***xPBAy***. The phase behaviour under different conditions (heating up and cooling down) was investigated by polarization microscopy and DSC measurements.

All the substances are with the same length of the aliphatic chain in the backbone x = 6, but with the different spacer lengths y = 8, 12 or 13. 6PBA8 has different phase behaviour when the substance is heated up and cooled down. In the first case it presents S_X phase (in brackets) and in the latter from S_C at 87°C it goes to crystal state. About 6PBA12 it is reported that there should come a nematic phase only when heating up. For 6PBA13 the substance goes through nematic and P_{SA} phases independently of heating up or cooling down the material.

3.1 ^{1}H NMR spectra

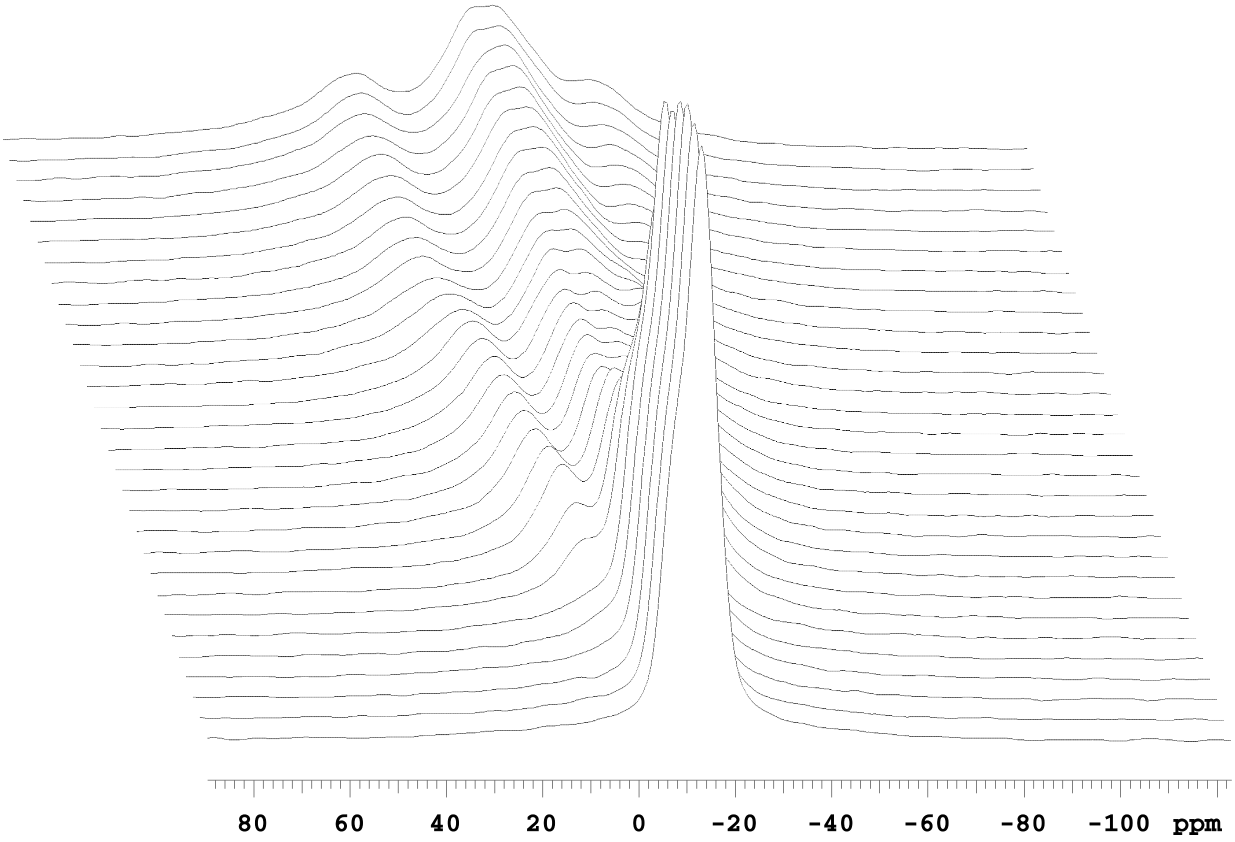

Figure 3.2 Stack of ^{1}H NMR spectra taken from 129° C (bottom) to 110 C (top) with a step of 1° C.

One stack of proton spectra taken from the 6PBA8 in the different temperature, varying from 130 to 100 °C is shown on the Fig. 3.2. The temperature was changed downwards when the sample was in the magnetic field of 9.3 T, with a speed of 1°C/min. The spectra above 119

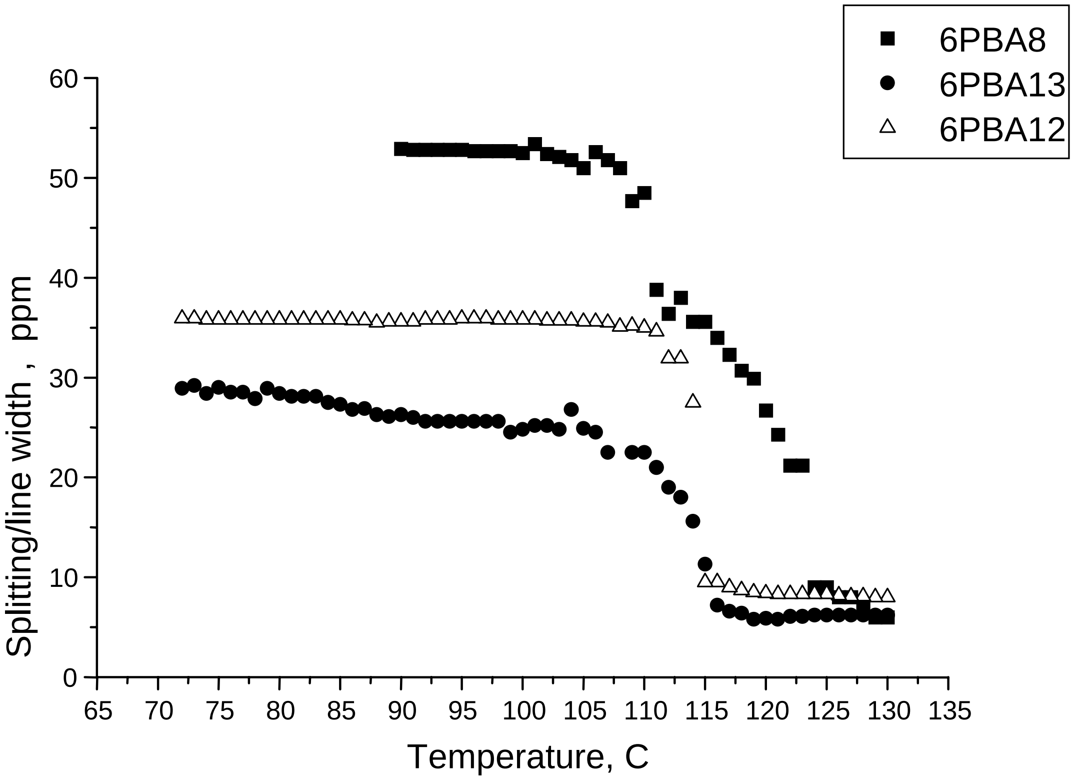

Figure 3.3 Dependence of the splitting/linewidth (the latter – for the temperatures above the isotropic-nematic phase transitions in the case of 6PBA8, 6PBA13, and for the whole range for the 6PBA12) on the temperature

°C, which is the isotropic-nematic transition point has only one line. This is the consequence of the fact that the substance is melted in isotropic state; one can not reveal any fine structure, all the protons (from the spacer, aromatic rings, main chain) form a single line. This can be explained with the fact that the individual line widths are larger than the chemical shift differences, because of high viscosity of the melt. It can be characterized by its line width at half height. During the further decreasing of the temperature protons give a typical wide-line spectra and one can follow the phase transitions of the substance. Below the clearing point a broad doublet appears which is typical for lateral protons of oriented phenyl rings and is caused by a dipolar interaction. The quantity of this splitting increases linearly with decreasing of the temperature. For a non-oriented sample no splittting occurs. The dependence of the splitting versus temperature has different slope for the different mesophase types (nematic, smectic) and it reaches a steady-state value for a glassy or crystal state (see Fig. 3.3). The aliphatic protons appear in the proton spectra between the aromatic splitting, but not exactly in the middle as the isotropic chemical shift for aromatics and for aliphatic protons are at different positions on the scale. Fig. 3.3 confirms that for 6PBA12 the substance directly jumps from isotropic in crystal state. There is no line splitting in this case observed, the proton spectra below the clearing point are again consistent of one line, like in the isotropic phase, with broader but constant during further cooling line-width. It was not possible to orient this sample.

3.2 ^{13}C NMR spectra:

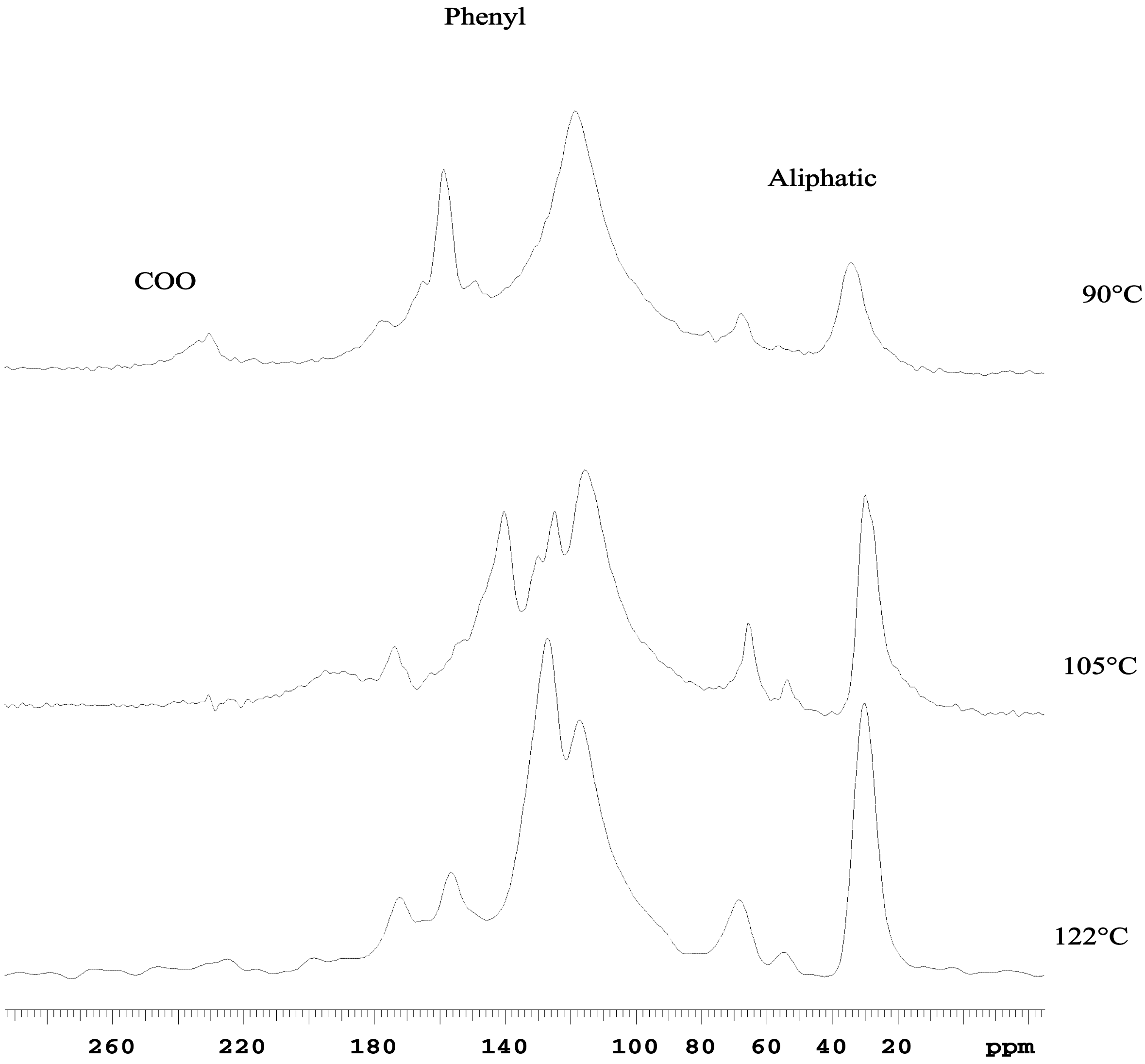

Figure 3.4 ^{13}C NMR spectra taken from 6PBA8 at isotropic (122 ° C), nematic (105° C), and glassy state (90° C); the temperature was decreased following the orientation procedure.

Fig. 3.4 shows static ^{13}C cross-polarization and decoupled NMR spectra of one of the samples taken (6PBA8) at different temperatures. For the other two samples the spectra look in the similar way. Here should be noted that the lines of the spectra taken above the clearing temperature in isotropic state are wider than those typical for liquids. This fact can be explained with the higher viscosity of the substance. The regions of the lines belonging to the aliphatic, aromatic and carboxylic ^{13}C of the isotropic spectra were assigned with the help of a spectral catalogue [62]. During transition into mesophase, some of the isotropic lines vanish and instead of this new resonances appear which are gradually shifted when temperature is changed. Only the methyl resonance is nearly constant in its position. In the glassy state the shifts reach their maximum.

3.3 Indication of the main chain orientation

Fig 3.5 shows two groups of ^{13}C spectra for 6PBA8 and 6PBA13 taken at room temperature but the samples are like frozen in the oriented state, it means that they have the same orientation like in the nematic phase. The orientation procedure was as described in chapter 3.1. The dependence is demonstrated of the spectra from the angle between the magnetic field and the sample director **N**. This angle δ was changed from 0 to 180° with a step of 10° or a total number of 19 FIDs for each substance. Each FID has a number of accumulations nt = 2000, which makes a total measuring time for each substance of 53 hours

An interesting feature was observed in the aliphatic region: the position of the aliphatic peak slightly moves in the case of 6PBA13 during the changing of the angle δ reaching a maximum relative shift of 30 ppm according to the initial position at 90°. This fact can be interpreted in the following manner. In the aliphatic line come all the nuclei **from the spacer** and the $(CH_2)_6$ groups in **the backbone**. When the ^{13}C resonance is excited under the conditions of proton decoupling, like in our case, the main interaction, which controls the line-shape is the chemical shift, which is characterized by its tensor elements σ_{11} σ_{22} and σ_{33} . On Fig. 3.6 a) the aliphatic chain is sketched, with one of the ^{13}C nucleus marked and the chemical shift tensor elements pointed out. For the aliphatic chain [63] the most shielded

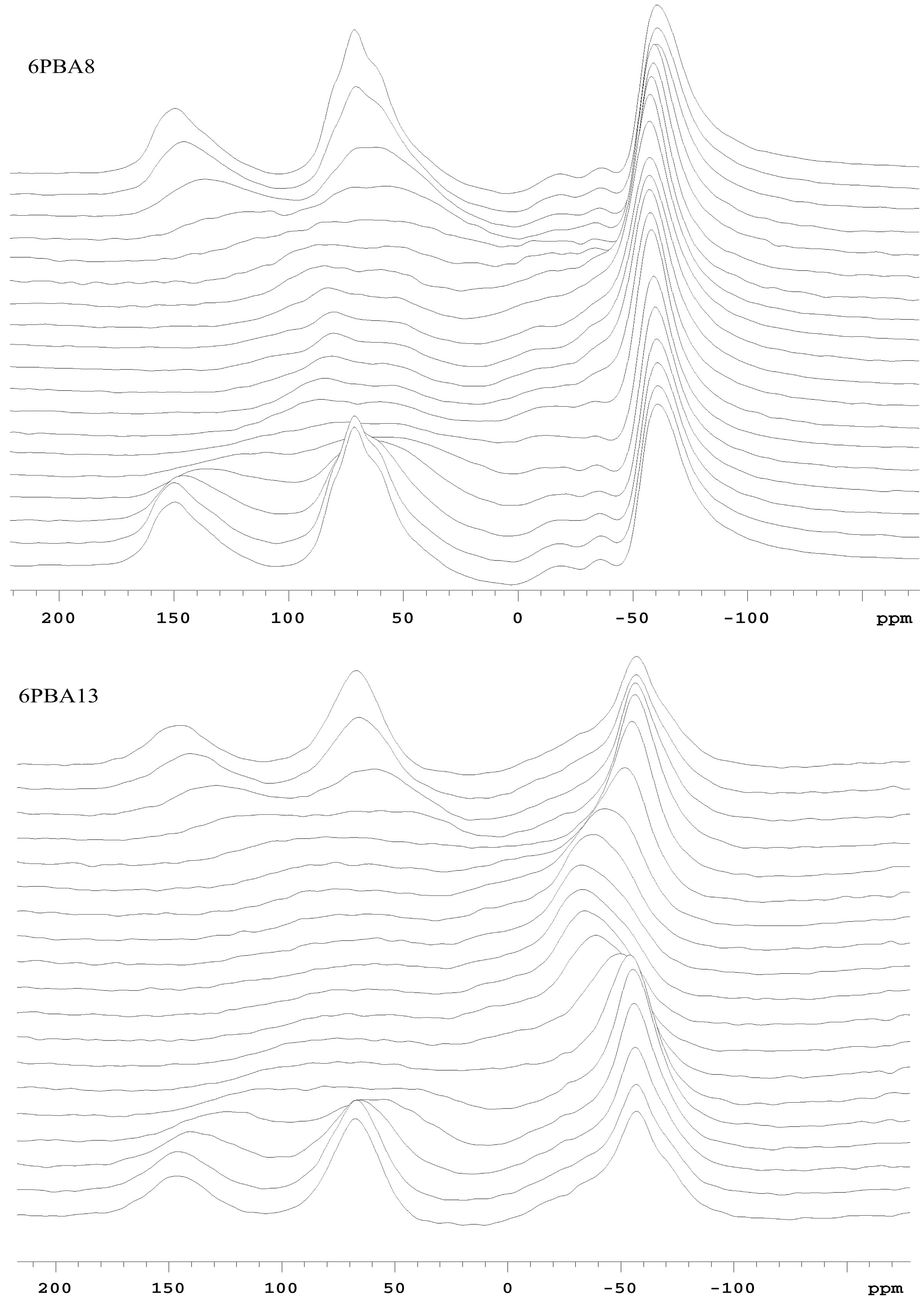

Figure 3.5 Angular dependence of the static ^{13}C NMR spectra on the angle δ between the magnetic field B_0 and the director N; variation of δ from 0 ° (bottom) to 180 ° with a step of 10 ° ; the samples (6PBA8 – top, and 6PBA13 – bottom) are frozen in oriented state.

element σ_{33} is directed along the chain, σ_{22} is directed perpendicular to the chain plane, and σ_{11} is directed to the bisector of the CH_2 bonds. On the Fig. 3.6 b) the NMR spectrum corresponding to this tensor for isotropic sample is schematically drawn. This is only an idealized form of the spectra for an non-axiallsymmetric tensor, in practice the isotropic chemical shift spectrum looks not with a sharp contours, but it is rounded-off (similar to the isotropic ^{29}Si spectrum shown on Fig. 2.2) because of the variations of the chemical surroundings for different nuclei and some differences of the conformations for different parts of the segment.

Lets first consider the case when MC II SC (main chain is parallel to the side chain) - Fig. 3.7 a). In this case we have all the ^{13}C aliphatics tensors from the main chain and from the side chain with a similar orientation, and the same tensor element (for example σ_{33}) will be oriented along the director **N** in the both parts. In the ideal case, when the **N** II $\mathbf{B_0}$ spectra of the fully ordered sample will look like a delta function appearing in the position of the σ_{33} - Fig. 3.7 b). Because of the rounding-off effects and only a partial orientation the real spectra looks like the sketch drawn on Fig. 3.7 c) a smooth and broadened line, centered to the σ_{33}.

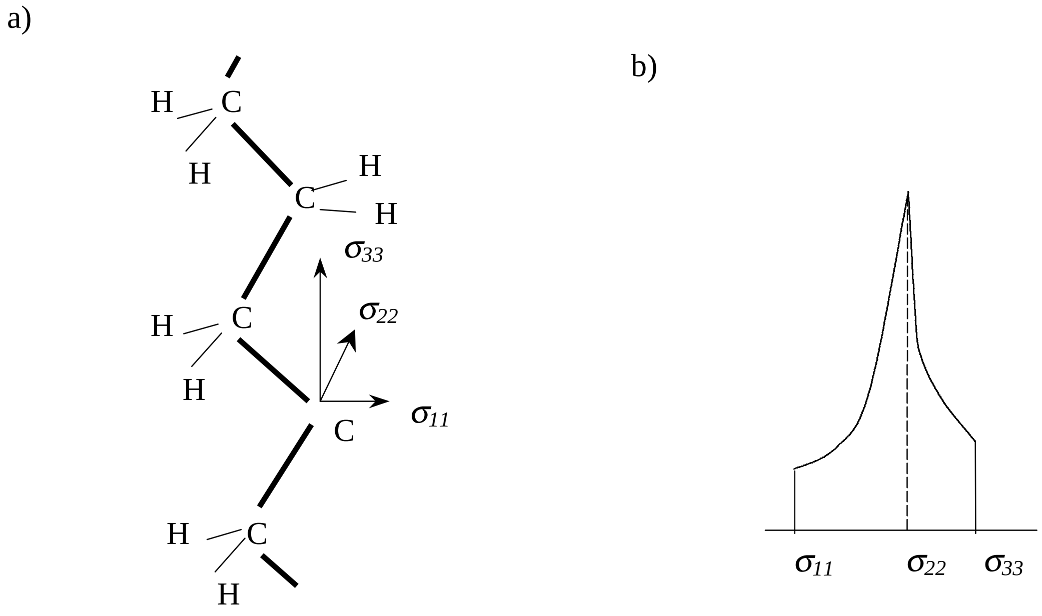

Figure 3.6 a) Scheme of the aliphatic chain with the ^{13}C chemical shift tensor elements pointed out; b) idealized sketch of the spectrum of an isotropic sample, corresponding to the ^{13}C tensor from a)

For the different spectra shown on Fig. 3.5 the angle δ between the magnetic field $\mathbf{B_0}$ and the director **N** is changed and the shift of the maximum for the aliphatic line is observed which is increasing with increasing of δ until $\delta = 90°$, where it reaches a maximum value. Lets see what is the situation with the position of the tensor when $\delta = 90°$ (Fig. 3.7 d)). In this

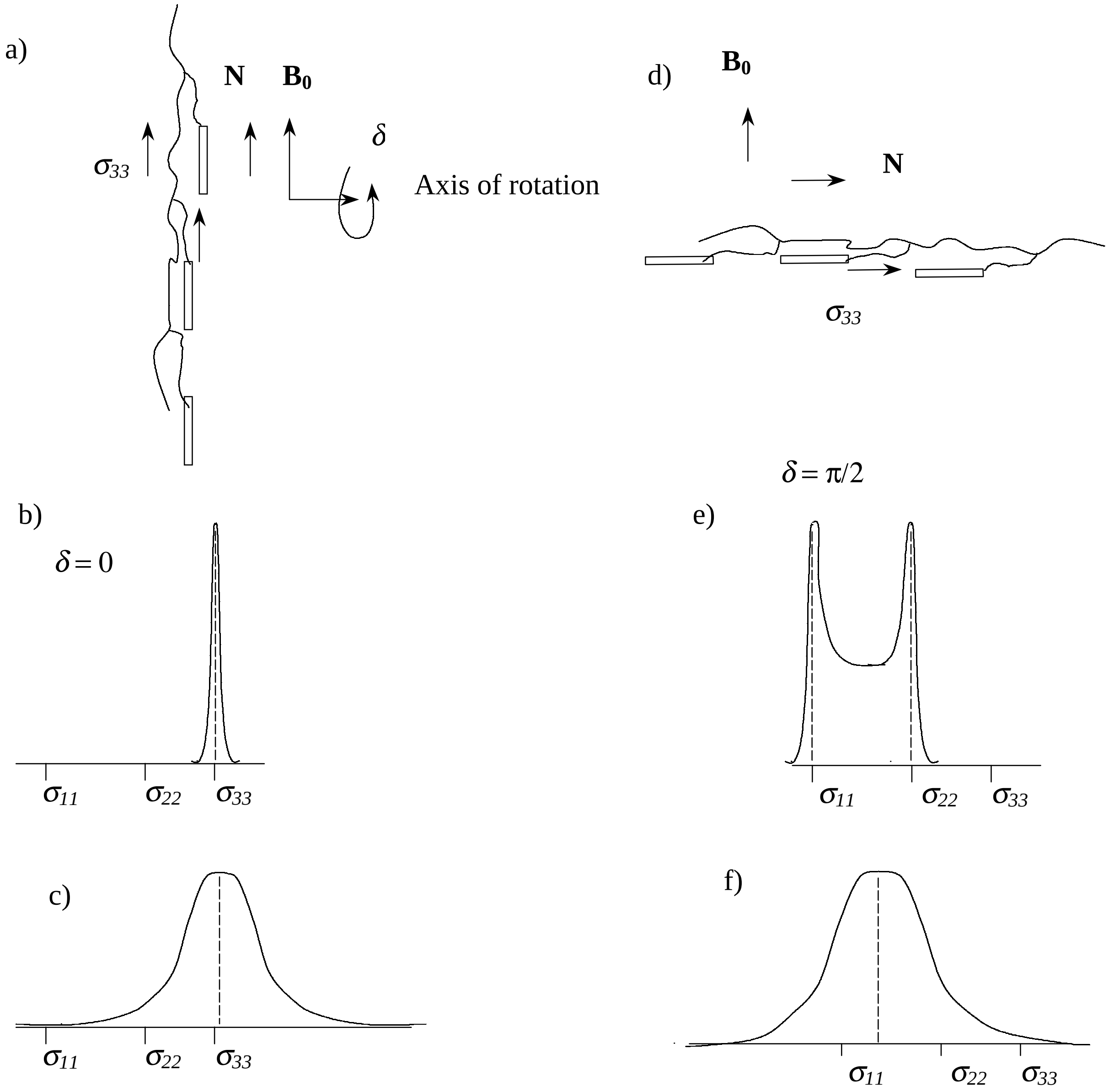

Figure 3.7 MC || SC a) scheme of the mutual orientation of the MC, SC (**N**) and $\mathbf{B_0}$ when $\delta = 0°$; b) idealized form of the spectrum for $\delta = 0°$; c) sketch of the line shape observed in reality for $\delta = 0°$; d) scheme of the mutual orientation of the MC, SC (**N**) and $\mathbf{B_0}$ when $\delta = 90°$; e) idealized form of the spectrum for $\delta = 90°$; f) sketch of the really observed line shape for $\delta = 90°$.

case the σ_{33} element of the chemical shift tensor is in the xy-plane and the magnetization vector is formed from the σ_{11} and σ_{22} elements. This case is considered by Opella and Waugh

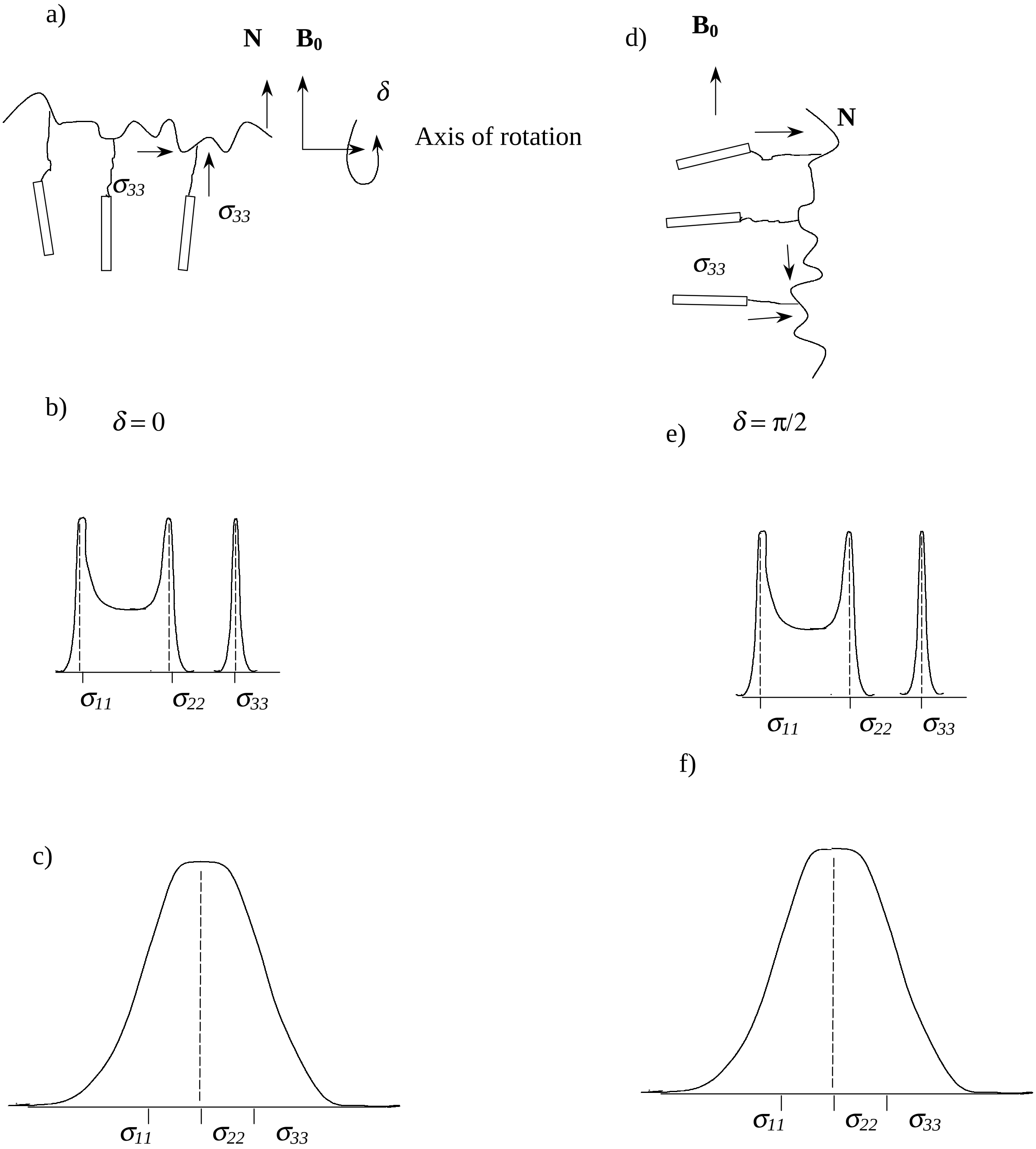

Figure 3.8 MC ⊥ SC a) scheme of the mutual orientation of the MC, SC (**N**) and $\mathbf{B_0}$ when δ = 0°; b) idealized form of the spectrum for δ = 0° ; c) sketch of the line shape observed in reality for δ = 0° ; d) scheme of the mutual orientation of the MC, SC (**N**) and $\mathbf{B_0}$ when δ = 90°; e) idealized form of the spectrum for δ = 90 ° (the same like in the case b); f) sketch of the really observed line shape for δ = 90°; no difference with c).

[64] and the shape of the line is like it is drawn on Fig. 3.7 e). In practice the real spectra looks like the sketch on Fig. 3.7 f) and it is centered between σ_{11} and σ_{22}. In this way changing the angle δ from 0 to 90° step by step the shifting of the position of the maximum in the aliphatic region can be explained: for $\delta = 0°$ it will be near σ_{33} and for $\delta = 90°$ - between σ_{11} and σ_{22}.

The case when main chain is perpendicular to side chain (MC⊥SC) is presented on Fig. 3.8. First, Fig. 3.8 a), when angle $\delta = 0°$, the tensors in the aliphatic part of the main chain and in the side chain have differently oriented principal axis referring to the laboratory frame - $\mathbf{B_0}$.

According to this all the tensor elements σ_{11} σ_{22} (from the main chain) and σ_{33} (from the side chain) contribute for forming the spectrum and it has the form of Fig. 3.7 b) superimposed to the principal form of Opella and Waugh [64] – Fig. 3.7 e). The real spectra has a rounded-off form of the smooth line as shown on Fig. 3.8 c). In the case $\delta = 90$ ° Fig. 3.8 d) σ_{11} σ_{22} (from the side chain aliphatics) and σ_{33} (from the main chain aliphatics) are aligned along the external field direction $\mathbf{B_0}$ and contribute to the forming of the line in the same manner like in the case b). That's why there is no difference expected for this case with changing of the mutual orientation between the **N** and $\mathbf{B_0}$. Here it should be mentioned that all the considerations above are only qualitative. In this case the quantitative estimation of the orientation degree is not possible because the line for the aliphatic ^{13}C is formed from main and the side chain ^{13}C nuclei and they can not be separated.

The qualitative considerations of the effects of the shift in the case of MC II SC (Fig. 3.7) and no-shift in the opposite case (Fig. 3.8) give a reasonable explanation of the experimentally observed fact of the shifting of the peak position for 6PBA13 and no-shift in the case of 6PBA8 with changing of δ. From the proton experiments (see Fig. 3.2, and Fig. 3.3) we know that the sample is oriented (at least it is sure for the mesogenic unit!). Non-oriented sample can be excluded for the 6PBA8 and 6PBA13. However it is not excluded that the spacer and the main chain could be non-oriented. Thus, in the case of 6PBA8 (see Fig. 3.5), when no difference of the position of the peak is observed this can mean either that the mutual orientation of the main and side chain is perpendicular or that the spacer and the main chain are highly disordered.

4 Characterization of the structure and order in partially oriented solids by 2D-magic-angle-spinning NMR

4.1 General idea of the method

As it was discussed earlier (see chapter 2.6) for expanding of the multitude of the liquid crystalline substances investigated with NMR with the aim to estimate the orientation distribution of the main chain, application of some ^{13}C methods is needed. It was mentioned also that the application of the static NMR techniques is not useful in this case, because the broad lines specific for a solid-state NMR from the many different functional groups of the whole macromolecule overlap with each other and this makes the quantitative analysis impossible. In this case some resolution enhancement techniques should be applied.

Such wide used in solid state NMR method increasing the resolution is the magic angle spinning – MAS. Magic-angle spinning experiment was introduced to NMR by Andrew [65], and Lowe [66] as a mean of spatially averaging inhomogeneous interactions in order to obtain well-resolved NMR spectra of solid samples. A typical MAS spectrum of a solid material consists of centerbands at the isotropical shift frequencies of the individual resonances, flanged by set of a narrow bands - rotational sidebands, at integer multiples of the spinning frequency: the intensities of these sidebands are a function of the symmetry parameter and the ratio of the chemical shielding anisotropy to the spinning angular velocity ω_R [66, 67]. However for the current purpose using of the simple 1D MAS is still not appropriate while the spectra are very complicated, there is a strong overlapping of the central and side bands from different functional groups. This problem can be overcome by choosing any appropriate 2D [22] or 3D [69] NMR method based on MAS which can extend the complicated 1D spectrum into second or third dimension.

If one spins an ordered sample, with the order axis not parallel to the rotor axis, one observes phase and intensity modulation of the centerbands and sidebands, which depend on the position of the rotor at the time the spectrum was excited [22, 70]. For any periodic process, with period τ_{rot} and the data which have recorded it (in the case of NMR – the free induction decay of the magnetization vector FID), Fourier analysis along rotor position gives the intensities of oscillation with ω_R, $2\omega_R$, … If sample is not oriented there is no position dependence and consequently no such Fourier coefficients. Thus, the existence of the coefficients and their magnitude contain information about the orientation state. Therefore by synchronizing data acquisition with the rotor position, for each resonance a sideband pattern in two dimensions can be obtained. In the one dimensional rotor-synchronized spectra mixing of absorptive and dispersive lineshapes occurs, with the dispersive components often broadening the lines in an intolerable fashion. Therefore, the orientation dependence of rotor-synchronized MAS spectra could only be fully exploited after it was discovered that a Fourier transformation against the rotor phase $\gamma_1 = \omega_R t_1$, applied to 2D datasets with $\gamma_1 = \omega_R t_1$

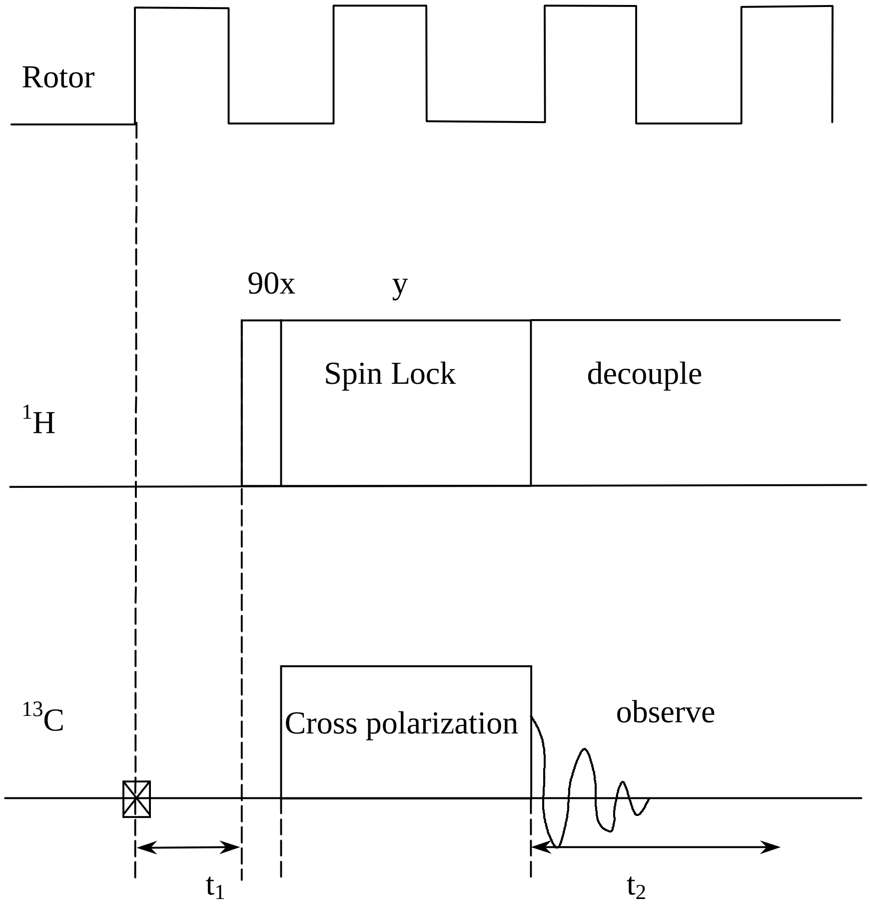

Figure 4.1 Pulse sequence for the rotor synchronized Harbison-Vogt-Spiess experiment

regularly incremented through 360° (see the pulse sequence presented on Fig. 4.1) under most circumstances produces absorptive lines along ω_2 for each fixed ω_1 value. An optical reflected signal from the mark on the bottom of the MAS rotor placed in the magnet triggers the start of the experiment. The start of the pulse program waits a time t_1 after the triggering with reflection mark which is a period of $N\tau$ where N is the number of increments and $\tau = 2\pi / N\omega_R$ before executing the 90° proton pulse. After the proton 90° pulse, the ^{13}C were cross-polarized under Hartmann-Hahn-matched conditions. Normal detection under conditions of high power proton decoupling occurs during t_2. After a two dimensional Fourier transform, no intensity is obtained for an isotropic sample outside the middle (ω_1 = 0) row which resembles the one-dimensional MAS spectrum and contains spinning sidebands spread along the ω_2 co-ordinate. However for an ordered sample sidebands are observed for $\omega_1 \neq 0$, and the intensities of the two dimensional sideband pattern reveal the orientation distribution function of any resonance site. Because of the rigorous cyclic, nondecaying behaviour of the experiment during t_1, it is valid to sample over a single rotor period, and the N slices of the 2D Fourier transform spaced by ω_R in ω_1, contain all the information available from the experiment.

4.2 Geometry conventions

Here for all the considerations it is appropriate to follow the generally accepted conventions and symbols used by Herzfeld and Berger [71].

Four coordinate systems are relevant for the case MAS experiment of partially oriented systems:

- Director frame (DF): this system is defined by the direction of the external forces that have produced the macroscopic anisotropy of the sample. In the case of drawn polymer, the Director **z**-axis is given by the draw direction; for liquid crystalline polymers **z**-axis is the direction of preferable orientation of the mesogenic groups;

- Molecular frame (MF): this molecular fixed system is defined in order to describe the orientation of particular molecule (or segment) with respect to the DF. In some cases, only one angle χ of one molecular axis **z** with respect to unique director axis is relevant, since the distribution $P(\chi)$ of the MF **z**-axis has axial symmetry with respect to DF **z**-axis. The choice

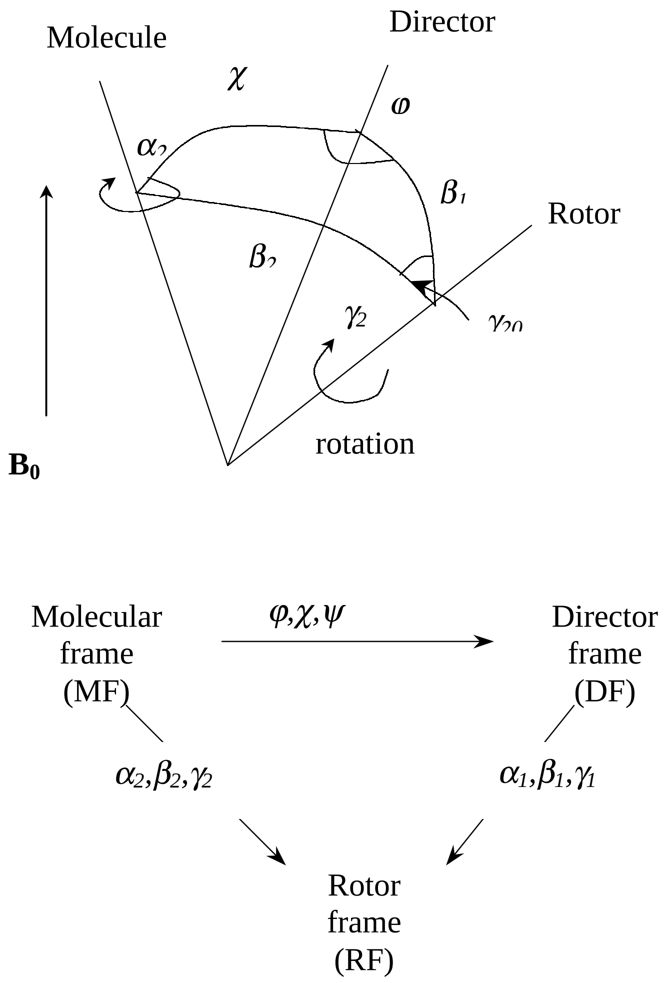

Figure 4. 2 Definition of the angles and different reference frames. An important role for forming of the 2D pattern has the angle between the director and the rotor β_1, for $\beta_1 = 0°$ no sidebands in the ω_1 dimension appear.

of the MF **z**-axis is rather arbitrary. It can be chosen with respect to some arbitrary feature of the molecular geometry, like chain axis of a polymer, the local axis of an aromatic ring, or the principal axis frame (PAS) of the shielding tensor itself.

- Principal axis system (PAS): the spin coupling parameters (shift anisotropy, quadrupolar coupling constants, etc.) are defined within the principal axis system x_k, y_k, z_k, of the anisotropic spin coupling tensor. The label k = 1, 2, 3,... , corresponds to the different spins within a molecule (or monomeric unit in a macromolecule) that contribute to the spectrum. It is important to know how this system is related with respect to the MF. Sometimes the z_k axis of an axially symmetric coupling tensor coincides with a particular bond direction, e. g. the principal axis of the ^2H quadrupole coupling tensor for many C-^2H bonds, but in some cases it is not clear and even not possible to find out how is the particular PAS oriented referring to any molecular axis.

- Laboratory frame (LF): usually in the static NMR experiments it is defined by the direction of the external magnetic field $\mathbf{B_0}$. Here for the case of MAS another definition is more convenient. As the magic angle spinning experiment takes place in a rotor which is rotating with certain angular velocity ω_R around the axis which is under 54,7° according to the direction of magnetic field $\mathbf{B_0}$ laboratory frame is defined so that it is static in the frame fixed to the rotor (RF).

First we have to establish the relationships between the three frames of reference pertinent to this consideration. The frame of reference of the axis of preferential orientation (DF) is related to the rotor frame of reference (RF), whose ***z*** axis is the spinning axis and *y* axis lies in the plane of rotor and magnetic field, by the Eulerian angles α_1, β_1, γ_1. It should be noted that RF is static in laboratory frame. A tensor, $\mathbf{T}$, in RF is given by:

$$\mathbf{T}_{RF} = \mathbf{R}(\alpha_1, \beta_1, \gamma_1)\mathbf{T}_{_{DF}}\ \mathbf{R}^{-1}(\alpha_1, \beta_1, \gamma_1) \tag{4.1}$$

where the rotation matrix $\mathbf{R}$ is given explicitly by Herzfeld and Berger [71]. The relationship between DF and RF is depicted in Fig. 3.2. It is clear that $\gamma_1 = \gamma_{10} + \omega_R \cdot t$ where γ_{10} specifies a particular rotor position, e.g., at the beginning of the FID. It is related to the rotor frame by:

$$\mathbf{T}_{RF} = \mathbf{R}(\alpha_2, \beta_2, \gamma_2)\mathbf{T}_{_{DF}}\ \mathbf{R}^{-1}(\alpha_2, \beta_2, \gamma_2) \tag{4.2}$$

where again γ_2 is time dependent $\gamma_2 = \gamma_{20} + \omega_R \cdot t$.

Finally we can relate DF and MF by:

$$\mathbf{T}_{DF} = \mathbf{R}(\varphi, \chi, \psi)\mathbf{T}_{_{MF}}\ \mathbf{R}^{-1}(\varphi, \chi, \psi) \tag{4.3}$$

and thus:

$$\mathbf{R}(\alpha_2, \beta_2, \gamma_2) = \mathbf{R}(\alpha_1, \beta_1, \gamma_1)\mathbf{R}(\varphi, \chi, \psi) \tag{4.4}$$

The relation between the three frames of reference is depicted schematically on Fig. 4.2. We denote that in the case of uniaxially ordered system the DF is defined by a single angle vector and choice of the Euler angle α_1 is free.

σ_{11} is defined as the downfield and σ_{33} as the upfield principal value of the shielding tensor **ó** . One of the next chapters (4.4) is dealing with the calculation of the sideband intensities in the two-dimensional MAS spectra. For a given rotor frequency ω_R, the intensity of the signal at the positions $M\omega_R$ in ω_1 and in $N\omega_R$ in ω_2 dimension is defined as I_{MN}. The indices M and N increase with increasing frequency (i.e. from right to left across the spectrum): for the centerband, $M = N = 0$. Sideband intensities are everywhere normalized such that the sum of intensities in conventional, unsynchronized 1D-MAS spectrum of single species equals 1, which means that the central trace of the 2D spectrum is normalized to intensity 1.

4.3 Chemical shift

Before to get into details about the theory of the 2D MAS rotor synchronized method and its capabilities for estimation of the ODF some brief introduction is needed about the chemical shift, like a property of the specific ^{13}C site in the substance as this method exploits namely this concrete interaction in the NMR phenomena.

The most typical and studied interactions in solid-state NMR spectroscopy are:

- Chemical shift;
- Dipolar coupling;
- Quadrupolar interaction.

A detailed definition and presentation of any of these interactions one can find in any of the following basic NMR books like [51, 16, 70]. Important for the aim of the current thesis is that it is hopeless to expect, that we can apply any NMR technique based on any other interaction except chemical shift, because as it was already discussed before, for a quadrupolar interaction a special sample treating is needed (selective deuteration in the main-chain segments), and for such a complicated materials to explore the dipolar-interaction pattern is even much more harder than for the chemical shift as the multi-spin interaction is much more complicated.

The chemical shielding interaction separates the resonance frequencies of nuclei based on their electronic environment. The magnetic field experienced or ‘seen’ by the nucleus of an atom in a molecule is affected by the electrons that surround the nucleus. The chemical shift tensor is a reflection of this orientation dependent interaction of the electronic environment of a nucleus with the external magnetic field. In general, a different value of the chemical shift will be observed for a nucleus for each orientation of that molecule in the magnetic field.

In the most general terms this chemical shift interaction is represented by a 3×3 Cartesian matrix:

$$\sigma = \begin{bmatrix} \sigma_{xx} & \sigma_{xy} & \sigma_{xz} \\ \sigma_{yx} & \sigma_{yy} & \sigma_{yz} \\ \sigma_{zx} & \sigma_{zy} & \sigma_{zz} \end{bmatrix} \qquad (4.5)$$

The resonance frequency that is observed in high resolution NMR spectroscopy is the one-third in the trace of the matrix shown in Eq. (4.5), or:

$$\sigma_{iso} = \frac{\sigma_{xx} + \sigma_{yy} + \sigma_{zz}}{3} \qquad (4.6).$$

There exists a frame, called **p**rincipal **a**xis **s**ystem (PAS), in which the matrix in Eq. (4.5) is diagonal; in this case three diagonal elements are known as the principal values of the chemical shift tensor (or tensor components), and are designated as $\sigma_{11}, \sigma_{22}\ and\ \sigma_{33}$. Another two parameters are often used to characterize the chemical shift tensor in PAS:

- CS tensor anisotropy: $\delta = \sigma_{33} - \frac{1}{2}(\sigma_{11} + \sigma_{22})$ (4.7);
- CS asymmetry parameter: $\eta = \frac{\sigma_{22} - \sigma_{11}}{\sigma_{33}}$ (4.8).

With MAS the chemical shift interaction is averaged to its isotropic value. The average chemical shift **ó** of a given nucleus in a sample that is rotating around and axis making an angle θ with respect to the external magnetic field is given by:

$$\sigma = \sigma_{iso} + \frac{1}{2}(3\cos^2\theta - 1)\left[\frac{1}{2}[(3\cos^2\beta - 1)(\sigma_{33} - \sigma_{iso}) + \frac{1}{2}\cos^2\beta\cos 2\alpha(\sigma_{11} - \sigma_{22})\right] \qquad (4.9)$$

where α and β are two of the three Euler angles which specify the orientation of the PAS in the frame if spinning system. At θ = 54,7°, the term $(3\cos^2\theta - 1)$ is zero, and the pattern of the spectra collapses to a single line at the frequency given by the isotropic chemical shift σ_{iso} provided that the rotation frequency ω_R is larger compared to the width of the powder pattern.

4.4 Determination of orientation distribution function

Orientation distribution function is the ultimate result to be extracted from the considered 2D NMR experiment. There are several different approaches to attain this angular distribution. Here we consider the simple case of one dimensional ODF - $P(\chi)$. This is the case in which the investigated system exhibits a transverse isotropy, or with other words:

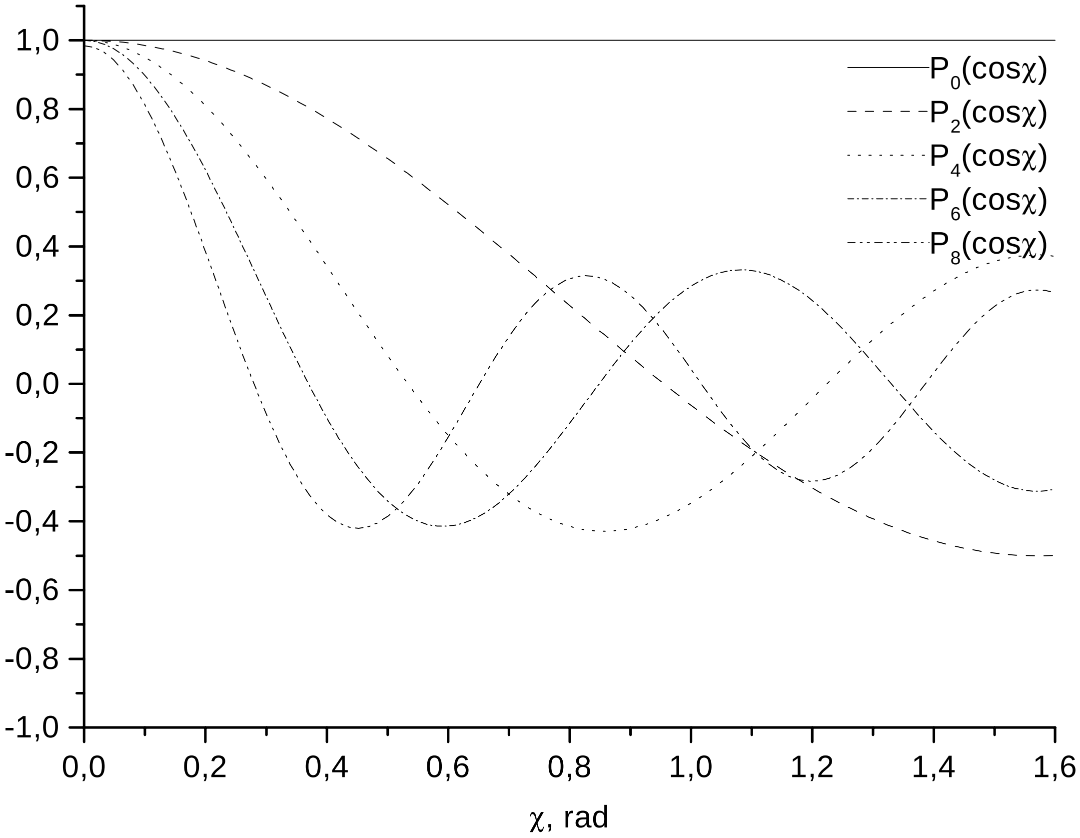

Figure 4.3 Plot of the Legendre polynomials

- the molecules are distributed uniformly around the order axis;
- molecular frame can be chosen, such that the shielding tensor principal axes are also distributed in an axialsymmetric fashion about a unique axis of this frame. This simplification is called ‘transverse isotropy’. In many cases it can be assumed, however there are indications that this is violated in polysiloxane side chain liquid crystal polymers [21]. Here this case will be discussed in some later stage (see Chapter 4.11).

- **Direct reconstruction**; it is the most convincing method of obtaining the distribution, but is not applicable in the current case. It requires that the spectrum contains a direct image of the angular distribution, that is, a single spectral peak for each angular peak, and no coincidence of spectral peaks. The distribution can then be reconstructed directly from the spectral intensity (see Chapter 2.4), as there is a following relation between the spectral density and ODF:

$$S(\omega)d\omega = P(\chi)d\chi \tag{4.10}$$

This relation is termed in [16] as ‘the principle of conservation of area of corresponding intervals’. This is relatively simple and robust procedure, it does not involve any data fitting at all. Direct reconstruction is possible with a number of experiments in the case of interactions with axialsymmetric spin interactions (η = 0). This is the case of ^{29}Si experiments with liquid crystalline polysiloxanes reported in Chapter 2.4.

- **Estimation of the expansion coefficients**. This ODF can be expanded into a series of Legendre polynomials (See Eq. 2.4, 2.5). The $P_L(cos\chi)$ for L = 0, 2, 4, 6, 8 are plotted on Fig. (4.3).

The expansion of the angular distribution in terms of Legendre polynomials $P_L(cos\chi)$ can be introduced as follows:

$$P(\chi) = \sum_{L=0}^{\infty} P_{L00} P_L(\cos\chi) \tag{4.11}$$

Here the moments of the ODF P_{L00} are related to the order parameters $\langle P_L \rangle$ by

$$\langle P_L \rangle = \frac{8\pi^2}{(2L+1)} P_{L00} \tag{4.12}$$

Each order parameter $\langle P_L \rangle$ characterizes the weight with which the corresponding $P_L(\cos\chi)$ contributes to $P(\chi)$:

$$\langle P_L \rangle = \int_0^1 d\cos\beta\, P(\chi) P_L(\cos\beta) \tag{4.13}$$

The set of coefficients $\langle P_L \rangle$ ($L = 0,1,2,...$) in principal contains the same information as $P(\chi)$. Therefore it is more favourable in some cases to estimate some of the $\langle P_L \rangle$ instead of $P(\chi)$. For some particular problems the information contained in $\langle P_2 \rangle$ and $\langle P_4 \rangle$ is sufficient. In fact several classical methods (such as birefringence or dichroism) for charactetization of orientation yield directly the ensemble averages of $P_2(\cos\theta)$ or $P_4(\cos\theta)$, which corresponds to orientational moments $\langle P_2 \rangle$ and $\langle P_4 \rangle$. The second moment $\langle P_2 \rangle$ is also convenient for roughly characterizing the width and the centre of the ODF.

In the following part two alternative methods for getting some of those coefficients are explained.

- **<u>Moment analysis</u>** this method was shortly introduced also in Chapter 2.4 (See Eq. 2.6). It relies on the fact that the orientation is reflected in the moments M_n of the resonance line.

$$M_n = \int (\omega - \omega_{iso})^n S(\omega) d\omega \tag{4.14}$$

Introducing than in this expression $S(\omega)$ from (4.10) one gets the dependence between the expansion coefficients $\langle P_L \rangle$ and the spectral moments M_n. In this manner via calculating of the spectral moments M_n from experimental data one can reconstruct the ODF $P(\chi)$.

- **<u>Expanding of the NMR spectra into subspectra:</u>**

The conventions expect that $P(\chi) = 1$ for an isotropic distribution. The NMR line shape can conveniently be calculated using this expansion (4.11) by realizing that the spectrum can likewise be written as a superposition of subspectra $S_L(\omega)$:

$$S(\omega)_{\exp} = \sum_{L=0}^{\infty} \langle P_L(\cos\chi) \rangle S_L(\omega) \tag{4.15}$$

Where $S_L(\omega)$ is the following integral over χ of $S(\omega,\chi)$ - the line shape for a fixed χ, multiplied by the Legendre polynom $P_L(\cos\chi)$:

$$S(\omega)_{\exp}=\sum_L\frac{(2L+1)}{8\pi^2}\langle P_L\rangle\underbrace{\int_0^{\pi/2}S(\omega,\chi)P_L(\cos\chi)\sin\chi d\chi}_{S_L(\omega)}\qquad(4.16)$$

Or with other words $S_L(\omega)$ is a $P_L(\cos\chi)$ weighted spectrum. If $S(\omega)$ is a 1D spectrum, the $S_L(\omega)$ are 1D spectra or the sideband intensities I_N . If $S(\omega_1,\omega_2)$ is a 2D MAS spectrum, the $S_L(\omega_1,\omega_2)$ like wise, are 2D spectra and the continuous functions $S(\omega_1,\omega_2)$ and $S_L(\omega_1,\omega_2)$ can be replaced by sideband intensities I_{LMN} , resp. That means

$$\widetilde{I_{MN}}=\sum_L\frac{2L+1}{8\pi^2}\langle P_L\rangle\int_0^{\pi/2}I_{LMN}P_L(\cos\chi)\sin\chi d\chi\,.\qquad(4.17)$$

When one uses the expansion of ODF into Legendre polynomials it is necessary that this expansion is convergent, or at least the expansion coefficients should converge rapidly. This is in most cases fulfilled for moderately ordered systems. For the 2D MAS this approach is applicable in general, MAS mixes contributions from all single crystallite patterns into each sideband. This leads to a destructive interference within the rapidly oscillating high-order Legendre polynomials.

In practice there are two approaches for reconstructing the ODF from the 2D MAS NMR experiment:

- order parameters $\langle P_L\rangle$ can be obtained by solving a linear system of equations connecting experimental sideband intensities $\widetilde{I_{MN}}$ with calculated subspectral intensities I_{LMN} .
- by fitting procedure: the calculated by the (4.16) 2D spectrum can be fitted to the experimental one, with $\langle P_L\rangle$ like a fitting parameters; or assumption of the shape of ODF (for example Gaussian) can be done. Then all $\langle P_L\rangle$ are linearly dependent and by fitting the width of the ODF all coefficients can be obtained automatically (see Chapter 4.5).

In some respects, the moment expansion if applied like a fitting procedure incorporates more *a priori* information than the direct expansion like for instance on the position of the centre of the distribution. Without such information the moment expansion does not produce the desired results. Lets say that we have incorporated the position of the maxima to be at $\chi = 0°$. But if the real peak distribution occurs at $\chi \neq 0°$, say at 50°, the second moment $\langle P_2 \rangle$, weighting $P_2(\cos\chi)$ which has no maximum whatsoever near $\chi = 50°$, does not at all reflect the width of the distribution around this maximum. For all fitting procedures, problems arise at the singularities (sharp maxima) in the spectra: at those points the frequencies are independent of the angle to the first approximation so that the resolution is low. In addition, small mismatches of experimental and theoretically assumed line widths produce large differences between experimental and theoretical spectra.

Therefore we think that the former approach, namely the direct extraction of expansion coefficients is better for analizing the data, compared to the fitting procedure. The detailed form of the system will be shown in the next chapters after introducing the basic computation formulae.

4.5 Calculation of the sideband intensities in systems of perfect order

On the basis of Herzfeld-Berger [68] analysis Harbison *et al.* [71] have derived the formula for the intensity of a N-th order sideband for a specific site **in single crystal**, assuming a shielding tensor diagonal in MF:

$$(I_N)_{SC} = \frac{1}{2\pi} e^{iN\gamma_2} F^*(\alpha_2, \beta_2, \gamma_2, \sigma) \int_0^{2\pi} e^{-iN\vartheta} F(\alpha_2, \beta_2, \vartheta, \sigma) d\vartheta \tag{4.18}$$

$$F(\alpha_2, \beta_2, \vartheta, \sigma) = e^{i[A_2 \sin(2\vartheta) + B_2 \cos(2\vartheta) + A_1 \sin(\vartheta) + B_1 \cos(\vartheta)]} \tag{4.19}$$

$$A_1 = -\frac{2\sqrt{2}\omega_L}{3\omega_R} \sin(\beta_2)\cos(\beta_2)[\cos^2(\alpha_2)(\sigma_{11} - \sigma_{33}) + \sin^2(\alpha_2)(\sigma_{22} - \sigma_{33})] \tag{4.20}$$

$$B_1 = -\frac{2\sqrt{2}\omega_L}{3\omega_R} \sin(\alpha_2)\cos(\alpha_2)\sin(\beta_2)(\sigma_{22} - \sigma_{11}) \tag{4.21}$$

$$A_2 = -\frac{\omega_L}{6\omega_R} \{[\cos^2(\beta_2)\cos^2(\alpha_2) - \sin^2(\alpha_2)](\sigma_{11} - \sigma_{33}) + [\cos^2(\beta_2)\sin^2(\alpha_2) - \cos^2(\alpha_2)](\sigma_{22} - \sigma_{33})\} \tag{4.22}$$

$$B_2 = -\frac{\omega_L}{3\omega_R} \sin(\alpha_2)\cos(\alpha_2)\cos(\beta_2)(\sigma_{22} - \sigma_{11}) \tag{4.23}$$

ϑ is a variable of integration defined by Herzfeld and Berger, and ω_L is the nuclear Larmor frequency.

The 2D spectra correspondent to the rotor-synchronized experiment of Harbison-Vogt-Spiess will appear when arraying the macroscopical angle variable γ_2, which is describing the rotation about the rotor axis and consequently reveals the orientation dependence for all the nuclei in the sample. γ_2 is incremented in equal steps over one rotor period and for every γ_2 a separate FID is stored. The final 2D spectra is obtained by a 2D Fourier transformation of the *ni* FIDs (where *ni* is the number of increments). By Fourier transformation against γ_2 we obtain the 2D sideband intensity in our rotor synchronized experiment:

$$(I_{MN})_{SC} = \frac{1}{4\pi^2}\int_0^{2\pi} e^{i(N-M)\gamma_2} F^*(\alpha_2,\beta_2,\gamma_2,\sigma)\int_0^{2\pi} e^{-iN\vartheta} F(\alpha_2,\beta_2,\vartheta,\sigma)\,d\vartheta\,d\gamma_2 \tag{4.24}$$

This equation assumes that the experiment is begun at the certain moment of the rotor cycle; that is that $\gamma_2 = 0$ when $t_1 = 0$. Because γ_2 is a microscopic variable which we may not be able to determine, and because in a disordered sample there may be a range of γ_2 values, all of which cannot be zero simultaneously, this cannot in general be assured. A Fourier transformation against angle γ can be done, where the new variable γ is introduced like: $\gamma = \omega_R t_1$. The equation will then include a phase factor to allow for the fact that $\gamma_2 \neq 0$ at $t_1 = 0$: $\gamma_{20} = \gamma_2 + \omega_R t_1$

$$I_{MN}(\alpha_2,\beta_2) = \frac{1}{4\pi^2} e^{-iM\gamma_{20}}\int_0^{2\pi} e^{i(N-M)\gamma} F^*(\alpha_2,\beta_2,\gamma_2,\sigma)\int_0^{2\pi} e^{-iN\vartheta} F(\alpha_2,\beta_2,\vartheta,\sigma)\,d\vartheta\,d\gamma_2 \tag{4.25}$$

This equation, derived by Harbison *et al.* gives the 2D sideband intensities for a perfectly ordered system. (α_2, β_2, γ_2) can be replaced by (α_1, β_1, γ_1) if the shielding tensor is diagonal in the rotor frame of reference at the time $t_1 = 0$. In general however, this will not be the case. Since we know (α_2, β_2, γ_2) as a function of the other two sets of Euler angles, we can continue to assume a molecular frame coincident with the principal axis frame (PAS), and replace (α_2, β_2, γ_2) by (α_1, β_1, γ_1) and (φ,χ,ψ). For the coefficients A_1, A_2, B_1, B_2 given with expression (4.20) - (4.23) the diagonal form of the tensor is supposed. For the nondiagonal tensor the coefficients has another form, which can be found in [71].

Finally for a uniaxially ordered system i.e. when the tensors are arranged on a cone around any preferable axis (line director) (4.25) was integrated over α_2, and Harbison *et al.* got:

$$I_{MN}(\beta_2) = \frac{1}{8\pi^3} e^{-iM\gamma_{20}} \int_0^{2\pi} K_{MN}(\alpha_2, \beta_2, \sigma)\, d\alpha_2 \qquad (4.26)$$

where: $$K_{MN}(\alpha_2, \beta_2, \sigma) = \int_0^{2\pi}\int_0^{2\pi} e^{i(N-M)\gamma} e^{-iN\vartheta} F^*(\alpha_2, \beta_2, \gamma, \sigma) F(\alpha_2, \beta_2, \vartheta, \sigma)\, d\gamma\, d\vartheta \qquad (4.27)$$

4.6 Properties of sideband spectra

Harbison *et al.* found the following properties for the sideband intensities:

❶ $\boldsymbol{I_{MN}}$ is real;

❷ $$I_{MN} = I_{-MN-M} \qquad (4.28)$$

❸ $$\sum_{N=-\infty}^{\infty} I_{MN} = 0 \quad M \neq 0 \qquad (4.29)$$

❹ $$\sum_{N=-\infty}^{\infty} I_{0N} = 1 \qquad (4.30)$$

Property ❶ is fulfilled for any kind of order. For a 1D rotor synchronized spectra single crystals give dispersive part of the signal, but in two dimensions these modulations are converted to real intensity. The linear phase correction should be applied in ω_1 direction if the experiment is not started at ($\gamma_2 = 0$). In addition to that I_{0N} must be not only real but positive, and that therefore no negative sidebands will appear in the ($M = 0$) slice.

❷ follows obviously if one sees the relation (4.25) and comes from the both exponential integration terms out of the F-function.

❸ and ❹ were derived from Harbison *et al.* by applying the Bessel addition theorem [72]. These two properties simply mean that the sideband slices contribute no net intensity to the spectrum. The centerband slice is that which would be obtained by random unsynchronized acquisition.

All these properties ❶ - ❹ are important for checking in the next stage if the numeric simulations of the subspectral sidebands I_{LMN} are correct or not, and also for general checking if the pulse sequence gives a proper experimental spectrum.

4.7 Calculation of the subspectra

Inserting Eq. (4.25) for the sideband intensities for a single crystal into Eq. (4.16), which describes the dependence of the experimental line shape (in our case sideband intensities for the 2D rotor-synchronized experiment) and the ODF one gets:

$$I_{LMN} = \frac{(2L+1)}{16\pi^4}\int_0^{\pi}\int_0^{\pi}\int_0^{2\pi} \sin(\beta_2)L(\beta_1,\beta_2,\gamma_2)e^{-iM\gamma_2}K_{MN}(\alpha_2,\beta_2,\sigma)d\gamma_2 d\beta_2 d\alpha_2 \qquad (4.31)$$

This is the experession for the intensity of sideband MN of the L-th polynomial subspectrum $S_L(\omega_1,\omega_2)$ for a given β_1 (see Fig. 4.2).

$$L(\beta_1,\beta_2,\gamma_2) = P_L[\sin(\beta_1)\sin(\beta_2)\cos(\gamma_2)+\cos(\beta_1)\cos(\beta_2)] \qquad (4.32)$$

and $K_{MN}(\alpha_2,\beta_2,\sigma)$ as defined in Eq.(4.27). We can perform the integration over γ_2 (see Fig. 4.2 for the angles) analytically, yielding:

$$I_{LMN} = \begin{cases} \dfrac{(L-|M|)!}{4\pi^3(2L+1)(L+|M|)!}P_L^M(\cos\beta_1)\displaystyle\int_{-1}^{1}\int_0^{2\pi} P_L^M(\cos\beta_2)K_{MN}(\alpha_2,\beta_2,\sigma)d\alpha_2 d(\cos\beta_2) & \mathit{for}\ N \geq |M| \\ 0 & \mathit{for}\ N < |M| \end{cases}$$

$$(4.33)$$

Using this expression we can readily calculate subspectra for tensors of arbitrary size and orientation. Here P_L^M are again the associated Legendre polynomials defined in (4.45). This expression is convergent with increasing of L since there is a destructive interference between high-order Legendre polynomials, which oscillate more rapidly with increasing of L and strongly oscillating expression for the single crystallite pattern (4.25).

The subspectra slices obey the same symmetry rule, as do the slices for single crystallites.

$$I_{LMN} = I_{L,-M,N-M} \tag{4.34}$$

This follows from the fact that the associated Legendre polynomials defined in (4.45) have symmetric property:

$$P_L^M(\cos\beta) = P_L^{-M}(\cos\beta) \tag{4.35}$$

The summed intensity of each subspectral slice is zero, except for the central slice S_0 where it is 1; the P_0 polynomial corresponds to an isotropic powder distribution over a sphere $\{P_0[\cos(\chi)]=1\}$ and therefore I_{00N} is just the Herzfeld and Berger sideband intensity I_N. Since all polynomials are orthogonal to P_0, they can give rise to no net intensity in the sideband spectra. Additionally, because S_0 is simply the MAS spectrum of an isotropic powder, it has no intensity except in the central slice ($I_{LMN} = 0$ for $M \neq 0$); as it was previously mentioned, there are no sidebands in the ω_1 dimension. This is actually a special case of the general rule: $I_{LMN} = 0$ if $L < |M|$ which follows from the fact that $P_L^M[\cos(\beta)]$ in Eq. (4.33) is zero if $L < |M|$ [72 p. 334]. Thus the subspectrum S_2 contains only slices up to $M = \pm 2$, S_4 up to ± 4, and so on. Significant sideband intensity in the ($M = 3$) slice, for example, therefore means that subspectra of order 4 or higher are contributing to the overall spectrum, and that $\langle P_4 \rangle$ must be significant.

It follows that, any spectrum which can be described by an uniaxial distribution of molecules with tensor orientation fixed relative to the molecular axis must correspond to a weighted linear sum of these easily calculable by numeric integration subspectra.

Since the convergence of the expansion in the case of poor orientation, means that high-order polynomials may be ignored, the problem of getting the information about ODF from the experimental data, namely the measured sidebands I_{MN}, can be solved by applying the **multilinear regression procedure and solving the system of linear equations, according to the order parameters** $\langle P_L \rangle$**.**

Effectively, for a spectrum where $\langle P_0 \rangle$ to $\langle P_L \rangle$ are significant, we have to solve the system of linear equations:

$$\begin{aligned}
\widetilde{I_{0N}} - I_{00N} &= I_{20N}\langle P_2 \rangle + I_{40N}\langle P_4 \rangle + I_{60N}\langle P_6 \rangle + \ldots.. \\
\widetilde{I_{\pm 1N}} &= I_{2\pm 1N}\langle P_2 \rangle + I_{4\pm 1N}\langle P_4 \rangle + I_{6\pm 1N}\langle P_6 \rangle + \ldots.. \\
\widetilde{I_{\pm 2N}} &= I_{2\pm 2N}\langle P_2 \rangle + I_{4\pm 2N}\langle P_4 \rangle + I_{6\pm 2N}\langle P_6 \rangle + \ldots.. \\
\widetilde{I_{\pm 3N}} &= \qquad\qquad\;\; + I_{4\pm 3N}\langle P_4 \rangle + I_{6\pm 3N}\langle P_6 \rangle + \ldots.. \\
&\ldots
\end{aligned} \tag{4.36}$$

where $\widetilde{I_{MN}}$ are the sideband intensities obtained from the 2D rotor-synchronized experiment and I_{LMN} are the calculated subspectral sideband intensities as given in Eq. (4.33). As it was defined in Chapter 3.2. index N for experimental sideband corresponds to the index in the ω_2 dimension of the spectra. Varying M from $-M_{max}$ to M_{max} , and also N from $-N_{max}$ to N_{max} we obtain a system with $(2M_{\max}+1)(2N_{\max}+1)$ equations for the unknown $\langle P_L \rangle$. Lets say for example $M_{max} = 2$ (which is in some real cases the largest index in the ω_1 direction for which the sidebands can be obtained for a moderately oriented system with a certain chemical shift) and $N_{max} = 5$, than we obtain 55 equations for system (4.36). Typically only the order parameters $\langle P_L \rangle$ up to $L = 6$ or 8 are significant for the spectra, which means that we get an overestimated system as the number of equation is greater than the number of the unknown variables. If we denote the left-hand side of the system (4.36) like the vector $\mathbf{b} = \{\widetilde{I_{MN}}\}$, and the unknown order parameters like the vector $\mathbf{x} = \{\langle P_L \rangle\}$ and the calculated subspectral sidebands we transform in the matrix $\mathbf{A} = \{I_{LMN}\}$ which has the L/2-colons (as the odd numbered $\langle P_L \rangle$ =0 and L is even by default) and (2M+1)(2N+1)-rows then the system (4.36) can be simply presented in the formalism of linear algebra as:

$$\mathbf{b} = \mathbf{A} \cdot \mathbf{x} \tag{4.37}$$

Instead of exact solution we are searching for that $\mathbf{x}$ which produces a $\mathbf{b}$ vector with least square deviation to the original $\mathbf{b}$, i.e.

$$\|\mathbf{A}\cdot\mathbf{x}-\mathbf{b}\|^2 \rightarrow Min.; \qquad \sum_{i=-N}^{N} \Big(\sum_{j=-M}^{M} a_{ij}x_j - b_i \Big)^2 \rightarrow Min. \tag{4.38}$$

This condition leads to the result, that $\mathbf{x}$ is the solution of the linear system of equations [73]:

$$\mathbf{A}^T \cdot \mathbf{A}\mathbf{x} = \mathbf{A}^T\mathbf{b} \tag{4.39}$$

This is already a linear system against $\mathbf{x}$, which has number of equations equal to the number of the unknown variables, as multiplication of $\mathbf{A}^T \cdot \mathbf{A}$ gives a quadratic matrix with $L/2$ columns and $L/2$ lines. This means that we come to the linear system of $L/2$ equations and $L/2$ variables which is then normally solved. The results are the values for $\langle P_2 \rangle$, $\langle P_4 \rangle$ up to $\langle P_L \rangle$ which make the best fit to the sideband intensities $\widetilde{I_{MN}}$.

The regression method is both intuitive and computationally simple, and is not susceptible to problems of local minima, which beset iterative fitting procedures. It gives more realistic output with comparison to the procedure described in Chapter 3.7. as it does not *a priori* suppose any form of the ODF. In fact in the nature there is no a general rule that the distribution of the orientation should have a Gaussian form. Generally it can be of any other kind. And lets remind again that this method is appropriate for the case of axially symmetric tensor, or where transverse isotropy is known or can be assumed. Only in this case the ODF can be approximated with one-dimensional function. In some cases [69] it is combined with an iterative variation of the tensor orientation to give the best fit.

4.8 Dependence of the sideband intensities on experimentally adjustable parameters

From Eq. (4.24) the values of I_{MN} depend explicitly on some independent parameters, like the tensor elements, rotation frequency ω_R, β_1, etc. Of these, two are under the control of the experiment.

- The reduced shielding anisotropy μ defined [68] as:

$$\mu = \frac{\omega_L}{\omega_R}(\sigma_{33} - \sigma_{11}) \tag{4.40}$$

  can typically be varied over an order of magnitude or more by adjusting ω_R.
- The angle β_1, that is the angle between rotor and director axis, can be set between 0° and 90° during sample preparation.

In order to provide the most informative conditions for the experiment it is necessary to discuss the influence of these parameters on I_{MN}. To allow the influence of other nonadjustable parameters to be discounted, we shall assume here a standard case of an axially symmetric shielding tensor with its unique axis parallel to the director axis.

4.8.1 Effect of reduced shielding anisotropy

For very small chemical shielding tensor anisotropies (this is the case for the aliphatics ^{13}C for instance) μ is small and consequently for a moderate and fast rotation (big ω_R) the I_{MN} will vanish to zero for all $M \neq 0$ and $N \neq 0$, or no sidebands will appear.

From the other side very large anisotropy (up to 150 ppm for carboxylic ^{13}C) and slow rotation makes large μ , which produces too many sidebands, overlapping to each other. The result is a 2D spectrum, which is quite complicated and difficult to analyze.

However, Harbison *et al.* [71] discovered, that in the indirect dimension the sidebands do not decrease so rapidly as in the direct dimension when ω_R is enhanced, i. e. μ is decreased. This gives the work also at small anisotropy resonances with moderate spinning speeds. This effect is explained from Harbison *et al.* with the fact that for certain bands (where $M = N$ or $N = 0$), the sideband intensity goes to zero effectively as a M-th order Bessel function, whereas sidebands in 1D experiment approach zero quadratically in the Bessel function.

In [71] Harbison *et al.* have discussed also the dependence of the absolute intensity of each slice $\sum_{N=-\infty}^{\infty} |I_{MN}|$ on μ . There is a general form of this dependence for every M that $\sum |I_{MN}|$ first increases monotonically from zero, more slowly with higher values of M and eventually oscillates about any asymptote, even for large anisotropies. There is no advantage in increasing μ (by decreasing the rotor speed) beyond the point at which the highest sideband order observed in spectra in ω_1 dimension approaches its asymptote. Therefore for the sake to optimally observe the system it will be desirable in some cases to spin very slowly.

4.8.2 Effect of the angle β_1

The angle β_1 between the director and rotor axis can usually be freely chosen at the time of sample preparation. As it will be shown in some later stage, the dependence of the line intensities $\widetilde{I_{MN}}$ on β_1 is proportional to the associated Legendre polynom $P_L^M(\cos\beta_1)$ (4.33). This means that it is very important how to chose the angle β_1 during sample preparation. It is so that the function $P_L^M(\cos\beta_1)$ and consequently the $\widetilde{I_{MN}}$ is zero when $\beta_1 = 0°$, and it is also zero for odd numbered slices when $\beta_1 = 90°$. A study of the influence of the choice of β_1 on the total intensity has been presented graphically in [71]. The sum of the intensities of the first slice has a fairy broad maximum in the range 30° - 60° when the shielding anisotropy is small. For larger tensors the dependence of slice intensities on β_1 is even less marked, and for the extreme value of $\mu = 25$, the intensity of the low-order slices is an oscillatory plateau between 5° and 85°. For a very wide range of β_1 the choice of this angle does not influence significantly the sensitivity. Individual sidebands however, depend often strongly on β_1 and it is frequently essential that it should be known accurately (to within a few degrees).

For the sake of best sensitivity most frequently chosen is the angle in the middle of the interval from 0° to 90°, namely, near 45°.

4.9 Disorder and sideband intensities treated by Gaussian distribution

The rotor-synchronized 2D MAS NMR technique was proposed by Harbison *et al.* for investigating systems which are disordered to greater or lesser extend, i.e. some liquid crystal partially ordered polymers. To treat theoretically the problem of partial orientation merely needs being able to perform weighted power averages over α_2, β_2 and γ_2 in the expression for the line intensities I_{MN} (4.26) for a perfectly ordered system. There are different types of weighting functions, which can be employed for approximation of ODF. Harbison *et al.* first consider a simple analytical form of the ODF; spherical Gaussian [15]. This weights all orientations of the molecular frame making an angle to the director frame by the probability function $P(\chi)$:

$$P(\chi) = C\exp\left\{\frac{-\sin^2(\chi)}{2\sin^2(\bar{\chi})}\right\} \tag{4.41}$$

C being normalized constant. The probability $P(\chi)$ of finding a given angle is determined by a single parameter $\overline{\chi}$, the root-mean-square angular deviation from the order axis, or with other words one can follow in broad terms the influence of disorder on sideband intensities in two dimensions. The function expressed by (4.41) is then simply added in (4.26) by assuming that the sample consists of a distribution of molecular orientations about the mean order axis, and that within the MF the tensor orientation is fixed. This can be visualized physically as a set of rigid rods with a Gaussian distribution of orientations. The angle of deviation of the MF from the DF, χ, can be expressed in terms of β_1, β_2 and γ_2.

Treating the disorder as a Gaussian distribution is a good illustrative method to show overall effects of disorder, but it is not the optimal way to analyse experimental data. First of all, Gaussian may not adequately fit the spectrum, and more importantly, the non Gaussian nature of real systems may be a considerable part of their interest and may in fact, be strongly indicative of their physical nature.

4.10 Expansion of multidimensional ODF

In Chapter 4.7 all the expressions for the subspectral sidebands I_{LMN} rely on the assumption that ODF is a one dimensional function of the form $U(\cos\chi)$. This assumption is reasonable in the most cases, namely when:

(*) Axialsymmetry: the molecules are distributed uniformly around the order axis:

(**) A molecular frame can be chosen, such that the shielding tensor principal axes are also distributed in an axially symmetric fashion about a unique axis of this frame.

If one of these two conditions is violated a complete description of the ODF demands the other Euler angles to be considered:

- if (*) is violated the ODF should be a function of $V(\varphi,\chi)$;
- if (**) is violated ODF should be of the form $V(\chi,\psi)$;
- if both (*) and (**) are violated than ODF must be described by $W(\varphi,\chi,\psi)$.

This functions are to be expanded into 2D and 3D basis spherical harmonics functions, resp. Most convenient is to represent these functions by Y_{lm} for the 2D or D^{L}_{MN} for the 3D expansion functions respectively.

If the system is transverse isotropic, the ODF can be expanded in terms of Legendre polynomials see Eq. (4.11) in Chapter 4.4. If condition (**) is violated, the system may be uniaxially ordered macroscopically, but it lacks transverse isotropy. The ODF then also depends on the angle φ and may be expressed in terms of Wigner rotation matrices:

$$V(\varphi,\chi)=\sum_{L=0}^{\infty}\sum_{M=-L}^{L}P_{LM0}D^{(L)}_{M0}(\varphi,\chi,0) \tag{4.42}$$

or in terms of spherical harmonics:

$$V(\varphi,\chi)=\sum_{L=0}^{\infty}\sum_{M=-L}^{L}(\frac{2L+1}{4\pi})^{1/2}P_{LM0}Y^{*}_{LM}(\varphi,\chi) \tag{4.43}$$

The Y_{LM} , in turn can be related to the associated Legendre functions:

$$Y_{LM}(\varphi,\chi)=\left[\frac{(2L+1)(L-M)!}{2\pi(L+M)}\right]^{1/2}P^{M}_{L}(\cos\chi)e^{-iM\varphi} \tag{4.44}$$

Here P^{M}_{L} is defined as follows:

$$P^{M}_{L}=(-1)^{M}\sin^{M}(\chi)\frac{d^{M}}{d[\cos(\chi)]^{M}}\{P_{L}[\cos(\chi)]\} \tag{4.45}$$

Finally for general case where condition (*) is also violated, $W(\varphi,\chi,\psi)$ must be expanded in terms of the full set of elements of the Wigner rotation matrices [13]:

$$W(\varphi,\chi,\psi)=\sum_{L=0}^{\infty}\sum_{M=-L}^{L}\sum_{N=-L}^{L}P_{LMN}D^{(L)}_{MN}(\varphi,\chi,\psi) \tag{4.46}$$

And this is the most general case for describing the ODF.

In our case, for the purposes of estimation of the distribution of the distribution of the tensors of interest (namely COO ^{13}C in the 6PBAy substances), axialsymmetry for the carboxylic tensor is assumed. There are no preliminary evidences that transverse isotropy is fulfilled for this tensor but we will use this approximation for the further evaluation of the data, as in the opposite case the analysis of the orientation by a multidimentional ODF is extremely sophisticated.

4.11 Uniaxial system without transverse isotropy

Harbison *et al.* have considered also the calculation of the subspectra for the case where the system exhibits no transverse isotropy. Then the subspectra $S_{LK}(\omega_1,\omega_2)$ should be expanded about the angles χ and φ using the definition of spherical harmonics given in Eq. (4.44). The powder integration for calculating of $K_{MN}(\alpha_2,\beta_2,\sigma)$ can be performed over (φ,χ,ψ) instead of of $(\alpha_2, \beta_2, \gamma_2)$ (it can be done for any complete set of Euler angles). By rotating the shielding tensor by $\mathbf{R}(\varphi,\chi,\psi)$ one can calculate K_{MN} in the same frame (director frame) for each crystallite, avoiding in this way the problem of normalization as the integrating and weighting are done in the same frame of reference. Than the expression for the MN –th sideband of $S_{LK}(\omega_1,\omega_2)$ in a uniaxial system ($\alpha_1=\psi$) is then [71]

$$I_{LKMN}=\frac{1}{8\pi^3}\left\{\frac{(L-|K|)!}{2\pi(2L+1)(L+|K|)!}\right\}^{1/2}\int_0^{\pi}\int_0^{\pi}\int_0^{2\pi}\sin(\chi)Y^*_{LK}(\varphi,\chi)K_{MN}(\alpha_1,\beta_1,\sigma')d\varphi d\chi d\alpha_1 \qquad (4.47)$$

$$\sigma'=\mathbf{R}(\varphi,\chi,0)\sigma\mathbf{R}^{-1}(\varphi,\chi,0) \qquad (4.48)$$

and $K_{MN}(\alpha_1,\beta_1,\boldsymbol{\sigma})$ and $Y_{LK}(\varphi,\chi)$ as already defined. This expression produces similarly to the former case of transverse isotropy (4.33) a basis set of subspectra, which are completely independent of all but measurable parameters (tensor principal value, spinning speed and director orientation). It is computationally simple, but however, requires a considerable amount of time.

The intensities I_{LKMN} follow the same rules as observed for I_{LMN}. There are no odd-numbered subspectra for either K or L and $S_{L,-K}=S_{LK}$. As $|K|$ is always equal to or less than L, the number of subspectra up to a given degree L is limited; there are, however, considerably more than for a simple Legendre polynomial expansion, namely $(L^2+6L+8)/8$ subspectra compared with only $(1+L/2)$. For highly non-symmetric tensor $(\eta\approx 1)$ subspectra of the same degree L but different order K are about equally significant, and therefore experimental data must fit the full set (for example, 10 subspectra for an expansion up to degree 6).

4.12 2D ^{13}C -experiment with 6PBAx liquid crystalline samples

On Fig. 4.4. the experimentally obtained slices with $M = 0, \pm 1, \pm 2, \pm 3, \pm 4$ from the substance 6PBA8 (see Table 3.1) are presented. The rotor synchronized ^{13}C experiment was hold under rotational speed of 5000 Hz, on a 400 MHz (9.4T) Unity Varian NMR spectrometer with the pulse sequence shown on the Fig. 4.1 in a cross-polarization magic-angle spinning (CP-MAS) 7 mm rotor probe. The experimental conditions were as follow: pulse length of the excitation pulse for the proton channel was $pw = 3.8\ \mu s$; acquisition time was $at = 10\ ms$; number of points in the FID was $np = 1216$; the contact time between protons and carbons was $p_2 = 1\ ms$; recycling delay between the last acquisition point and the start of the next excitation pulse was $d_1 = 4\ s$; the number of increments over one rotor period was $ni = 64$, that means for the 5000 Hz or a rotor period of 2 ms, the incrementation step for t_1 (see Fig. 3.1) was 3.125 μs; number of transients of any of the 64 FID-s was $nt = 900$, which means a total acquisition time of 64 hours.

The preparation of the sample was done on the following manner. As the clearing temperature for the 6PBA8 substance was too high for the capability of the 7 mm CP-MAS probe, the rotor was first put in a wide-line probe in a special folder, providing an angle of 45° between the external field (in which the director should be aligned) and the rotor axes. Or it means that the angle β_1 will be 45°. After that the probe was put in the magnet (9.4 T) and the temperature control was switched on. First the sample was heated up until 125 °C, and left for a 20-25 minutes under this temperature to ensure that the substance is fully melted and reaches isotropic phase. After that a slow cooling down was started; the temperature was decreased with a step 1°C/minute from 125°C until 105°C and left for 30 minutes at this temperature. After that the temperature was abruptly set to the measuring temperature (the measurement was done at room temperature) assuring in this way that the macromolecules keep the same orientation as it was at 105° or in the mesophase. The orientation state was like ‘frozen’ in a certain sense. After that immediately the rotor was put into the CP-MAS probe and put back into the magnet and the experiment can run after some routine adjustments of the pulse width, Hartman-Hahn condition, tuning and etc. 64 hours measuring time for acquiring the spectra shown on fig. 3.4. (here not all the 64 slices are shown but only the informative one in which any sidebands from the ω_1 dimension appear) was quite long but nevertheless all the experimental parameters were stable at the whole time of the measurement and the rotational speed was also stable within ± 10 Hz, and the system was in equilibrium – no any reorientation processes take place during the measurement.

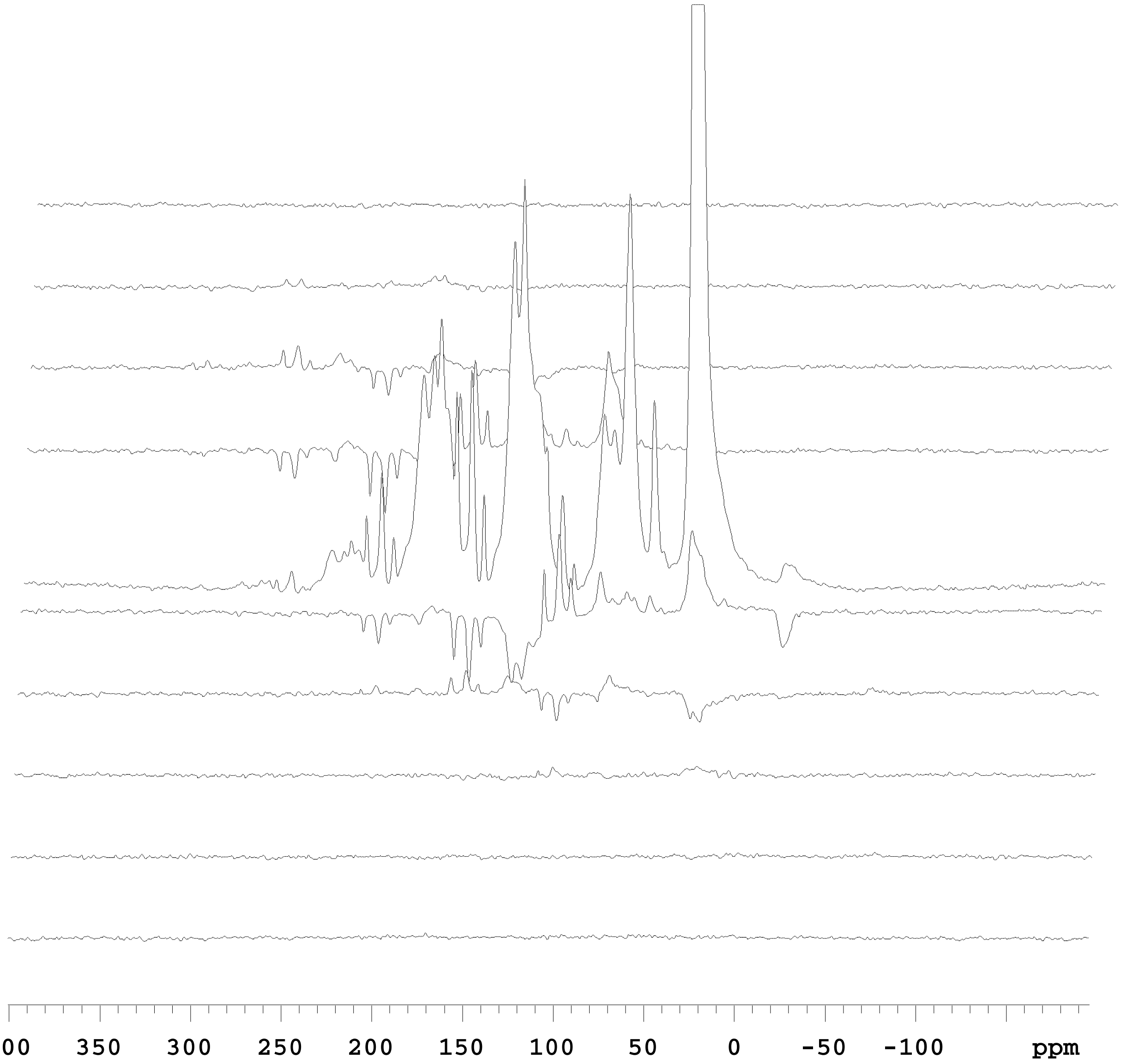

Figure 4. 4 Slices ($M = 0, \pm 1, \pm 2, \pm 3, \pm 4$) from the 2D spectrum obtained by MAS rotor synchronized experiment for 6PBA8 (see Table 3.1). Spinning frequency was $\omega_R = 5000$ Hz.

The data processing of the obtained FID consisted of 2D Fourier transformation (against directly detected dimension t_2 and the incrementation time t_1) and linear phase correction and it was done automatically with the VNMR software. The obtained spectrum was absorptive as it was commented in Chapter 4.5. There is a certain qualitative evidence that the system is oriented, as in the slices neighbouring to the central one ($M = 0$) one can see the presence of sidebands. It is known (see chapter 4.6) that the absence of any sidebands in the slices with M

≠ 0 means either a complete disorder, or that the angle between the director and rotor axis is 0°. Obviously this is not the case.

The next step is to extract the quantitative information contained in this spectrum by the method described in Chapter 4.7. For this we need the following most important things:

- to measure the sideband intensities $\widetilde{I_{MN}}$ from the spectra for the OOC specie contained in the main chain;

- to calculate the subspectral intensities I_{LMN} as defined in (4.33).

(#) is obviously not possible in this case. As the macromolecule contains more than 10 different ^{13}C species the whole spectra is quite complicated because all different ^{13}C sites are concentrated in the interval from the most left-one to the most right one of about 150 ppm on the ω_2 scale on the spectra. The line of interest for us –OOC– comes on the most right hand site (to the higher shielding) and typically such a tensor has a relatively big anisotropy of about 150 ppm [62]. Next to it only several ppm shifted is the resonance line for one of the ^{13}C contained in the aromatic rings, which is also characterized by a large anisotropy. And large anisotropy means many sideband. Even for this high rotational speed of 5000 Hz it is obvious that we can not separate and analyse the lines. There is very strong overlapping of the sidebands from the different species!

Calculation of (##) is the problem of numerical integration but still the knowledge about the chemical shift tensor elements σ_{11}, σ_{22} and σ_{33} is absent. More details about the practical realization of this computation will be given in Chapter 6.

So the problem of overlapping and assigning of the lines makes the task for measuring the $\widetilde{I_{MN}}$ impossible at this stage. Another NMR technique is needed which can solve the problem of the overlapping and makes possible to resolve and assign the lines from the different ^{13}C species.

5 Order resolved sideband separation in magic angle spinning NMR

For complicated systems as it was reported in the previous chapter the gain in resolution by applying the MAS technique is not always sufficient to allow the necessary peak intensities to be measured because of overlap of different sets of sidebands. Several 2D NMR techniques, which separate the isotropic and anisotropic parts of the chemical-shift interaction have been proposed as solutions to this type of problem. Some of these involve the reintroduction of the powder patterns into the first dimension while retaining the high resolution MAS spectrum in the second. This is achieved by changing the speed of the rotor [74, 75] or the orientation of its axis with respect to the static field [76, 77] just before the detection period or by applying pulse trains synchronized with the rotor, which interfere with the formation of rotor echoes during the evolution time [78, 79, 80]. A second class of experiments gives only the central lines in the first dimension and the full sideband spectrum in the second. These involve synchronous sampling in the evolution period with chemical shift scaling [81, 82] to reduce the isotropic shift differences to less than a rotor frequency or the suppression of the sidebands in the first dimension of TOSS [83]. Many of these experiments have associated technical difficulties or are limited in applicability by conditions imposed by rotor frequency.

In this chapter two methods will be presented which can solve the problem of overlapping and overcome the limitations of the other similar techniques.

5.1 Increased resolution in MAS NMR spectra by 2D separation of sideband order (2D ORDER)

The main idea of this technique – to separate isotropic from anisotropic shift - exploits the fact that in MAS sideband spectra the signal intensity appears only at the discrete sideband locations $\omega_{iso} + N\omega_R$, or with other words the sample spinning has periodic effect on the anisotropic part of the chemical shift. During the evolution time t_1 the magnetiazion is stored parallel to the magnetic field, ensuring that during this time there is no modulation of the signal by the isotropic chemical shift. This results in signal in t_1, which is periodic with the rotor frequency and so in the ω_1 dimension the spectrum appears as a set of delta functions. Thus the 2D sideband pattern occupies a grid in which ω_1 is measured in multiples of ω_R and

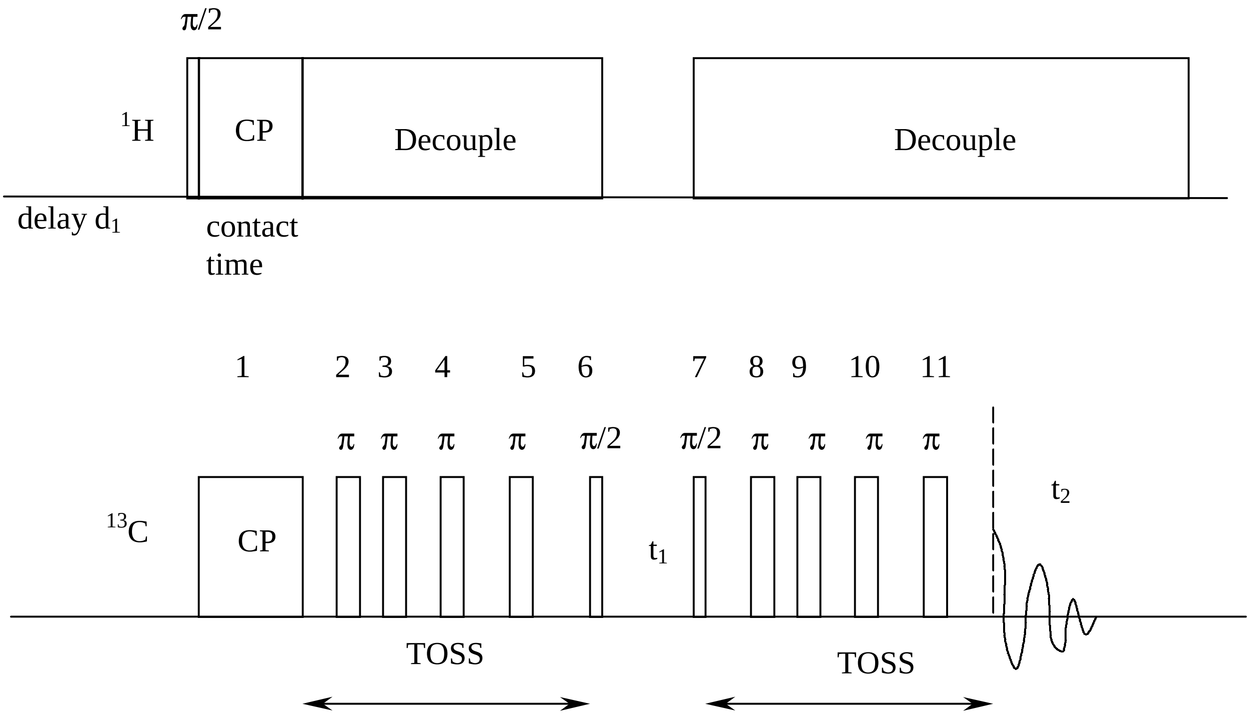

Figure 5.1 Pulse sequence for the 2D ORDER MAS method proposed by De Lacroix *et al.* [84] for separation of the sidebands by their order

the sidebands are separated in this dimension according to their order. It is therefore necessary to sample in t_1 only as many points as there are expected MAS sidebands, in practice 8 or 16 points spanning a single rotor period. Isotropic shifts appear in ω_2 , permitting resolution of different chemical species. The intensities of the observed sidebands correspond to those for MAS and can be used in a Herzfeld-Berger analysis to extract the components of the chemical-shift tensor.

As starting point for the theoretical basis of such experiment should be noted that the FID from a simple MAS experiment for a single crystallite can be written as [51, 85]:

$$s(t) = F^*(\gamma_2)F(\gamma_2 + \omega_R t)e^{i\omega_L \sigma_{iso} t}e^{-t/T_2} \tag{5.1}$$

where σ_{iso} is the isotropic chemical shift, T_2 is the spin-spin relaxation time and the F-function is as defined in Eq. (4.19) and describes the evolution of the anisotropic part of the shift. Coefficients A_1, A_2, B_1, B_2 are as defined in (4.20) – (4.23) and depend on the components of the chemical shift tensor σ_{11} ,σ_{22} ,σ_{33} in the molecular frame and Euler angles $\alpha_2, \beta_2, \gamma_2$ which relate this frame to the rotor frame. Here α_2 represents a rotation about the molecular **z**-axis and the rotor axis. These coefficients are independent of γ_2, the third Euler angle, which represents the rotation about the rotor axis. Thus [84] after Fourier analysis and synthesis give we obtain the formula for the powder average FID *S(t)*:

$$S(t) = \sum_N e^{iN\omega_R} e^{i\omega_L \sigma_{iso} t} e^{-t/T_2} \int_0^{2\pi} d\alpha_2 \int_0^{\pi} \sin\beta_2 d\beta_2 \int_0^{2\pi} F^*(\gamma_2) e^{iN\gamma_2} d\gamma_2 \int_0^{2\pi} F(\vartheta) e^{-iN\vartheta} d\vartheta \qquad (5.2)$$

where the product of the third and forth integral gives (real and positive) intensity of the MAS sideband of order N at $N\omega_R$ from the isotropic shift.

In order to separate the spinning sidebands over two frequency dimensions in the manner described above, an additional time dependence must be introduced but only into the anisotropic part of the chemical of the signal. For a single crystallite the desired 2D FID is:

$$s(t_1, t_2) = F^*(\gamma_2) F(\gamma_2 + \omega_R t_1 + \omega_R t_2) e^{i\omega_L \sigma_{iso} t_2} e^{-t_2/T_2} \qquad (5.3)$$

After doing the Fourier analysis and synthesis and averaging over a powder:

$$S(t_1, t_2) = \sum_N e^{iN\omega_R t_1} e^{iN\omega_R t_2} e^{i\omega_L \sigma_{iso} t_2} e^{-t_2/T_2} \int_0^{2\pi} d\alpha_2 \int_0^{\pi} \sin\beta_2 d\beta_2 \int_0^{2\pi} F^*(\gamma_2) e^{iN\gamma_2} d\gamma_2 \int_0^{2\pi} F(\vartheta) e^{-iN\vartheta} d\vartheta \qquad (5.4)$$

Indeed comparison with Eq. (5.2) shows that this represents a sideband pattern with the correct MAS intensities but spread over the indirect frequency dimension according to sideband order. It should be noted that the t_1 dimension is unaffected by the isotropic shift or spin-spin relaxation as the magnetization is stored along the *z*-axis.

Because TOSS pulse sequence is two times present in the 2D MAS method which is described now, some short summary of the TOSS experiment should be done. Dixon [86] has concluded that if in the MAS signal given with (5.1) one has instead of multiplication of the F-functions $F^*(\gamma_2)F(\gamma_2 + \omega_R t)$ just $F(\gamma_2 + \omega_R t)$, then all the spinning sidebands should be removed. Dixon [86] has introduced sequences of four (or generally $2m+2$) properly spaced

180° pulses that do essentially suppress the factor $F^{*}(\gamma_2)$ in the time signal and thus achieve Total Suppression of Sidebands (TOSS) [87]. The samples must exhibit cylindrical symmetry with respect to the rotor axis; powder samples in particular fulfil this condition. The number of sidebands should not be too large, otherwise small or even negative intensities result in after TOSS. The last pulse should be separated from the start of the acquisition by more than $100\mu s$, so no receiver deadtime problems occur in the signal detection.

The pulse sequence which generates a spectrum which separates the sidebands by their order is shown on Fig. 5.1 [84]. Cross polarization is followed by a TOSS sequence, after which a ^{13}C $\pi/2$ pulse restores one component of the magnetization to the **z**-axis. Both real and imaginary components are required to give the FID of Eq. (5.3); they are obtained from separate experiments and combined in the data processing such that the MAS intensities can be retrieved from the experiment. After the evolution time t_1 , a second ^{13}C $\pi/2$ pulse flips the magnetization back to the transverse plane where it is sampled after application of a second TOSS sequence. So far here it is assumed for the sake of simplicity that the TOSS sequences last for an integral number of rotor periods and the spin-spin relaxation during them can be neglected. If the evolution time between the two ^{13}C $\pi/2$ pulses is simply sandwiched without the two TOSS sequences one might expect that the signal of Eq. (5.3) could be generated in the fashion similar to Fig. 5.1. For an isotropic powder however, the signal so generated is independent of t_1 and thus cannot separate the sidebands into two dimensions.

Applying the described pulse sequence after successive acquisition and 2D Fourier transformation one should obtain a pure absorptive spectrum. The number of slices in ω_1 direction will be equal to the number of increments over the t_1. The zero-th slice ($N = 0$) is similar to the TOSS spectrum, or it contains only the isotropic centerband of each species in the sample. Successive ω_1 traces contain a single MAS sideband for each of the carbon atoms, separated in the 2D spectrum according to their order N, which is indicated on the ω_1 axis in the spectra. There is no overlap between sidebands in the 2D pattern since sidebands of different order appear on different ω_1 traces. Of course such experiment cannot separate two sets of sidebands whose isotropic chemical shifts are the same. The intensities of the sidebands taken from the 2D spectrum can be used to extract the components of the shift tensors by a Herzfeld-Berger analysis since Eq. (5.4) shows that they correspond to the normal MAS intensities.

Equation (5.4) indicates that a projection of the 2D spectrum on the ω_2 axis correspond to the conventional MAS spectrum and this provides a useful means of testing the accuracy of the shift tensor components extracted from such spectra. If there are any intensity variations there are likely to be due to TOSS sequence imperfections which have been well documented elsewhere along with methods for overcoming them [88, 89]. In order to minimize such problems using of the composite ^{13}C π -pulses [92] for both TOSS sequences and a four-step phase cycle based on symmetry considerations [89] was recommended in practice. This basic phase cycle shown in Table 5.1 also serves for removing any magnetization which is not along the ***z***-axis during the evolution time, t_1. The two components necessary for the extraction of MAS intensities from the spectrum are obtained by a $\pi/2$ shift of the phase of the ^{13}C pulse prior to t_1 . This means that for the one dataset one has to use for the first $\pi/2$ pulse the phase given for the pulse 6, and for the other dataset the 6b phase is needed.

Pulse Nr.	Phase cycling															
1	-x	-y	-x	-y												
2	x	y	-x	-y												
3	-x	-y	x	y												
4	y	x	-y	-x												
5	-x	-y	y	x												
6	-y	x	y	-x												
6b	x	y	-x	-y												
7	x	x	x	x	y	y	y	y	-x	-x	-x	-x	-y	-y	-y	-y
8	x	x	x	x	y	y	y	y	-x	-x	-x	-x	-y	-y	-y	-y
9	-x	-x	-x	-x	-y	-y	-y	-y	x	x	x	x	y	y	y	y
10	y	y	y	y	x	x	x	x	-y	-y	-y	-y	-x	-x	-x	-x
11	-y	-y	-y	-y	-x	-x	-x	-x	y	y	y	y	x	x	x	x
Receiver	x	x	x	x	y	y	y	y	-x	-x	-x	-x	-y	-y	-y	-y

Table 5.1

The two datasets recorded in this way are combined to give the signal of Eq. (5.4):

$$S(t_1,t_2) = S_{real}(t_1,t_2) - iS_{imag}(t_1,t_2) \qquad (5.5)$$

This condition comes from the following. The fool 2D FID signal can be represented with the exponent:

$$e^{i(\omega_1 t_1+\omega_2 t_2)} = \cos\omega_1 t_1 \cos\omega_2 t_2 - \sin\omega_1 t_1 \sin\omega_2 t_2 + i(\sin\omega_1 t_1 \cos\omega_2 t_2 + \cos\omega_1 t_1 \sin\omega_2 t_2) \qquad (5.6)$$

In the quadrature detection we have from one dataset:

$$\begin{array}{ll} \cos\omega_1 t_1 \cos\omega_2 t_2; & \cos\omega_1 t_1 \sin\omega_2 t_2 \\ \sin\omega_1 t_1 \cos\omega_2 t_2; & \sin\omega_1 t_1 \sin\omega_2 t_2 \end{array} \qquad (5.7)$$

To get all the information for the signal it is necessary to acquire a second data set, which has this 90° shift of the pulse 6. Thus we get in the other dataset:

$$\begin{array}{ll} -\cos\omega_1 t_1 \sin\omega_2 t_2; & \cos\omega_1 t_1 \cos\omega_2 t_2 \\ -\sin\omega_1 t_1 \sin\omega_2 t_2; & \sin\omega_1 t_1 \cos\omega_2 t_2 \end{array} \qquad (5.8)$$

Thus to obtain the missing parts for (5.6) one has to combine the first row of (5.7) and the secodn row of (5.8). Or this is the detailed form of equation (5.5).

After Fourier transformation over t_2 a standard complex transform performed over the 8 or 16 points in the t_1 domain results in the 2D spectrum and the ω_2 slices can be phased to pure absorption mode. In contrast to some other 2D experiments [83] there is no problem with mixed-phase lineshapes in this experiment despite the fact that the signal is phase modulated since the resulting spectrum has delta functions in ω_1 . The representation of the data in pure absorption mode maximizes the resolving power of the experiment. Any of the possible TOSS timings given in literature [16, 86, 91] may be used, but in general these last for an arbitrary time. In the previous discussion it was assumed that the TOSS sequences last an integral number of rotor periods. Failure to satisfy this condition means that a ω_1 – dependent phase correction must be applied in order to correct for the resulting addition, but constant phase offset.

5.2 Order-resolved sideband separation by MAS 2D-PASS NMR technique

An alternative pulse sequence for separating the sidebands and also for deriving ODF of ordered solids was reported in [92]. The application of this pulse sequence under the conditions of MAS produces an 2D spectra which resolves on different slices the different sidebands, like in the experiment described in the previous chapter. First this method was introduced only for separation of isotropic and anisotropic chemical shift interactions in powder samples [93]. This method was called 2D-PASS (**p**hase **a**djusted **s**pinning **s**idebands) and is based upon the manipulation of the phase of spinning sidebands using sequence of 5 π-pulses. In [92] this method is combined with rotor synchronization to develop a set of methods for ordered samples. The sync-PASS schemes are capable of providing the same information like Titman *et al.*'s 3D experiment [69] but one uses only half of the number of radiofrequency pulses and do not discard signal deliberately.

The scheme starts with conventional cross-polarization from protons to establish enhanced ^{13}C transverse magnetization. This evolves over one rotor period $T = 2\pi/\omega_R$ containing 5 π pulses at especially chosen intervals. The transverse magnetization is allowed to evolve during the time t_2 , with the MAS signal observed in the presence of ^{1}H decoupling.

For the first increment of the 2D experiment ($t_1 = 0$), the five π pulses are evenly spaced (separated by $T/6$) and symmetrically disposed about the centre of the single PASS rotor period. In this configuration, it may be shown that the subsequent MAS FID during t_2 is unaffected by the π pulses during the PASS element apart from relaxation losses and a trivial sign change. In other words, the first increment in the 2D experiment is essentially identical to the unmanipulated MAS signal.

For the subsequent t_1 increments of the 2D scheme, the position of the π pulses are varied along the rather peculiar curves shown besides the pulse sequence. Strong π-pulses are placed at times $\tau_1, \tau_2, \tau_3, \tau_4, \tau_5$ after the beginning of the pulse sequence, i.e. at time points $-T + \tau_1$, $-T + \tau_2$, $-T + \tau_3, -T + \tau_4, -T + \tau_5$. The ^{1}H –spin irradiation is turned off during each π-pulse to avoid loss of magnetization through undesirable Hartmann-Hahn contact.

In the 2D PASS scheme (Fig. 5.2) the timing for the 5 π-pulses are coupled through non-linear equations to a single parameter Θ called the pitch. In general, the pulse sequence timings satisfy the equations:

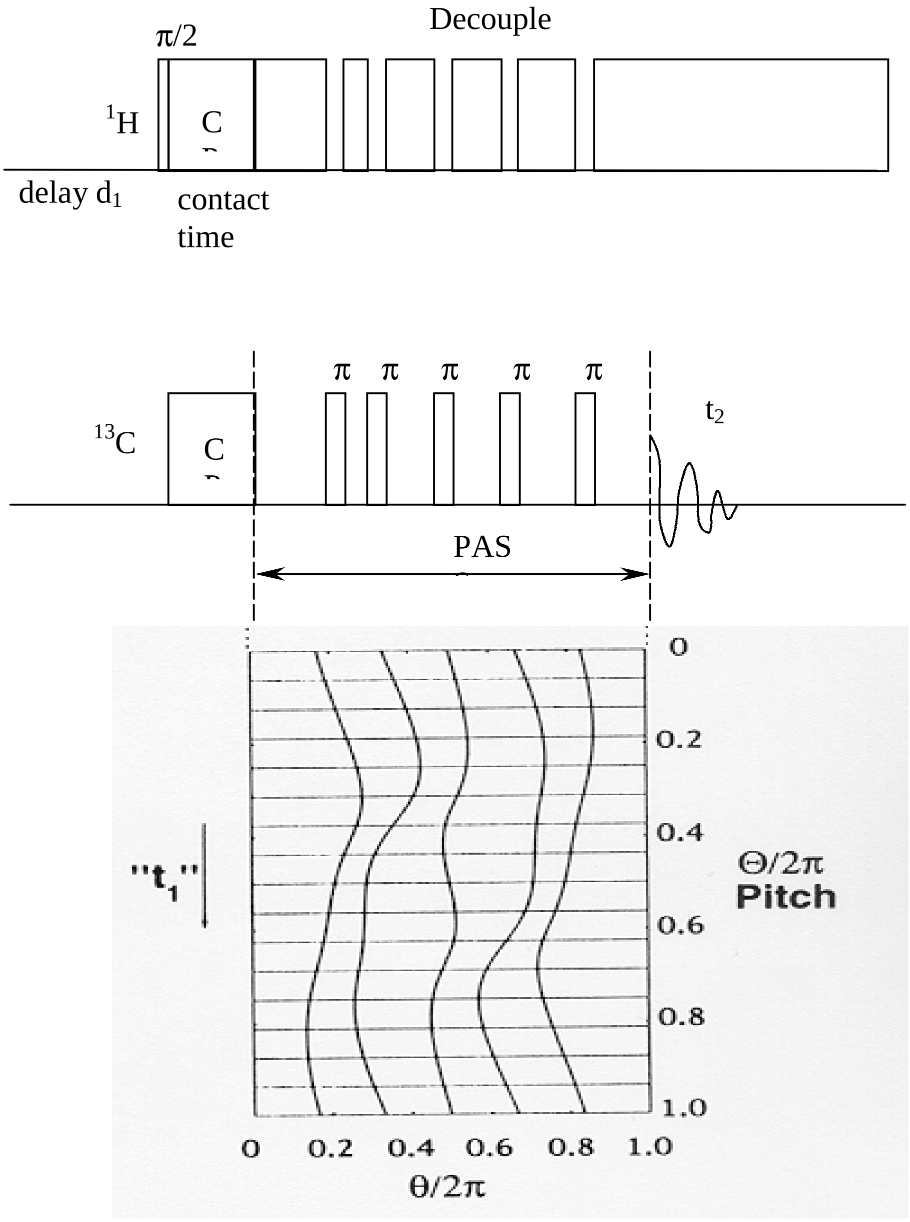

Figure 5.2 Pulse sequence for the 2D PASS experiment. On the horizontal axis is time in fractions of a rotational period. The vertical axis is pitch.

$$2\sum_{q=1}^{5}(-1)^{q}\exp(im\theta_{q})+1+\exp[im(\Theta+\theta_{T})]=0 \tag{5.9}$$

$$2\sum_{q=1}^{5}(-1)^q\theta_q+\theta_T=0 \qquad (5.10)$$

where $\theta_q=\omega_R\tau_q \quad (q=1,....,5)$ and $\theta_T=\omega_R T$, the equations being solved simultaneously for $m=1$ and 2. A table of solution for θ_q at 16 pitches $\Theta=\{0,\ 2\pi/16,\ 4\pi/16,...,\ 30\pi/16\}$ and $\theta_T=2\pi$ is given in Ref. [93]. Sideband separation is achieved by acquiring a 2D data set $s(t_1,t_2)$ in which the pitch Θ is varied according to $\Theta=\omega_R t_1$, and the NMR signals are acquired with respect to time variable t_2. Complex Fourier transformation in both dimensions gives a 2D spectrum in which all spinning sidebands are separated in ω_1 dimension according to their sideband indices M. This means that the sidebands displaced from the isotropic chemical shift frequency by $M\omega_R$, where M is an integer, appear on the same slice parallel to the ω_2 –axis in the 2D spectrum.

In Ref. [93, 92] it is also shown that sideband separation in ordered systems is achieved if the synchronization delay τ_{sync} is also coupled to the pitch Θ. (It should be inserted in the pulse sequence shown on Fig. 5.2 before the cross polarization. This means that for ordered samples experiment should start by waiting until the rotor reaches some defined position of the pen mark on the rotor, and after that waiting a time τ_{sync} before the $\pi/2$ –pulse on the proton channel). A 2D PASS scheme for ordered samples is defined by timings:

$$\theta_{sync}=\omega_R\tau_{sync}=\theta^0_{sync}-\omega_R t_1$$

(5.11)

where θ^0_{sync} is an arbitrary constant. Thus at the same time as the angle Θ defining the pulse sequence timings is incremented, the synchronization delay τ_{sync} is progressively contracted.

Molecular order resolution in this case can be achieved by incorporating a further variation of the synchronization delay. There are two possible variants.

(1) An independent synchronization shift is superimposed on that required to achieve sideband separation, forming a 3D experiment. The synchronization angle variable now reads:

$$\theta_{sync}=\theta^0_{sync}+\omega_R t_1-\omega_R t_2 \qquad (5.12)$$

The NMR signal is acquired with respect to a third time coordinate t_3. Independent incrementation of t_1, t_2, and t_3 complies a three dimensional data matrix $s(t_1,t_2,t_3)$. This data matrix has precisely the same form as that generated by the experiment described by Titman *et al.* [69] but has at least twice the signal-to-noise ratio and is obtained using half the number radiofrequency pulses. Three-dimensional transformation yields a spectrum $S(t_1,t_2,t_3)$ in which all spinning sidebands are separated according to both 'molecular order' and 'sideband index'.

(2) Since the digital resolution required in the 'order' dimension and 'sideband' dimension are usually rather low, it is feasible to avoid the 3D Fourier transform. The synchronization delay is varied as:

$$\theta_{sync} = \theta_{sync}^{0} + \omega_{sync} t_1 - \Theta \tag{5.13}$$

and the pitch variable is:

$$\Theta = \omega_R t_1 \tag{5.14}$$

where ω_{sync} is a small submultiple of ω_R , i.e. $\omega_{sync} = \omega_R / n_{sync}$ and n_{sync} is an integer. In practice, this simply means that τ_{sync} is contracted at a slightly smaller than would be necessary to match the pitch Θ exactly. A complete 2D data set $S(t_1,t_2)$ is compiled by varying t_1 over the range $\{0, 2\pi n_{sync} / \omega_R\}$ in small steps, acquiring the signal with respect to the time coordinate t_2 . Double Fourier transformation of this data set generates a 2D spectrum with the same information content as the 3D spectrum, providing that the sidebands associated with molecular orientational order do not extend beyond indices $\pm(1/2)n_{sync}$. The resulting 2D spectrum can be viewed as a skew projection of the 3D spectrum onto a slightly inclined plane.

This method spreads out namely the peaks in a 2D-PASS spectrum according to the underlying degree of order. The separated sideband manifolds are split further along the ω_1 axis, according to the ODF of individual chemical shift tensor. The frequency displacements are multiples of ω_{sync}. If n_{sync} is larger than the number of order generated sidebands, there is no spectral overlap. This version of the experiment requires the same total number of transients as the 3D experiment of Titman *et al.* [69]. The only advantage is that 3D Fourier transformation, which is unavailable on some instruments is avoided.

Some details of the phase cycle for the π -pulses are now given. Each t_1 increment of the 2D data matrix is the sum of 243 transient signals, multiplied by individual complex factors

$\exp(-i\phi_{data})$ before co-addition. The post-digitalization phase shift ϕ_{data} , the phase ϕ_{CP} of the cross-polarization ^{13}C field, the phases $\phi_1,...,\phi_5$ of the π -pulses , and the reference phase of the receiver ϕ_{rec} , were varied according to the phase cycle:

$$\begin{aligned} \phi_{CP} &= 0 \\ \phi_q &= \frac{2\pi}{3} floor(3^{1-q} m_2) \\ \phi_{data} &= \frac{\pi}{2} m_2 \end{aligned} \tag{5.15}$$

with $q = 1,...,5$ and ϕ_{rec} adjusted to satisfy the equation

$$\phi_{CP} - 2\phi_1 + 2\phi_2 - 2\phi_3 + 2\phi_4 - 2\phi_5 + \phi_{rec} + \phi_{data} = 0 \tag{5.16}$$

Here m_2 is the transient counter, $m_2 = 0, 1, 2, ..., 242$ and $floor(x)$ is defined as the largest integer not greater than x .

5.3 Comparison between both methods

Both of the methods (de Lacroix or also called 2D ORDER [84] and PASS [93]) allow the separation of the sidebands in 2D pattern by their sideband order.

2D ORDER method has the following disadvantages. First, the scheme involves many pulses, at least four π -pulses for each of the two TOSS blocks, plus two $\pi/2$ –pulses. Pulse imperfections cause loss of signal and perturbations of the sidebands amplitude. PASS sequence contains also several π -pulses, but only one 5 π -pulses block is used, so the effects of pulse imperfections are expected to be smaller. Second, for the de 2D ORDER method, the magnetization storage scheme only stores one magnetization component at a time; thus it loses a factor of $\sqrt{2}$ by discarding one magnetization component during t_1 and the results from two separate experiments with different pulse phases must be combined. Actually Varian software permits by extension of the phase table to avoid accumulating of two data sets, but this does not improve the resolution. In contrast to that PASS method keeps the magnetization transverse, avoiding the longitudinal storage step (during t_1 in de 2D ORDER sequence) and retaining thus the full intensity. At the same time by using PASS sequences which have the same overall duration for every transient, the problems of transverse relaxation should be avoided.

5.4 Herzfeld-Berger analysis and chemical shift

Before to present the measured data with the two methods described above and discuss the results one need still some brief introduction about the Herzfeld-Berger method of graphical determination of the principal values of the chemical shift tensor [68]. In its very basic paper in 1980 Herzfeld and Berger have derived a general integral and series expressions for the intensities of the sidebands observed in magic angle spectra of inhomogeneously broadened powder systems with spin $I = 1/2$. The expressions are evaluated for a wide range of shift parameters and the results were used to construct graphical and numerical methods for extracting the principal values of chemical shift tensors from the intensities of just a few sidebands.

The expression for the sideband intensities I_N is very similar to the Eq. (3.17) but still a powder averaging over the Euler angles α_2 and β_2 should be done, or:

$$I_N = \frac{1}{2\pi} e^{iN\gamma_2} F^*(\alpha_2, \beta_2, \gamma_2, \sigma) \int_0^{2\pi} \int_0^{\pi} \int_0^{2\pi} e^{-iN\vartheta} F(\alpha_2, \beta_2, \vartheta, \sigma) d\alpha_2 d(\cos\beta_2) d\vartheta \qquad (5.17)$$

It can be shown that:

$$\sum_{N=-\infty}^{\infty} I_{\mathrm{N}} = 1 \qquad (5.18)$$

and also:

$$\lim_{N \to \pm\infty} I_{\mathrm{N}} = 0 \qquad (5.19)$$

and

$$\lim_{\omega_R \to \pm\infty} I_{\mathrm{N}} = \begin{cases} 1 & for\ N = 0 \\ 0 & for\ N \neq 0 \end{cases} \qquad (5.20)$$

and the last important property of Eq. (5.17) is that it gives a real number.

In order to efficiently cover the full range of values of the chemical shift parameters, it is convenient to choose a different set of variables. Here the following convention is chosen: $\sigma_{33} > \sigma_{22} > \sigma_{11}$. In this case the quantity:

$$\mu = \frac{\omega_L(\sigma_{33} - \sigma_{11})}{\omega_R} \qquad (5.21)$$

is always positive for positive ω_R and the quantity:

$$\rho = \frac{\sigma_{11} + \sigma_{33} - 2\sigma_{22}}{\sigma_{33} - \sigma_{11}} \tag{5.22}$$

has a value between –1 and 1, the extreme values corresponding to axially symmetric tensors. Therefore, it is sufficient to have the calculated line intensities for just the half strip $\mu \geq 0$ and $-1 \leq \rho \leq 1$. Knowing of μ and ρ together with the knowledge of the σ_{iso} which from one side can be exactly fixed from the spectra and from the other side is:

$$\sigma_{iso} = \frac{\sigma_{11} + \sigma_{22} + \sigma_{33}}{3} \tag{5.23}$$

allows us by solving a simple system of 3 equations (5.21), (5.22) and (5.23) to obtain the tensor elements $\sigma_{11}, \sigma_{22}, \sigma_{33}$.The experimental intensities must be normalized in order to compare them directly with the theoretical values. This requires accurate measurements of the concrete I_N line intensity taking the relative value, according to the zero-th order sideband I_0. The contour maps showing the dependence of I_N / I_0 for $N = \pm 1, \pm 2$ are shown on the Fig. 5.3.

The displayed contour plots may be used to graphically obtain μ and ρ from an NMR spectrum (and in our case from the any of the 2D spectra obtained from the method of 2D ORDER or the PASS. If the contours corresponding to the experimentally measured values of $I_{\pm 1} / I_0$ or $I_{\pm 2} / I_0$ are taken, by interpolation, from the appropriate contour maps they will intersect at the corresponding values of μ and ρ. In general, owing to experimental errors and errors in interpolation, the lines will not all intersect at one point and the degree of dispersion gives a measure of the uncertainty in μ and ρ. In addition any pair of contours may intersect more than once and enough contours must be considered in order to determine which intersection corresponds to the true values of μ and ρ. Alternatively some intersection point can be excluded by *a priori* knowledge of the order of magnitude of μ and ρ.

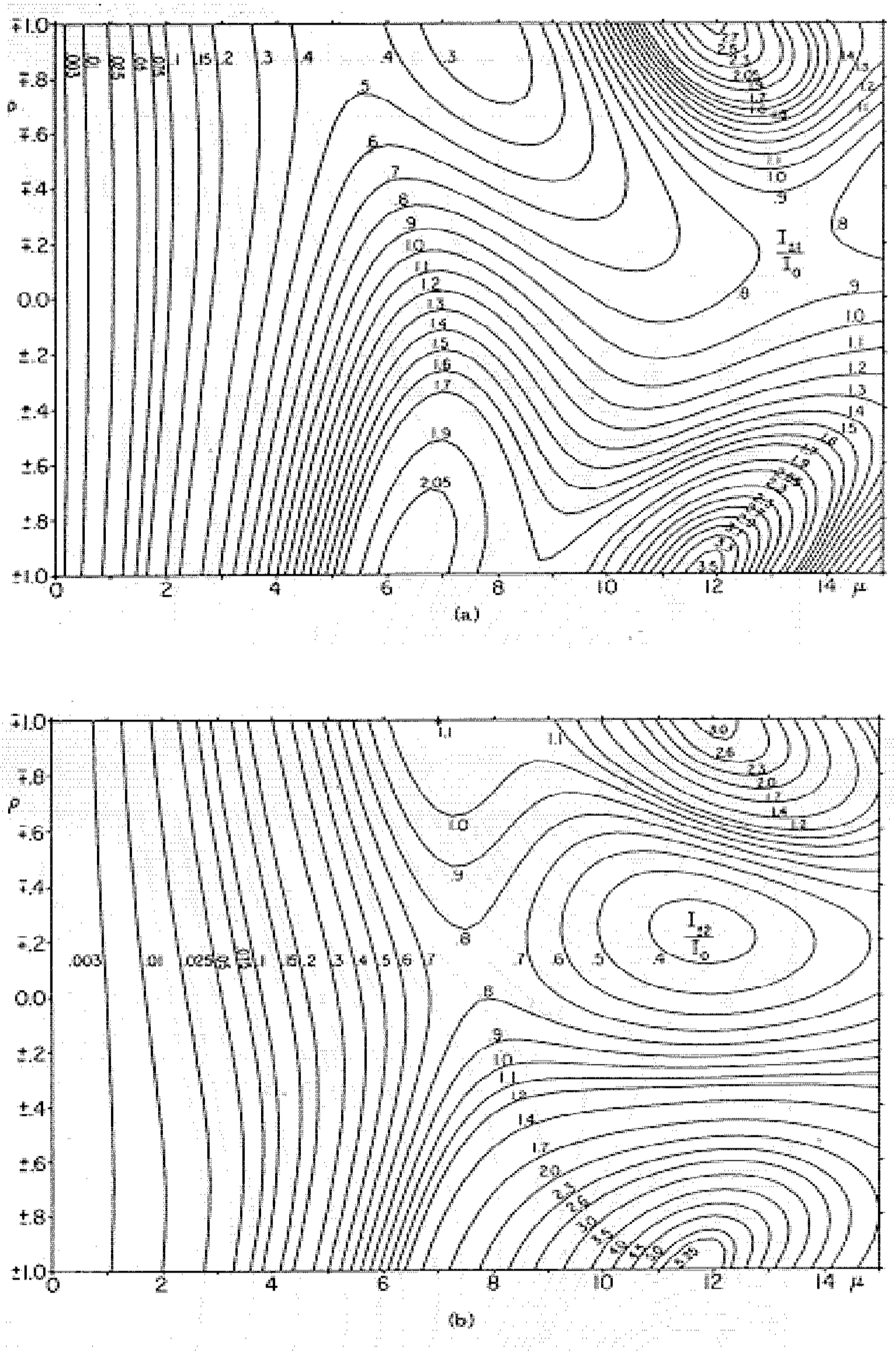

Figure 5. 3 Contour plots of I_N/I_0 for N=±1 (a), ± 2 (b) adopted from [68]

In all this, it is important to be consistent about the sign of ω_R . The convention chosen here implicitly takes ω_R as positive. The sidebands are then passed as $\pm N$ accordingly, to obtain the corresponding values of μ and ρ . The principal values of the chemical shift tensor are then obtained from Eq. (5.21) - (5.23) using the positive values of ω_R . However, it is equally valid to take ω_R as negative. The assignment of the sidebands is then reversed and the sign of ρ obtained is also reversed. However, the principal values of the CS tensor using the negative ω_R are unchanged (although σ_{11} and σ_{33} are interchanged).

μ and ρ may also be obtained numerically by doing a least-square fit of the experimental values of I_N / I_0 . The nearly exact recovery of the single crystal chemical shift values, shown in Ref. [68] indicates the method and makes the graphical analysis and least-square fit procedure equivalent.

5.5 Application of the de 2D ORDER and PASS methods and experiments completed with isotropic samples

Applying any of the not conventional and not every day used techniques requires some special preliminary work like:

- preparation of the pulse sequence for the concrete method which is controlling the automatic process of long acquisition;
- testing of the pulse sequence with the test substance, which has good signal-to-noise ratio and also simple spectra (like dimethyl sulfone – DMS which has only one ^{13}C line and even after 16 scans one can obtain a good ^{13}C signal); testing with the DMS serves also for checking if the pulse sequence works as it is supposed to be and for adjusting of some experimental parameters like the pulse width of the $\pi/2$ pulse and etc.

5.5.1 2D tests with DMS

Dimethyl sulfone - $(CH^*_3)_2SO_2$ - is organic material which has the following properties at room temperature:

- it is isotropic powder;

- all the $^{13}C*$ nuclei in the molecule are charaterized with the same chemical shift tensor elements, or namely, as reported in [94, 95]:

	Temperature, ° C	σ_{iso} , ppm	σ_{11} , ppm	σ_{22} , ppm	σ_{33} , ppm
DMS	22	44	63	63	7
	-248	44	62	62	9

Table 5.2

2D ORDER method:

The source code for the pulse sequence shown on Fig. 5.1 was programmed and compiled with the 'seqgen' shell in the VNMR 6.1 software. As the pulse sequence is quite complicated, and before executing it in practice, one needs usually to test and optimize different parameters, it was programmed in such a manner, that by controlling of different user-defined flags one can 'switch off' and 'switch on' different parts of the sequence. Or it was possible to choose in the same pulse sequence between:

- simple cross polarization and acquisition; this is very convenient for adjusting of the Hartmann-Hahn condition;

- cross polarization + TOSS; this is needed for adjusting the pulse width of the $\pi/2$ –pulse. In this case it is of high importance to adjust very well the exact $\pi/2$ –pulse width (pw), as **the method is very sensitive for any pulse imperfections, and the effectiveness of the application of this method depends very strongly on even very small (in the order of 0.1 μs) misadjustment of the correct $\pi/2$ –pulse width**! An certain adjustment procedure was used before any measurement for determination of the correct $\pi/2$ –pulse width, by varying with the isotropic sample (DMS) the pw in small increment steps and choosing after a certain number of transients which is the pw with the best suppression of side bands.

- CP + TOSS + $\pi/2$ + t_1 +$\pi/2$ + TOSS; or the full sequence shown on Fig. 5.1.

The next important practical problem was the choosing of the proper **TOSS timing intervals** or with other words the relative according to the rotational speed and ω_R time intervals ($\Delta t_1, \Delta t_2, \Delta t_3, \Delta t_4, \Delta t_5$) between the 4 TOSS pulses. In the original paper of de Lacroix [84] it is recommended for the 2D ORDER to use such a combination of ($\Delta t_1, \Delta t_2, \Delta t_3, \Delta t_4, \Delta t_5$) which gives a sum of integer number of rotor period, for example $\sum_{n=1}^{5} t_n = 2T$, where $T = \frac{\omega_R}{2\pi}$. The following two combinations of timing intervals were tried:

	Ref. Nr.	$\triangle t_1 / T$	$\triangle t_2 / T$	$\triangle t_3 / T$	$\triangle t_4 / T$	$\triangle t_5 / T$	$\sum_n \triangle t_n / T$
1.	Dixon [86]	0.1885	0.2297	0.8115	1.7703	2.0000	4
2.	Schmidt-Rohr [16]	0.1885	0.0412	0.5818	0.9588	0.2297	2

Table 5.3

One should keep in mind that for the full length of the pulse sequence this time-length should be taken twice, or the total length of the de 2D ORDER pulse sequence is:

$8T + t_1$ if the Dixon timing is used, and

$4T + t_1$ if the second timing is applied.

And as it was mentioned above t_1 varies in the interval from 0 to one rotor period – T. For testing of the timings the pulse sequence was executed on DMS with its full length, but fixing $t_1 = 0$. This should give a spectrum the same or similar to the simple MAS pattern, because in ideal case when $t_1 = 0$ after acting of all the pulses, if there is no significant relaxation the magnetization vector should be the same like in after normal CP excitation under MAS. It is not realistic to hope that after so many pulses the effect of relaxation should not be significant, and that’s why different timings were tried and compared. Using of the Dixon timing gave quite poor signal (intensities 3 or 4 times less than in the simple MAS 1D) and it turned out that it is not appropriate for further using. The second timing, which was two times shorter gave much better result with DMS. The line-intensities were again reduced compared to the simple MAS taken at the same ω_R but the loosing of the intensity caused of the effect of relaxation was not so strong. And from the other side there is a hardware limitation of the minimal space between the pulses. It has no sense to reduce $\sum_{n=1}^{5} \frac{t_n}{T}$ to less than 2 because than there will appear some additional effect of pulse form imperfections which also has a strong influence on the correct application of the method. So as the optimal compromise between these two conditions the timing from the Schmidt-Rohr [16] was fixed for all the further measurements.

The **phase table** shown on Table 5.1 was included in the program. It reduces strongly the effects of the pulse imperfections and other effects which cause loosing of the intensity. Using of such kind of phasing need an increased **b**lock **s**ize (see ‘bs’ in [96]) of the blocks of data stored in the acquisition processor from 4 (which is normally used in other routine NMR measurements) to 16. And additionally as 2 data sets are acquired, for the correct 2D Fourier transformation one needs a special vector of 8 coefficients to be specified for data processing according to Eq. (5.5). According to the topic ‘wft2d’ in [96] and Eq. (5.5) the following correct combination for the Fourier transformation of the 2D acquired data was derived:

$$wft2d(1, 0, 0, -1, 0, 1, 1, 0) \tag{5.24}$$

Before the 2D transformation, first an simple 1D Fourier transformation is executed and any linear phase correction was added if necessary. The next step - 2D transformation - should give a pure absorption pattern.

PASS method:

For the PASS method a ready pulse sequence was used. It was originally taken from the library of the Varian pulse sequences and modified from Dr. Detlef Reichert, a member of the NMR group of the Fachbereich Physik, Martin-Luther-Universitaet, Halle. It was only necessary to test it, and make some simple adjustments. In this case the block size (bs) was increased to 64 scans.

On Fig. 5.3 the 2D spectra (on the bottom) obtained from DMS with de 2D ORDER pulse sequence is shown. The 2D spectra obtained with PASS from DMS is not shown, as like it should be expected, the pattern looks very similar to the displayed one. Actually the effect on the isotropic samples of the both 2D methods is the same! The result in both cases is a 2D pattern with diagonal structure, and one should get so many diagonals (all parallel to each other), as many isotropic lines are contained in the substance. Along any of the diagonals one sees the corresponding sidebands for the specific line. So for the case of DMS, where only one ^{13}C line appears in the spectra we obtain a simple pattern with only one diagonal. The spectra was measured at 1500 Hz rotational frequency, which for DMS chemical shift anisotropy of 56 ppm (see Table 5.4) provides significant sidebands with order up to ±2. On the same figure (see the top) an 1D MAS spectra of DMS, taken at the same rotational frequency – 1500 Hz is shown. As it was mentioned in the theoretical explanation of the both 2D methods, for the isotropic samples, one should obtain lines with equal intensities like in the normal 1D MAS measurement, taken at the same ω_R . This can be used like a criterion if the method is working properly or not. One has to compare the line intensities of the sidebands of the 1D MAS spectra with the line intensities of the sidebands obtained for the

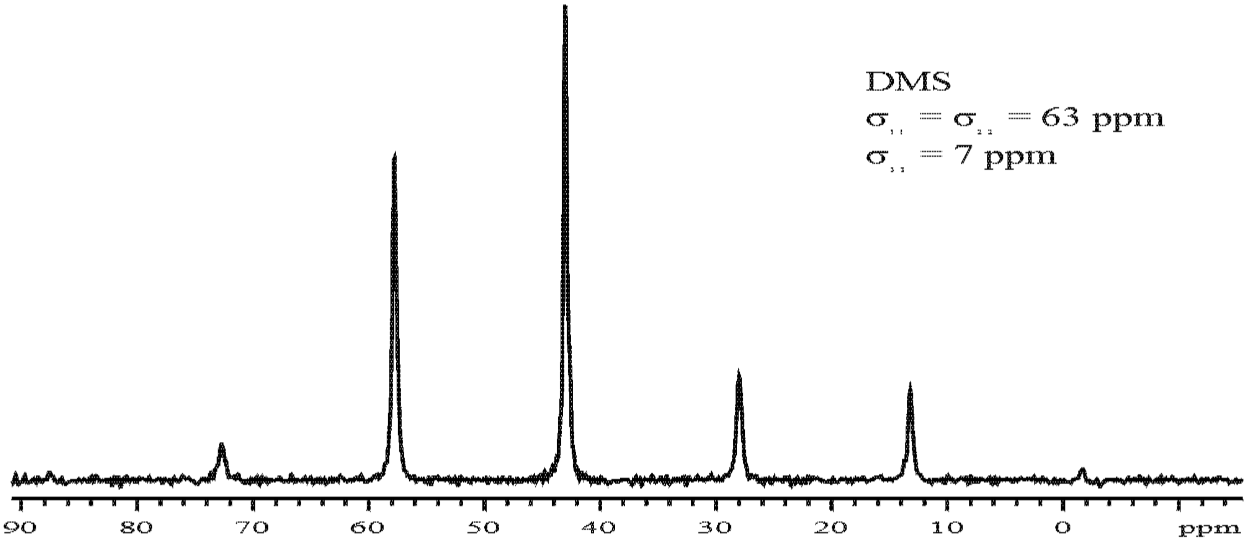

(a), Simple 1D MAS

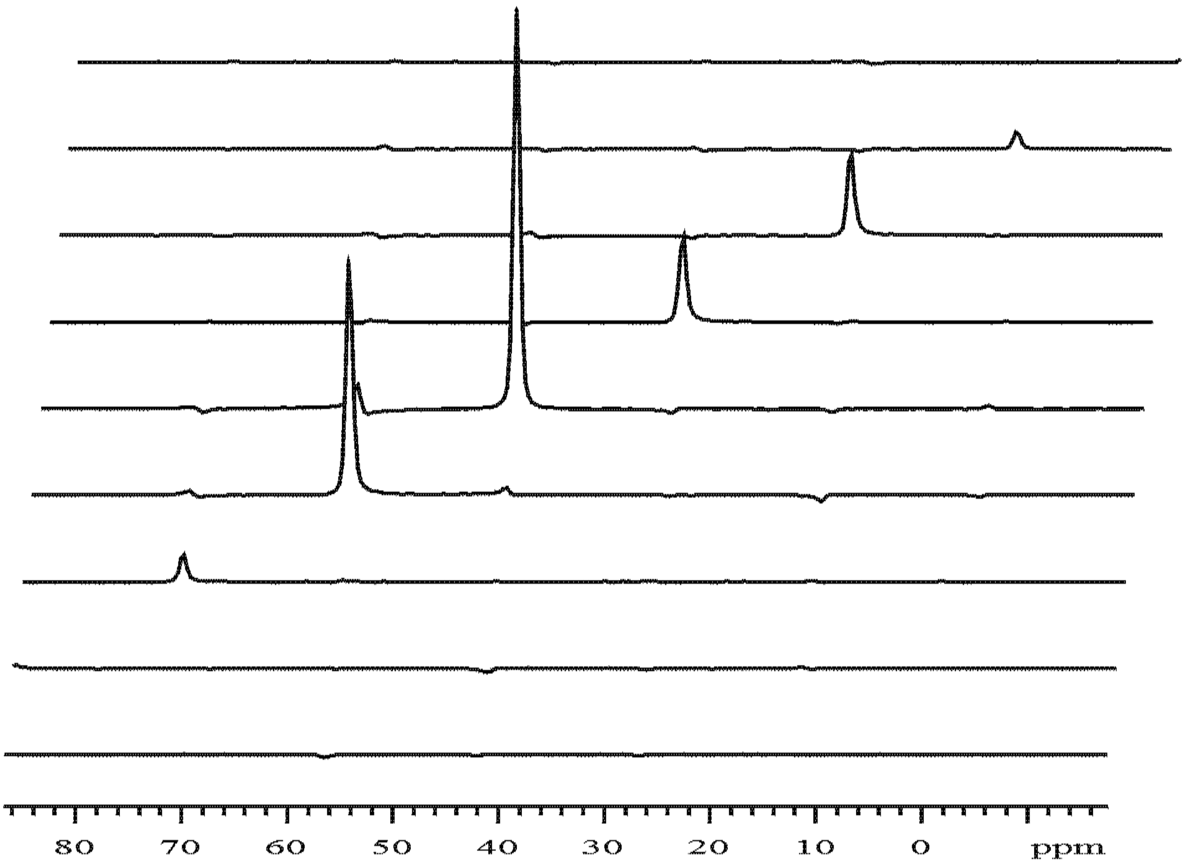

(b), 2D ORDER

Figure 5. 4 a) 1D MAS spectrum taken from DMS at ω_R =1500 Hz; b) 2D ORDER spectrum taken from DMS at ω_R = 1500 Hz.

same chemical site in any of the both 2D Spectra. If there is a significant difference (reducing of the sidebands intensity is expected!) it means that either the effect of the pulse imperfections or the effect of the transversal relaxation of the magnetization because of the too long pulse-sequence length are too strong.

In Table 5.4 the line intensities I_M ($M = 0, \pm 1, \pm 2$) for the DMS sidebands measured at 1500 Hz from the three different experiments (1D MAS, 2D ORDER, PASS) are shown together with simulated data, for the same frequency (details about the simulation are given in the next chapter).

M	I_M, DMS, σ (63, 63, 7) ppm, σ_{iso} = 44 ppm			
	1D MAS	Simulation	2D ORDER	PASS
-2	0.09	0.09	0.08	0.08
-1	0.74	0.74	0.67	0.69
0	1	1	1	1
1	0.31	0.33	0.28	0.29
2	0.25	0.24	0.24	0.24

Table 5.4

The line intensities were measured by using the procedures supported in the Varian-software (VNMR) for volume integration in 1D and 2D spectra. All the sideband intensities are normalized to the volume of the I_0 which is defined to be 1. One can see an excellent agreement between 1D MAS and simulated I_M . The correspondence of the 2D – data for I_M with 1D MAS is also satisfactory and it seems that the effects of losing of the intensity because of any reasons is not so strong. Nevertheless, especially for the $I_{\pm 1}$ the effect of decreasing in the PASS line is smaller than for the de 2D ORDER line. And this can be the effect of significant reducing of the pulse-sequence length for the PASS compared to the de 2D ORDER method (from 11 to 5 pulses!).

5.5.2 2D measurements with liquid crystal substances

Several attempts were done for applying the 2D ORDER on the liquid crystal substances in isotropic phase method introduced in Chapter 3 and Table 3.1. The aim of this measurements was to get the information about the chemical-shift tensor elements for the carboxylic group,

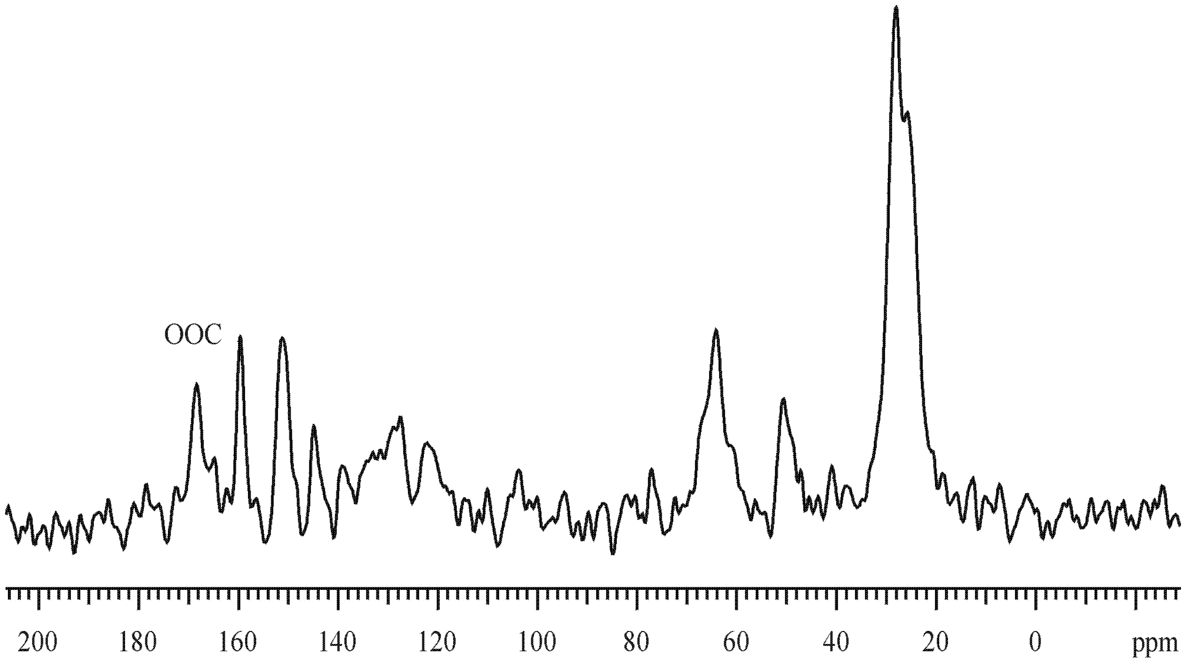

Figure 5. 5 TOSS spectrum taken from 6PBA8 (see Table 3.1) at ω_R = 3000 Hz

located in the main chain of the macromolecule. The TOSS spectra of the substances of this group (6PBAy) look as the spectrum shown on Fig. 5.5. The spectrum was taken at ω_R = 3000 Hz , $\pi/2$ –pulse width was pw = 4.8 μs , number of transients was nt = 1000, total experiment time was 1 hour and 7 minutes. From this spectrum exact position of σ_{iso} for OOC group can be specified and it is:

σ_{iso} = 168.5 ppm

One 2D ORDER spectrum obtained from the 6PBA8 sample, taken at 3000 Hz rotational speed is shown on Fig. 5.6.

This spectra was taken with 16 increments in t_1 dimension, for each of the 16 FID an accumulation of nt = 1600 scans was acquired. The pulse width of the $\pi/2$ – pulse was pw = 3.5 μs and acquisition time at = 5 ms . Knowing that delay of d_1 = 4 s should be established for each scan after the last acquisition point and before starting the next excitation pulse, and that two data sets were acquired it leads to the total acquisition time for this measurement of

57 hours (here not all the 16 slices are shown, but only the interesting one – from slice 5 to 12, or those in which any sidebands appear.

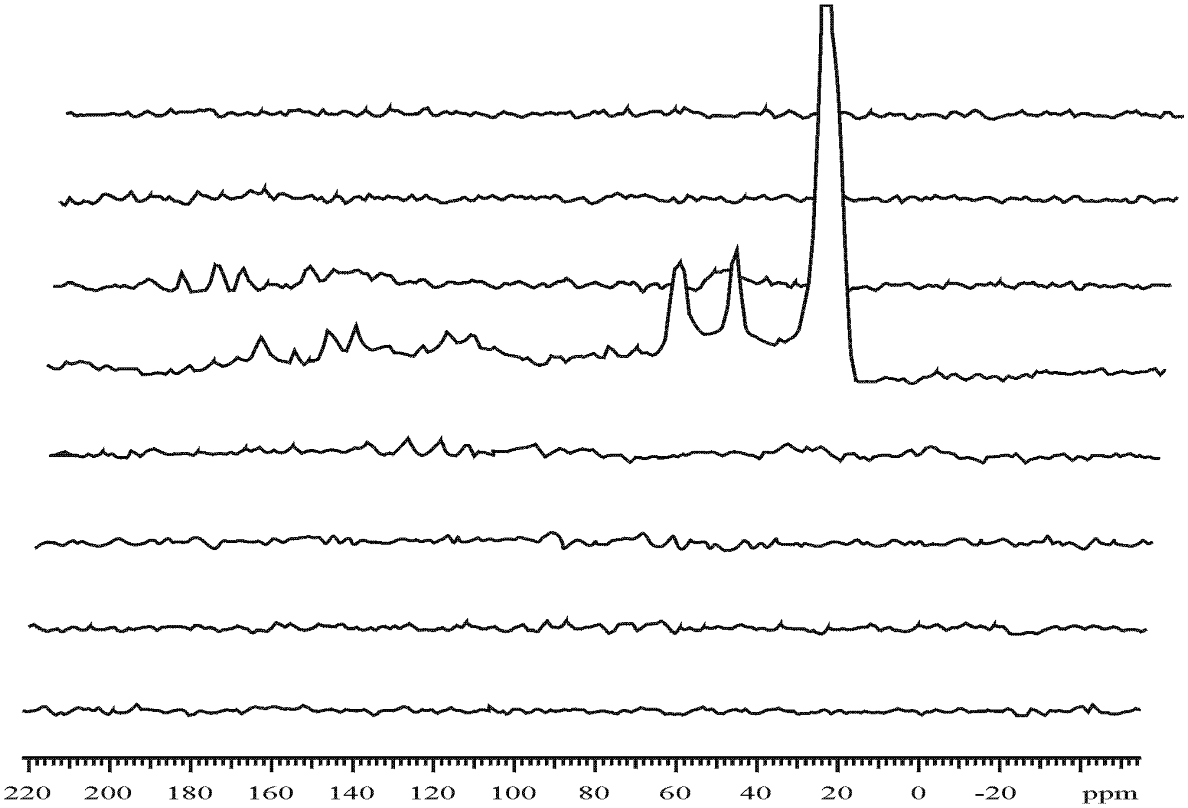

Figure 5. 6 2D ORDER spectrum obtained from the 6PBA8 sample, taken at ω_R = 3000 Hz

The following conclusion can be done from this spectrum. The signal to noise ratio is very bad and it is not senseless to analyze quantitatively such a spectra. Nevertheless, a separation of the sidebands can be seen, along the diagonal which for the carboxylic region is the most left one, the line intensities are comparable to the noise. Obtaining of such a poor signal can be explained most of all by the small volume of the substance which was sampled in the 7mm CP – MAS rotor. The hole mass of the substance available from any of the materials from this group (6PBA8, 6PBA12, 6PBA13) was only 100 mg. It was not an industrially produced material but an product of special synthesis procedure. The spectra obtained with another two samples (6PBA12 and 6PBA13) look similar way. Another feature observed was that the signal was quite less compared to the simple 1D MAS spectra get from the same sample at the same frequency. This can be the effect of significant transverse relaxation during the time of the hole sequence. Different rotational speed were also tried. It is known that the more sidebands one has (smaller ω_R) the more intersection points can be searched for the Herzfeld-

Berger analysis (Fig 5.3). At least one should get an ±1, ±2 sidebands. This is the minimum to find one intersection point. From the other side when trying different ω_R (1500 Hz, 3000 Hz, 4000 Hz) it was observed the slower the rotation is the worse is the signal-to-noise ratio.

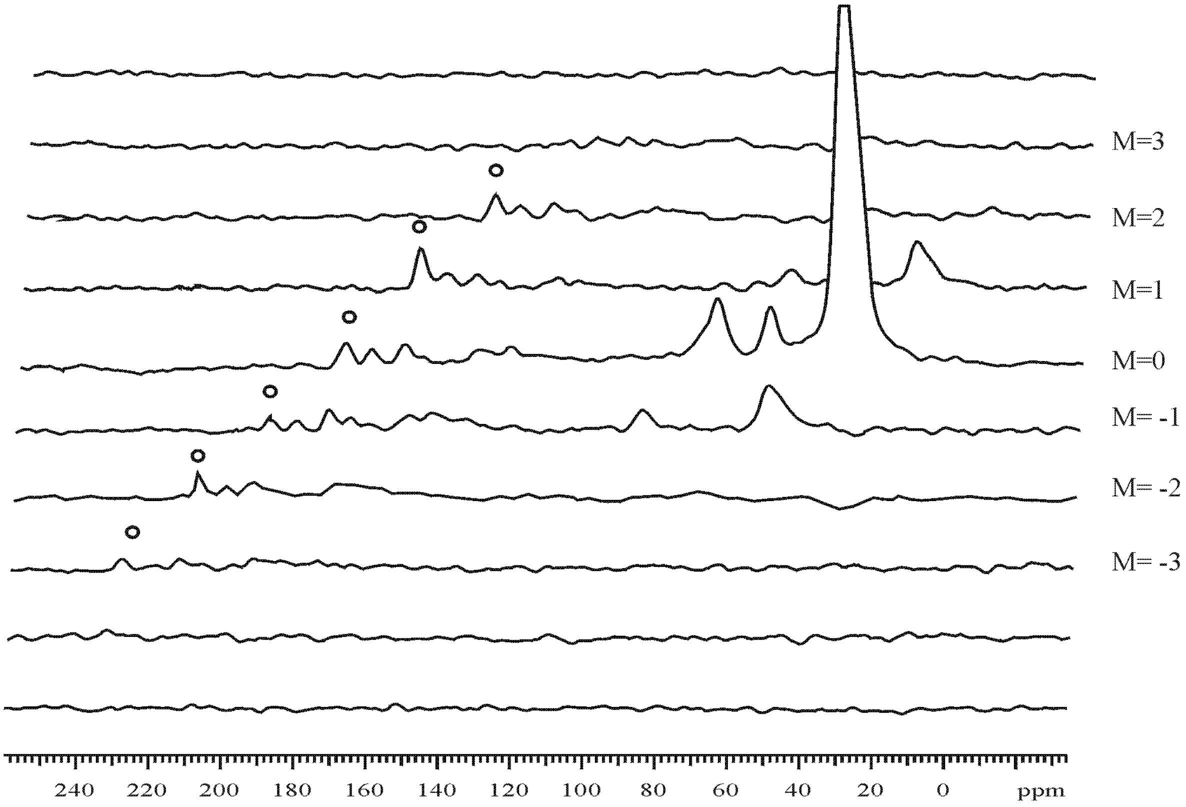

Figure 5.7 PASS spectrum taken from not oriented 6PBA13 at ω_R = 2000 Hz

The PASS method seemed to be more promising for improvement of the resolution as it has the advantage of shorter total pulse length. A spectrum is shown on Fig. 5.7 obtained with PASS, from 6PBA13.

The experimental conditions were as follows: rotational frequency ω_R = 2000 Hz, pulse width for the $\pi/2$ –pulse pw = 3.6 ms , number of transients for each FID nt = 2240 and total acquisition time 40 hours. In increasing of the resolution compared to the former spectra can be observed. The lines of interest for us belonging to the carboxylic group OOC are depicted with a small open circle.

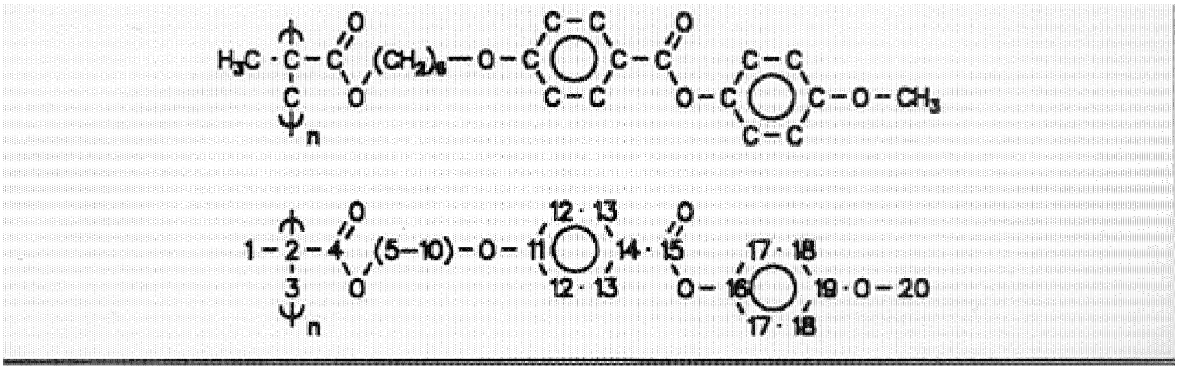

Figure 5.8 Structural formula of the PMA-OCH_3

Similar measurements were also done with PMA-OCH_3. This is a standard polymethacrylate liquid-crystalline side-chain polymer sample (Fig. 5.8). It was investigated by SANS (Chapter 2.1) as well as with ^2H –NMR technique (see Chapter 2.5).

Table 5.5

Nuclear number	σ_{iso} , ppm
1	17.1 ± 1
6-9	27.3 ± 0.3
2	45.2 ± 0.1
20	55.6 ± 0.3
5	65.868
10	68.278
12/18	114.3 ± 0.7
17	122.2 ± 0.6
13	132.5 ± 0.3
19	145.0 ± 0.1
16	157.5 ± 0.6
11	164.2 ± 0.4
4	177.7 ± 0.5

The successive phases are pointed out [33] as follows:

Tg 39° C S_{A1} 75° C N 108° C I

At a lower temperature the smectic phase appears according [33], although it has not always been identified in the literature [29]. The authors from [33] describe an orientation procedure of cooling down the sample with a very slow changing of the temperature, in the external magnetic field, namely 5° C/hour. It takes than about 25 ° C/day. It is possible that only with very slow cooling one can reach an smectic ordering structure. For our measurements only the nematic phase was investigated as it does not take such a long time and Varian spectrometer is always full-time occupied for researches and measurements.

A TOSS ^{13}C spectra of PMA-OCH_3 is shown on Fig. 5.9. The position of any of the ^{13}C nuclei from the structure of this compound can be seen and the assignment of the lines by their σ_{iso} is shown in Table 5.5.

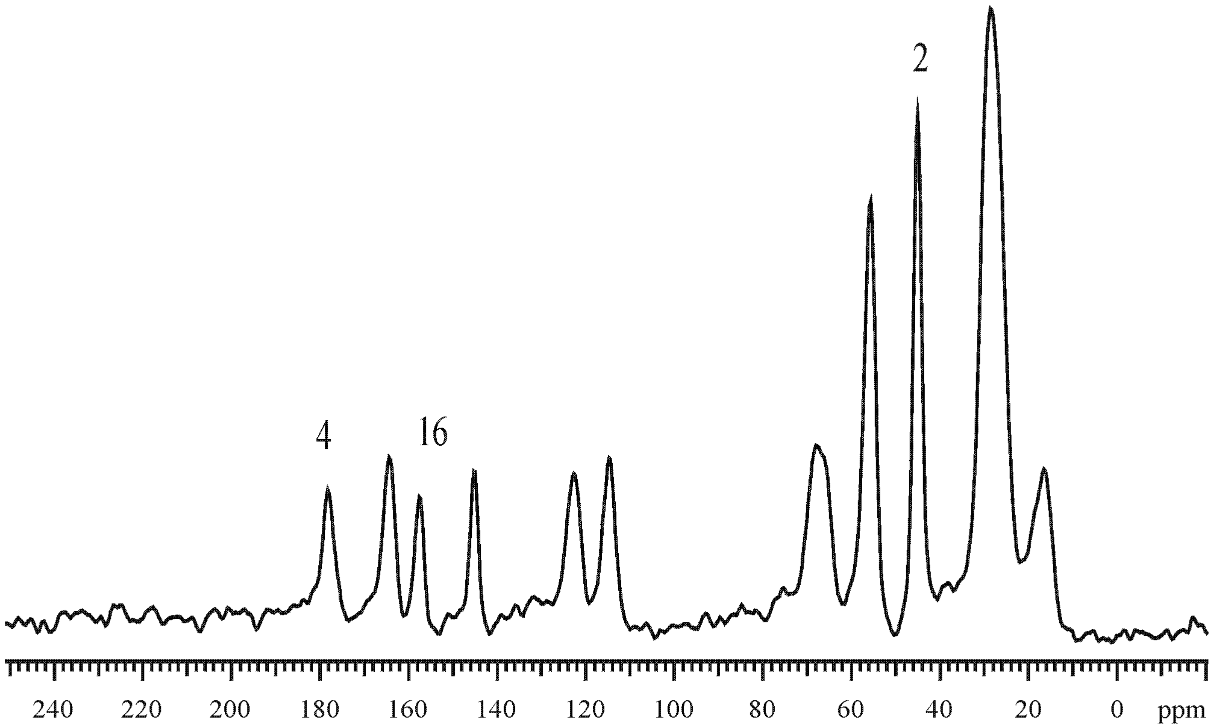

Figure 5.9 TOSS spectrum of PMA-OCH$_3$ measured at ω_R = 3000 Hz. The lines corresponding to the nuclei numbered as 16, 4 and 2 from the strcutural scheme given on Fig. 5.8 and Table 5.5 are pointed out.

This spectrum was measured under 3000 Hz rotational frequency, the pulse width for $\pi/2$ – pulse was pw = $3.7\mu s$, number of accumulations was nt = 300, total measuring time 20 minutes. Much better signal-to-noise ratio in comparison to the 6PBAy samples can be seen! The reason for this is that the mass of the available substance was not so strong limited like in the case of 6PBAy group, and hole the rotor can be filled! On the TOSS spectra one can see only the isotropic lines, and all the sidebands are suppressed. As the main aim of the current study is to estimate the orientation of the main chain the lines 2 and 4 are depicted on the Fig. 5.9 which are of interest for us. Actually only line 2 – the quaternary carbon - is located directly in the main chain. The carboxylic carbon denoted as 4, is attached directly to the main chain quaternary carbon. Typical for carboxylic ^{13}C is a tensor with quite big anisotropy (about 150 ppm) which is very convenient for our purpose as the bigger the anisotropy is, the more sidebands one expects in the 2D rotor-synchronized MAS spectra. A higher number of sidebands are desired for a better analysis. ^{13}C depicted as 16 on Fig. 5.8 and Fig. 5.9 and Table 5.5 belongs to the phenyl ring in the mesogenic unit. It will be used in the next step of evaluation of the orientation by the rotor-synchronized experiment for testing the reasonability of the estimation. As the orientation of the mesogenic unit is well studied from other researches, this ^{13}C can be used like a kind of reference for controlling of the calculations of the spectral moments $\langle P_L \rangle$ give a reasonable output or not.

On Fig 5.10 some slices of the 2D ORDER spectrum obtained from PMA-OCH$_3$ isotropic sample are shown.

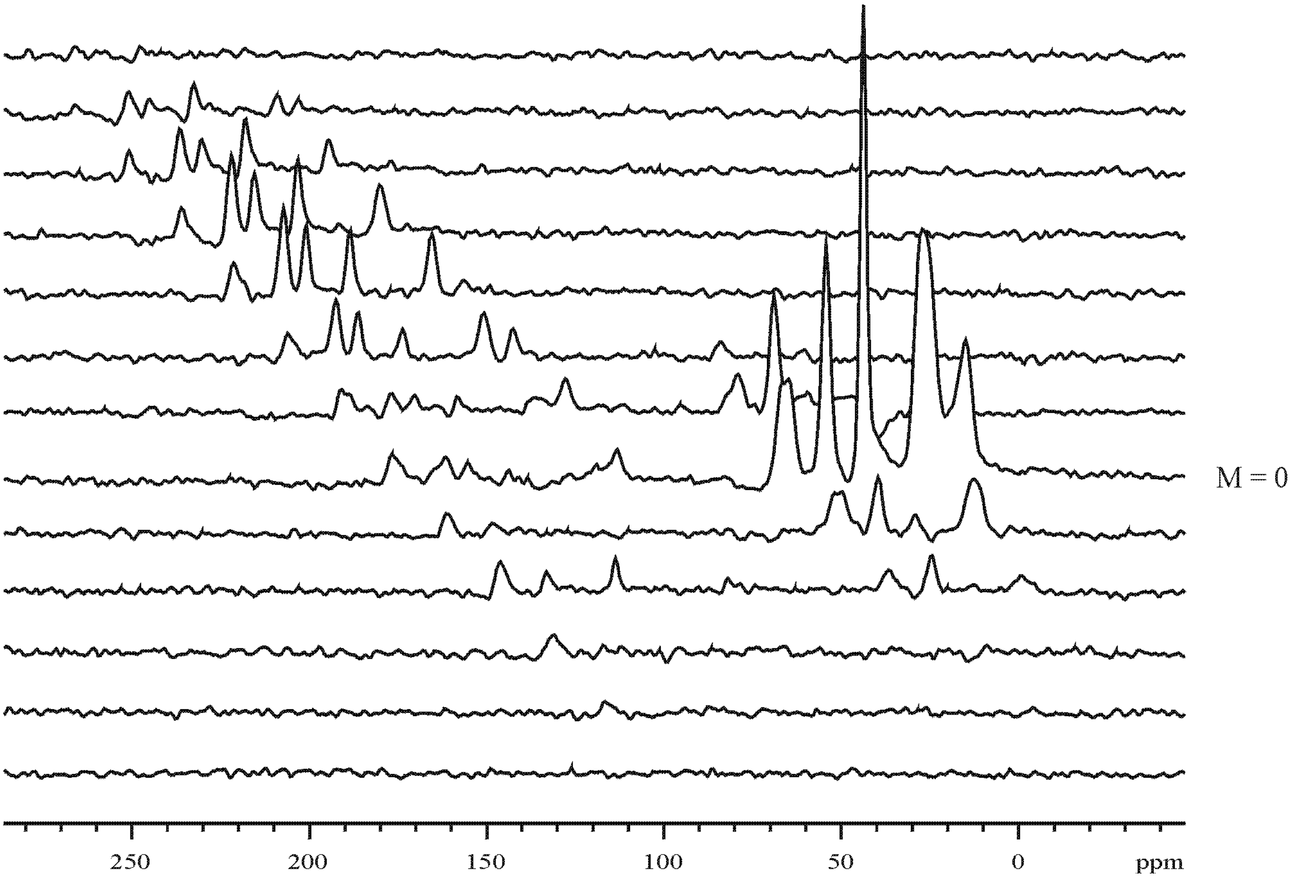

Figure 5.20 2D ORDER spectrum obtained from PMA-OCH$_3$ isotropic sample at ω_R = 1500 Hz

The spectrum was taken under rotation of ω_R = 1500 Hz, number of increments in t_1 dimension was ni = 16, pulse width pw = 3.4 μs , number of transients nt = 1920, and total measuring time of 34 hours. A considerable broadening of the sidebands for the carboxylic ^{13}C can be seen. This is in contradiction to the sidebands of the other types of ^{13}C which show narrow lines (especially for phenyl ^{13}C) and can be interpreted as there are variations in the chemical shift tensor of the hole ensemble of carboxylic nuclei.

The results of the Herzfeld-Berger analysis (see Chapter 5.4 and Fig. 5.3) carried on for the nuclei of interest located in- (6PBAy) or next- (PMA-OCH$_3$) to the main chain the 2D sideband order resolved experiments can be summarized in the following Table 5.6.

Table 5.6

Substance	Group	σ_{iso} , ppm	σ_{11} , ppm	σ_{22} , ppm	σ_{33} , ppm	$\Delta\sigma_{nn}$, ppm
PMA-OCH$_3$	COO	177.7	114	149	269	±4
6PBAy	OOC	168.5	97	183	220	±5

The accuracy of this analysis depends on the two main features: the accuracy of the integration procedure applied to measure the sidebands intensities from the 2D spectra and the standard deviation of this estimation and second factor influencing it is the error introduced by the determination of the intersection point in the graphical method of Herzfeld-Berger analysis. One can see on Fig. 5.3 that some curves with the same relative number of I_N / I_0 cross quite large area of the whole graph (for example curves for 0.4, 0.5 0.8 and 0.9 for Fig. 5.3 (a)) and this introduces a big factor of uncertainty for determination of the crossing point. So the two factors influencing the accuracy can be summarized as follows:

- error of integrating the line intensities and determining I_N / I_0 ;
- error of fixing of the crossing point or determining the μ and ρ .

Considering a correspondent standard deviation for any of these two factors the error of the final values obtained for σ_{11}, $\sigma_{22,}$ σ_{33} was estimated in the last column of Table 5.6.

6 Experimental determination of order parameters $\langle P_L \rangle$

6.1 Rotor synchronized three dimensional NMR method for extraction of orientation distribution function

Titman *et al.* proposed [69] the way of avoiding the problems with overlapping of the lines in the Harbison *et al.* [22, 71] rotor synchronized 2D MAS NMR method, which were also very significant in our measurements and make the analysis of the spectra impossible (see Chapter 4.12 and Fig. 4.4). Recently after the invention of the 2D ORDER [84] method for resolving the sidebands by their order (Fig. 5.1) Titman *et al.* [69] come to the idea to combine this new 2D method together with the experiment of Harbison *et al.* developing in this way a new three dimensional rotor-synchronized MAS experiment for measuring orientational distribution functions. To the 2D ORDER pulse sequence (Fig. 6.1) is added simply an triggering by an

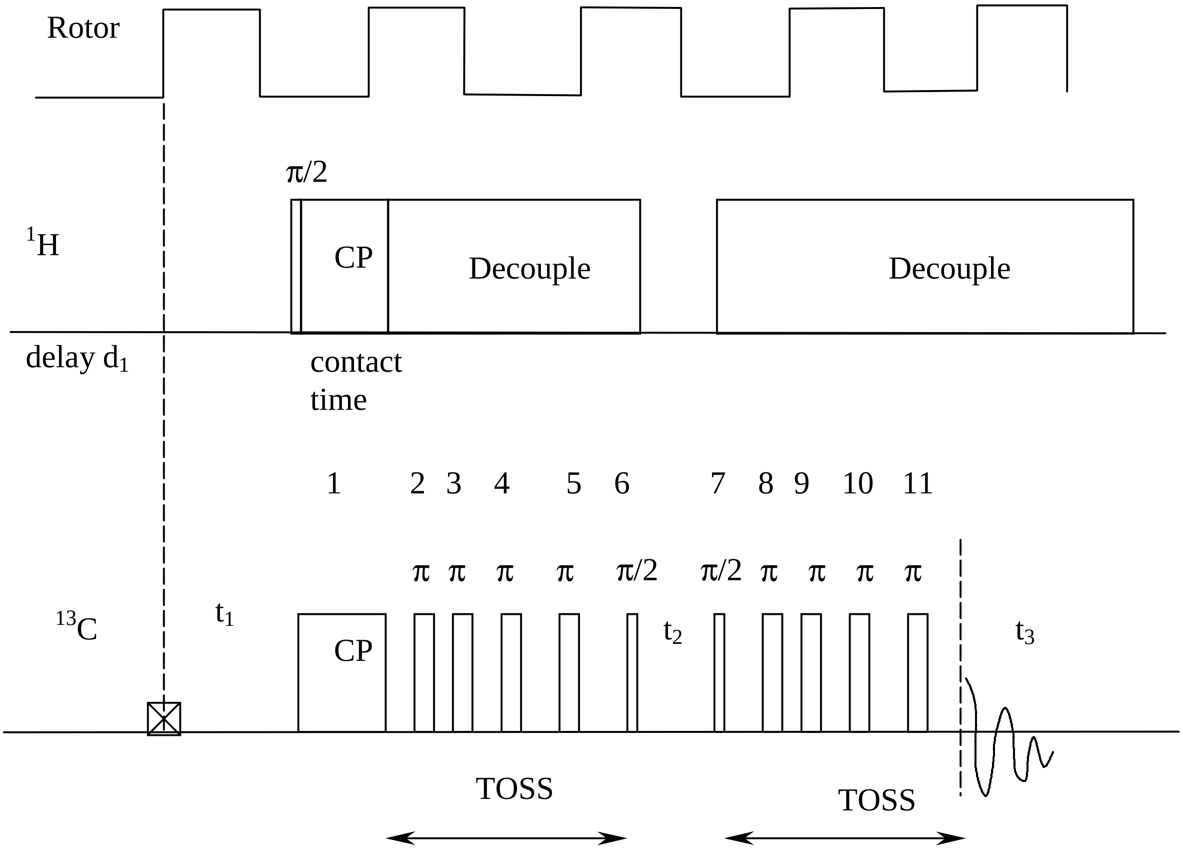

Figure 6.1 Pulse sequence for the 3D ORDER experiment [69].

optical signal reflected from the rotor ensuring in this way that the initial position of the rotor is the same for each acquisition and by incrementation of this synchronization time over one rotor period an orientational distribution information can be revealed from the spectra. Following Hagemeyer *et al.* [85] the MAS FID for single crystallite evolving under the chemical shift Hamiltonian can be written as:

$$s(t) = F^*[\gamma_2 + \varphi(0)]\, F[\gamma_2 + \varphi(t)] e^{i\omega_L \sigma_{iso} t} e^{(-t/T_2)} \qquad (6.1)$$

where the F- functions express the evolution of transverse magnetization under the isotropic part of the chemical shift interaction and is given by Eq. (4.19). The angle $\varphi(t)$ is the azimuthal angle of the rotor towards the laboratory frame and can be written as:

$$\varphi(t) = \varphi_0 + \omega_R t \qquad (6.2)$$

where φ_0 is a constant offset. The first two terms of (6.1) describe the phase of the transverse magnetization from a single crystallite. This consists of a constant term, which depends on the rotor and the crystallite orientation and a time-dependent term, which describes the precession of the transverse magnetization vector under the anisotropic part of the chemical shift Hamiltonian.

In the 2D rotor-synchronized experiment of Harbison *et al.* [71] the consistent phase term is made a function of an evolution period, t_1

$$\varphi_0 = \omega_R t_1 \qquad (6.3)$$

where any extra offset inherent in the method of rotor synchronization has been neglected for simplicity. Thus the 2D MAS FID can be written:

$$s(t_1, t_2) = F^*(\gamma_2 + \omega_R t_1)\, F(\gamma_2 + \omega_R t_1 + \omega_R t_2) e^{i\omega_L \sigma_{iso} t_2} e^{-t_2/T_2} \qquad (6.4)$$

From this expression the formula for line intensities Eq. 4.24 is obtained.

In order to separate overlapping 2D sideband patterns from different isotropic chemical shifts, the original experiment of Harbison *et al.* can be extended to three dimensions. A new evolution time t_2 , is introduced into the experiment during which the magnetization is parallel to the magnetic field, ensuring that during this interval there is no modulation of the signal by the isotropic chemical shift. The MAS rotor continues to spin during t_2 , and an extra phase modulation appears in the second term of Eq. (6.1). However, t_2 is introduced into the pulse sequence in a different way from t_1, such that the constant phase term of Eq. (6.1) is unaffected and there is therefore no special effect on an ordered sample. This means that the information about the order is contained in the ω_1 dimension, while in ω_2 each sideband appears at a frequency $N\omega_R$ corresponding to its offset of from the isotropic shift. Thus each ω_2 row in a given ω_2 -ω_3 plane contains a single sideband from each ^{13}C site. The required 3D FID is:

$$s(t_1,t_2,t_3) = F^*(\gamma_2 + \omega_R t_1)\, F(\gamma_2 + \omega_R t_1 + \omega_R t_2 + \omega_R t_3) e^{i\omega_L \sigma_{iso} t_3} e^{-t_3/T_2} \tag{6.5}$$

where the new detection time is t_3 . It should be noted that the isotropic shift and the spin-spin relaxation do not affect the signal in either t_1 or t_2 . Comparison with (6.4) shows that this represents a sideband pattern in three dimensions with intensities corresponding exactly to the I_{MN} of the original 2D spectrum . Each row of the original 2D spectrum of Harbison *et al.* is spread out into a plane with the coordinates of the Nth sideband in the new dimension given by $\omega_2 = N\omega_R$. Therefore, the projection of the M-th ω_2-ω_3 plane of the 3D spectrum onto ω_3 is exactly equivallent to the Mth row of the 2D one.

It should be noted also that all the properties of the 2D spectra of partially ordered samples mentioned by Harbison *et al.* are retained in some analogous 3D form. All the sidebands intensities in the 3D spectra are real implying that the whole spectrum can be phased to pure absorption, regardless of the degree of order. In addition, the sidebands in the middle plane (M = 0) plane are not only real, but also positive. The 3D spectrum shows the symmetry property:

$$I_{MN} = I_{-M,N-M} \tag{6.6}$$

so that the lines in the M –th plane are identical to those in the -M –th plane, except that their positions are shifted by the value equal to $M\omega_R$ in both the ω_2 and ω_3 dimensions. The sum of all intensities in any plane for which $M \neq 0$ vanishes since:

$$\sum_N I_{MN} = 0, \quad M \neq 0\,. \tag{6.7}$$

Because the isotropic chemical shift and the spin-spin relaxation affects only the t_3 part of Eq. (6.5) the three dimensional signal is cyclic over a single rotor period in both t_1 and t_2 and does not decay. This implies that the signal is completely defined by a minimal number of experiments with the two evolution times incremented in steps equal in length to some convenient fraction (say 1/16th) of the rotor period. After three dimensional Fourier transformation of this cyclic dataset the resonances in the ω_1 and ω_2 dimensions appear only at frequencies which are multiples of ω_R and have delta-function line shapes. All the information in the spectrum is contained in $16\times16\times n$ data points, where n is the number of points acquired in the normal acquisition period t_3 . Two dimensional Fourier transformation of a dataset which is phase modulated in t_1 normally results in undesirable mixed phase line shapes [97], but such problems are not encountered here because the dispersive contribution from a delta function is zero. This means that all the resonances can be phased to pure absorption in ω_3 provided the right combination of phase corrections in all three dimensions can be found. Because of the mixed phase nature of the line shapes in this experiment, phase correction in the ω_1 and ω_2 dimensions affects the phase in ω_3 , so that the appearance of the spectrum in the latter can be used to establish the frequency dependent phase corrections in the former.

6.2 3D ORDER and PASS measurements with oriented liquid crystalline polymers

For starting the practical application of the 3D method described in the previous chapter only a slight modification of the already existed and tested pulse sequence used for 2D ORDER method was necessary, and namely an rotor synchronization and corresponding time delay for it toward the beginning of the pulse program was included. After that a test acquisition was carried out with test substance DMS. First the data were acquired in two datasets, as it was needed (See Eq. (5.5) – (5.8)). The software problem was encountered during 3D transformation of the acquired data via Varian software. For the correct 3D transformation of the FID collected in 2 datasets one has to specify not 8 coefficients, as it was in the case of 2D transformation (see Eq. (5.24) in Chapt. 5.5.1) but a matrix of coefficients, which can have up to 5×8 elements. Following the rules described in the manuals certain table of coefficients was chosen, but the resulted spectra besides the DMS lines which are expected to come on the diagonal of the middle ω_1/ω_3 - plane contained some very strong additional sidebands located out of the diagonal. As the DMS is isotropic material, no any sidebands should appear in the other ω_1/ω_3 -planes with exception of the middle one, or the plane with number N = 0. A little modification of the phase table (Table 5.1) shown in Chapter 5.1 was done, after which it was not necessary to acquire the data in 2 datasets. By circumventing the 2 datasets acquisition a simple execution of the 3D Fourier transformation program without specifying any coefficients gave the correct spectra in which the lines from DMS come in the diagonal of the middle plane N = 0 and the intensities correspond to the normal 1D -MAS sidebands obtained for the same ω_R (see Table 5.4 and Fig. 5.4 in Chapter 5.5.1).

On Fig. 6.2 the some of the planes of 3D measurement taken from PMA-OCH$_3$ frozen in the nematic phase are shown. The orientation procedure was principally the same as described in Chapter 4.12. Phase transition temperatures relevant to the PMA-OCH$_3$ are given in Chapt. 5.5.2. The other experimental conditions are as follows: pulse width pw = 3.6 μs, number of increments in the first indirect t_1 dimension ni = 16, number of increments in the t_2 dimension $ni2$ = 16. It makes a total number of 256 FIDs in the whole dataset. The number of accumulations for every FID was 288 (it should be an integer number multiple of 32, as the block size for storing the data is 32). It gives a total accumulation time for the hole measurement of 83 hours. The resulting spectra contains after 3D transformation 16 planes every one of them consists of 16 slices. Two different presentations of the planes are possible: ω_1/ω_3 or ω_2/ω_3.

All the sidebands presented in the spectra for the carboxylic, phenyl and quaternary carbon nuclei (depicted as respectively 4 16 and 2 on Fig. 5.9 and Table 5.5) were evaluated by a volume integration and the corresponding sidebands intensities $\widetilde{I_{MN}}$ were all normalized to the volume of the $\widetilde{I_{00}}$ for the corresponding nuclei. According to the procedure for getting the order parameters $\langle P_L \rangle$ described in Chapter 4.7. one needs in addition to the measured sidebands intensities the calculated subspectral I_{LMN} values.

The source code for the program for numerical simulation for the formula (4.33) was written in the FORTRAN 77 and a Solaris Sparc 3.0.1 compiler was used for compilation. As the function which should be integrated in Eq. 4.33 is periodic it is proven [73] that in such case the rectangular formula for the integration of polynomials of degree ≤ 3 and for calculation of Fourier coefficients is as good as the Simpson formula. Formula for I_{LMN} includes four integrations, namely over θ γ_2 α_2 and β_2 . In practice because of some symmetry properties the integrations over θ and γ_2 are over an equivalent expressions with the only difference of a sign of one exponent. Thus the number of integrations can be reduced from four to three. As the input data for the calculation the program needs:

- ω_L - Larmor frequency for the resonating nuclei;
- ω_R – rotation frequency;
- σ_{11} σ_{22} σ_{33} – tensor elements for the chemical shift;
- β_1 - the angle between the director and $\boldsymbol{B_0}$

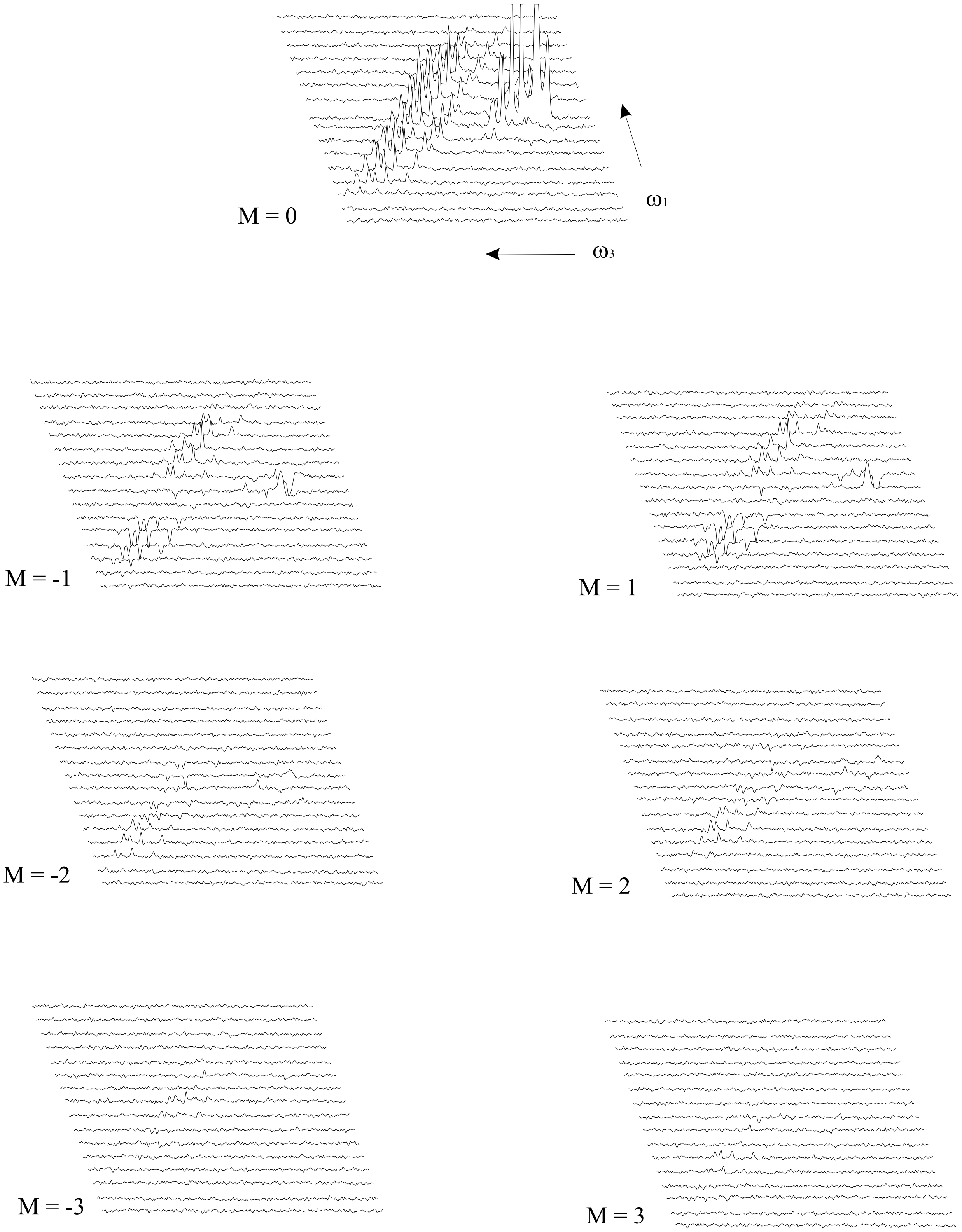

Figure 6.2 ω_1 /ω_3 planes obtained from oriented PMA-OCH$_3$ by 3D ORDER method.

The assigned Legendre polynomials $P_L^M(\cos\beta)$ were included in the program in the form of coefficient matrix for the individual powers of the argument.

For the first test the program was used for calculation of the subspectral sidebands I_{LMN} for DMS with the chemical shift data given in Table 5.2, Chapter 5.5.1. The following facts can be used for checking the correctness of the computation:

- the output for I_{LMN} are pure real numbers; in all cases the imaginary part of I_{LMN} is zero;
- the sum of all sidebands fulfils: $\sum_N I_{LMN} = 0$ for all fixed $M \neq 0$ *and* $L \neq 0$;
- $\sum_N I_{LMN} = 1$ for $M = 0$ *and* $L = 0$;
- the symmetry rule was valid for the calculated I_{LMN} and namely: $I_{L,M,N} = I_{L,-M,N-M}$

This were all the theoretical properties of the 2D sidebands intensities mentioned in Chapter 4.6. And in addition a good agreement with measured intensities from 1D MAS, as well as with 2D ORDER and PASS for ω_R = 1500 Hz can be seen (see Table 5.4).

In Table 6.1 the calculated by the linear regression procedure results for the order parameters $\langle P_L \rangle$ for PMA-OCH$_3$ are shown for three different ^{13}C species: carboxylic COO (attached adjacent to the quaternary ^{13}C from the backbone), quaternary CH$_2$ and phenyl ^{13}C from the aromatic ring of the mesogenic group (nuclei 16, Table 4.5). The same 3D NMR method was used in [69] for investigating of the order of the liquid-crystalline PA-OCH$_3$. This substance has very similar to the PMA-OCH$_3$ structure, with the only difference that near quaternary CH$_2$ carbon the -CH$_3$ group is absent. In Table 6.1 the results for the analysis of Titman *et al.* from [69] about the same groups are also shown for comparison. Nevertheless one should pay attention to the following factors:

- in the work of Titman *et al.* for estimation of the order parameters $\langle P_L \rangle$ the fitting procedure was used, which is in principal quite different than the linear regression procedure used in our case; in the fitting procedure it is preliminary assumed that the ODF has Gaussian form and the calculated order parameters depend only on the width of the Gaussian

PMA-OCH$_3$, ω_R =1.5 kHz, **COO**		**<P$_2$>**	**<P$_4$>**	**<P$_6$>**
σ (114, 150, 269) ppm, **σ_{iso}=177.7ppm**				
number of equations included in regression procedure ***k***	65	0.12	-0.03	0.06
	39	0.13	-0.09	0.05
	39, $\widetilde{I_{MN}} + 0.05\,\widetilde{I_{MN}}$	0.14	-0.08	0.06
	39, $\widetilde{I_{MN}} - 0.05\,\widetilde{I_{MN}}$	0.13	-0.10	0.06
	13	0.20	-0.10	-0.08
	13, $\widetilde{I_{MN}} + 0.05\,\widetilde{I_{MN}}$	0.10	-0.08	-0.13
	13, $\widetilde{I_{MN}} - 0.05\,\widetilde{I_{MN}}$	0.29	-0.12	-0.02
σ* (111, 150, 272) ppm, **σ_{iso}=177.7ppm**				
k = 39		0.14	-0.13	0.04
σ** (117, 150, 266) ppm, **σ_{iso}=177.7ppm**				
k = 39		0.15	0.06	0.10
PA-OCH$_3$ Titman *et al.* [69], COO, σ_{iso}= 175.2ppm, σ (115, 148, 263), ppm				
Gaussian distribution fitting		0.50	0.16	0.07
PMA-OCH$_3$, ω_R =1.5 kHz, **phenyl ^{13}*C* σ_{iso}=157.5ppm**, σ (70, 167, 237), ppm				
k	65	0.68	0.29	0.16
	39	0.69	0.22	0.16
	13	0.75	0.16	-0.26
PA-OCH$_3$ Titman *et al.* [69], phenyl ^{13}*C*, σ_{iso}= 157.9ppm, σ (70, 167, 237), ppm				
Gaussian distribution fitting		0.91	0.76	0.67
PMA-OCH$_3$, ω_R =1.5 kHz, **quaternary ^{13}*C* σ_{iso}=44ppm**, σ (36.5, 43, 52.5), ppm [98]				
k	27	-0.016	0.18	-0.065
	9	-0.091	0.22	-
PA-OCH$_3$ Titman *et al.* [69], quaternary ^{13}*C*, σ_{iso}= 41.5ppm, σ (27, 42, 56), ppm				
Gaussian distribution fitting		< 0.1	< 0.05	-

Table 6.1 Order parameters $\langle P_L \rangle$ for the COO, phenyl and quaternary ^{13}C of PMA-OCH$_3$

distribution; we have preferred the linear regression method for analysis as it is more general without assuming any preliminary presumptions for ODF;

- there is a structural difference between the PMA-OCH$_3$ which was investigated from us and PA-OCH$_3$ investigated in [69].

In the experimental data presented on Fig. 6.2 ω_3 corresponds to the directly detected dimension, the second indirectly detected dimension ω_2 corresponds to molecular order dimension (index M of the sidebands $\widetilde{I_{MN}}$) and ω_1 corresponds to the sideband dimension, or index N of the $\widetilde{I_{MN}}$.

The following comments to the Table 6.1 should be done.

- The influence of the number of equations (See Eq. (4.36)) included in the system was studied as well as the effect of inaccuracy in the experimental estimation of $\widetilde{I_{MN}}$ by the volume integration of the sideband peaks. As it is written in Chapter 4.7. the system (4.36) has an infinite number of equations and an infinite number of unknown variables $\langle P_L \rangle$. Varying M from $-M_{max}$ to M_{max} , and also N from $-N_{max}$ to N_{max} one obtains a system with $(2M_{\max}+1)(2N_{\max}+1)$ equations for the unknown $\langle P_L \rangle$. Here the calculation was done for:

(i) $M_{max} = 2$ and or it means slices from -2 to +2 in ω_1 direction; $N_{max} = 6$ and N from –6 to +6 – total number of $\boldsymbol{k} = 65$ equations for COO and phenyl ^{13}C $\langle P_L \rangle$;

(ii) $M_{max} = 1$ and M from –1 to +1 (slices –1, 0, +1 in ω_2 direction) and $N_{max}= 6$ or N from –6 to +6 – total number of $\boldsymbol{k} = 39$ for COO and phenyl ^{13}C $\langle P_L \rangle$; for quaternary carbon $M_{max} = 1$ and $N_{max}= 4$ or a total number of $\boldsymbol{k} = 27$;

(iii) $M_{max} = 0$ (zero-th slice) and $N_{max}= 6$ or N from –6 to +6 – total number of $\boldsymbol{k} = 13$ equations for COO and phenyl ^{13}C $\langle P_L \rangle$; for quaternary carbon $M_{max} = 0$ and $N_{max}= 4$ or a total number of $\boldsymbol{k} = 9$ equations.

The reason for choosing $M_{max} = 2$ and $N_{max}= 6$ for the case (i) was that in the experiment significant sidebands with indexes up to $\widetilde{I_{\pm 2,\pm 6}}$ were obtained for the chosen rotational speed, especially for the phenyl ^{13}C , whereas for the quaternary carbon which has a very small tensor anisotropy sidebands only up to $\widetilde{I_{1,\pm 3}}$ appear in the spectra.

As it can be seen the reduction of $\boldsymbol{k}$ from (i) to (ii) does not influence so strong the output values for $\langle P_L \rangle$. **The very big difference is there between the $\langle P_L \rangle$ calculated from only the zero-th slice and the more extended systems - case (i) and (ii)**. Therefore it can be concluded that for the more stable solutions of the system (3.46) it is better to include all the slices in which any sidebands $\widetilde{I_{MN}}$ from the nuclei of interest come.

The small variation of the measured sideband intensities in the limits of the maximal error of volume integration ($\widetilde{I_{MN}} \pm 0.05\widetilde{I_{MN}}$) affects very weakly the extended systems but it affects very strongly the $\langle P_L \rangle$ when they are calculated only from the zero-th slice sidebands!

- For checking how strong is the influence of the inaccuracy of determination by Herzfeld-Berger analysis of the tensor elements σ_{11} σ_{22} σ_{33} on the final output of the system for order parameters, $\langle P_L \rangle$ were computed for three different sets of tensor elements σ, σ^*, σ^{**}. σ - corresponds to the tensor resulted from the Herzfeld-Berger analysis done for the COO carbon of PMA-OCH$_3$ as described in Chapter 5.5.2 and the values displayed in Table 5.6. σ^* and σ^{**} are tensors which have elements slightly altered in the limits of the error of the **ó** elements as given in Table 5.6. For the former σ_{11}^* was altered to be $\sigma_{11}^* = \sigma_{11} - \Delta\sigma_{nn}$, and $\sigma_{33}^* = \sigma_{33} + \Delta\sigma_{nn}$, and σ_{22}^* was chosen so that the σ_{iso} should be unchanged. And for the latter $\sigma_{11}^{**} = \sigma_{11} + \Delta\sigma_{nn}$ and $\sigma_{33}^{**} = \sigma_{33} - \Delta\sigma_{nn}$ with $\Delta\sigma_{nn} = 3ppm$ for both cases. The conclusion can be done that the variation of the CS tensor values in such limits affects weakly the results for $\langle P_2 \rangle$.

Fig. 6.3 displays the graphics of ODF $U(\cos\theta)$ for θ between -90° and 90° constructed from the $\langle P_2 \rangle$, $\langle P_4 \rangle$ and $\langle P_6 \rangle$ given in Table 6.1 by:

$$U(\cos\theta) = \sum_{L=0}^{6} \frac{2L+1}{2} \langle P_L \rangle P_L(\cos\theta) \qquad (6.8)$$

The values for $\langle P_L \rangle$ shown in the table correspond to the order parameters connected with ODF of the corresponding tensor (for the COO, phenyl or quaternary ^{13}C) $\langle P_L \rangle_{CS}$ but not to the ODF of the molecular segment $\langle P_L \rangle_S$. In fact we are interested especially in $\langle P_L \rangle_S$ as $\langle P_L \rangle_{CS}$ characterizes the distribution of the electron surrounding near the ^{13}C but not the conformation of the molecular chain. If there it is reasonable to assume transverse isotropy (which means that the molecules are equally distributed around the angle γ, Fig. 2.3) than the following relation is proved [14]:

$$\langle P_L \rangle_{CS} = \langle P_L \rangle_S \cdot P_L(\cos\varepsilon) \qquad (6.9)$$

where ε is the angle between the ***z***-axis of the principal axis system (PAS) and the segment

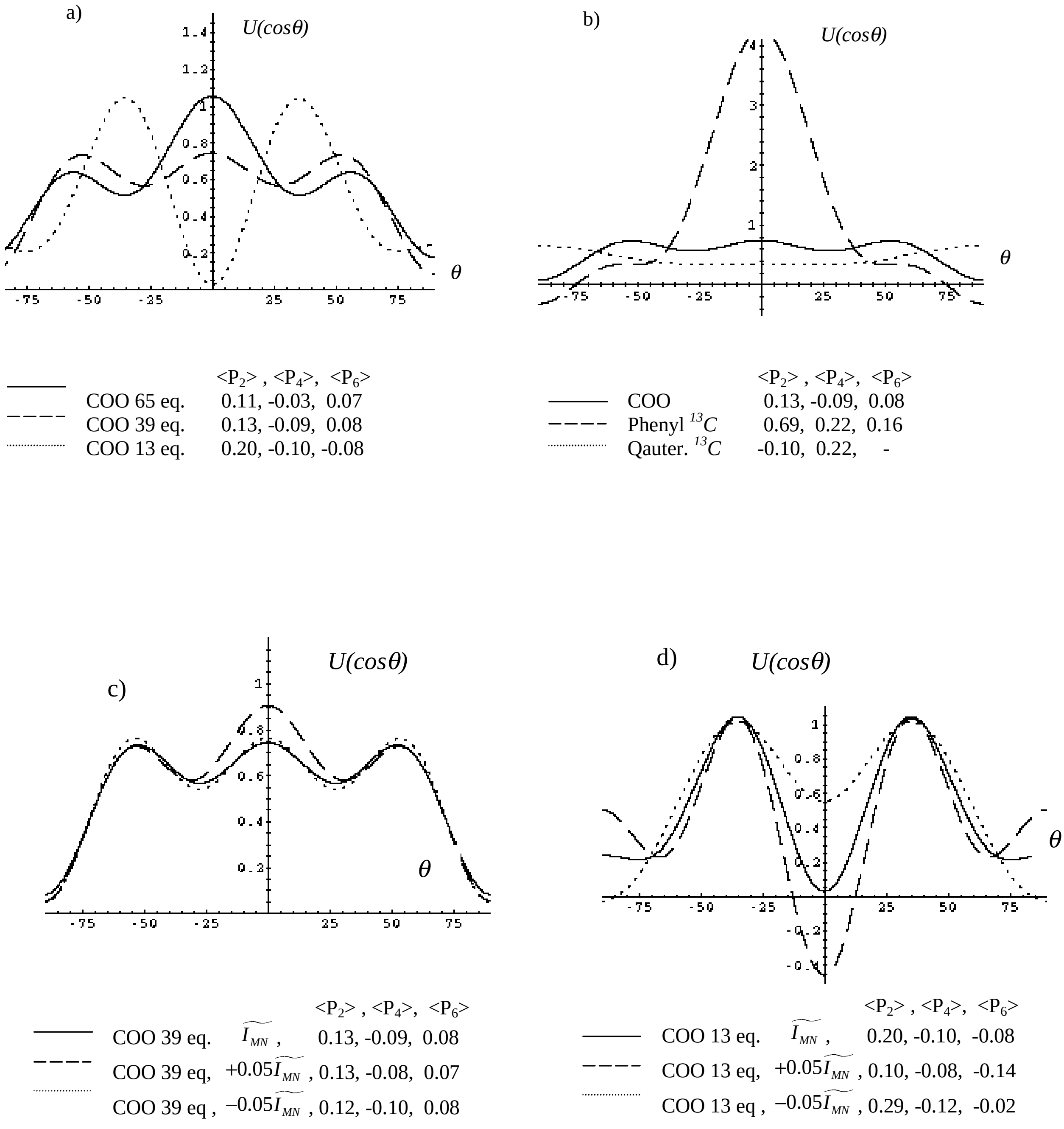

a)

		$\langle P_2\rangle$, $\langle P_4\rangle$, $\langle P_6\rangle$
——	COO 65 eq.	0.11, -0.03, 0.07
– – –	COO 39 eq.	0.13, -0.09, 0.08
········	COO 13 eq.	0.20, -0.10, -0.08

b)

		$\langle P_2\rangle$, $\langle P_4\rangle$, $\langle P_6\rangle$
——	COO	0.13, -0.09, 0.08
– – –	Phenyl ^{13}C	0.69, 0.22, 0.16
········	Qauter. ^{13}C	-0.10, 0.22, -

c)

		$\langle P_2\rangle$, $\langle P_4\rangle$, $\langle P_6\rangle$
——	COO 39 eq. $\widetilde{I_{MN}}$,	0.13, -0.09, 0.08
– – –	COO 39 eq, $+0.05\widetilde{I_{MN}}$,	0.13, -0.08, 0.07
········	COO 39 eq , $-0.05\widetilde{I_{MN}}$,	0.12, -0.10, 0.08

d)

		$\langle P_2\rangle$, $\langle P_4\rangle$, $\langle P_6\rangle$
——	COO 13 eq. $\widetilde{I_{MN}}$,	0.20, -0.10, -0.08
– – –	COO 13 eq, $+0.05\widetilde{I_{MN}}$,	0.10, -0.08, -0.14
········	COO 13 eq , $-0.05\widetilde{I_{MN}}$,	0.29, -0.12, -0.02

Figure 6.3 Graphs of the ODF *U(cosθ)* as reconstructed from $\langle P_L \rangle$ and Eq. (6.8)

axis ***u*** (see Fig. 2.3). For getting the order parameter of the segment $\langle P_L \rangle_S$ the segment axis ***u*** should be defined for any of the monitored groups. For the form of the orientation distribution the determining role has the $\langle P_2 \rangle_S$. The sign of $\langle P_2 \rangle_S$ is determining if the distribution has prolate (when $\langle P_2 \rangle_S > 0$) or oblate (when $\langle P_2 \rangle_S < 0$) shape. The next $\langle P_L \rangle$ for L = 4, 6, 8 … add only some oscillations in the ODF.

- **COO**. Here we define the segment axis ***u*** as the axis connecting two neighbouring ^{13}C . It is well known [51, 101] that the σ_{33} axis of the CS tensor lies perpendicular to the COO plane (Fig. 6.4). But relative to the segment σ_{33} are reported to be parallel to the local chain axis. In this case as can be seen from Fig. 6.4 the angle between σ_{33} and ***u*** ε = 0° . Thus as $P_2(\cos 0°) = 1$, than the Eq. (6.9) simplifies to:

$$\langle P_2 \rangle_{CS} = \langle P_2 \rangle_S \tag{6.10}$$

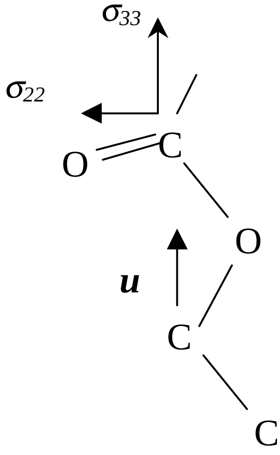

Figure 6.4 Sketch of the –COO part of the PMA-OCH$_3$ macromolecule with relative orientation of the chemical shif tensor elements

As it can be seen from the Table 6.1 the values for $\langle P_2 \rangle_S$ for the COO ^{13}C are positive (indication for the prolate form of the distribution) and in the interval from 0.12 to 0.29 which is indication for a relatively weak orientation of this part of the macromolecule. In this case we can relay on the assumption for the transverse isotropy, as it is quite unexpected that when there is such weak orientation there should be a strong anisotropy in the distribution of the orientations around the angle γ (See Fig. 2.3).

In comparison to the results obtained from Titman *et al.* [69] we can see quite big difference for $\langle P_2 \rangle_S$ for COO. They report $\langle P_2 \rangle_S$ = 0.50 whereas we get depending on the number of equations between 0.11 and 0.2. This difference can be explained with the following possible reasons:

- there is a difference in the structure of the substance; Titman *et al.* have studied PA-OCH$_3$ which is missing the CH$_3$ group attached to the main chain quaternary ^{13}C (see ^{13}C numbered as 1 in Fig. 5.8 and Table 5.5);
- it is possible that the orientation procedure applied from Titman *et al.* was different and the sample was more oriented;
- in the work of Titman *et al.* there was another procedure applied for extracting the order parameters $\langle P_L \rangle$. It was not like in our case the direct extraction by solving the system (4.36), but they have used the fitting procedure shortly explained in Chapter 4.4.

- **substituted phenyl ^{13}C :**(see ^{13}C numbered as 16 in Fig. 5.8 and Table 5.5); If we define segment axis ***u*** as to be along the line connecting the two substituted ^{13}C in the aromatic ring (namely ^{13}C 16 and 19 in Fig. 5.8) then we have similar mutual orientation between σ_{33} axis and ***u*** axis as in the case of COO[51, 99]. Angle $\varepsilon = 0°$ and Eq. (6.10) holds. As it can be expected for the mesogenic units and seen from Fig. 6.3 b) the has a pronounced maximum at $\theta = 0°$.
- **quaternary ^{13}C :** for this nuclei there is no clear evidence in the literature about how the tensor of this ^{13}C is oriented with respect to the local chain. Such information is not easy to obtain even with more complicated 2D methods as the CS anisotropy for this ^{13}C is quite small (only 16 ppm!). Therefore we can not make any conclusion about the $\langle P_2 \rangle_S$ of the segment. The values which we obtain for $\langle P_2 \rangle_{CS}$ (see Table 6.1) are extremely low (below 0.1) and negative, but nevertheless the presence of sidebands for this quaternary line in the 3D spectrum is an indication of the orientation for this part of the molecule as well. The form of the distribution of the main chain segment remains an open question. There was a former study by Böffel *et al.* [23] by ^2H NMR on the same substance, which proved that there is a perpendicular orientation between the main chain and the director.

It should be reminded that for the current analysis of the ODF of all the groups the transverse anisotropy is assumed. For evaluating how adequate is this assumption one can try to

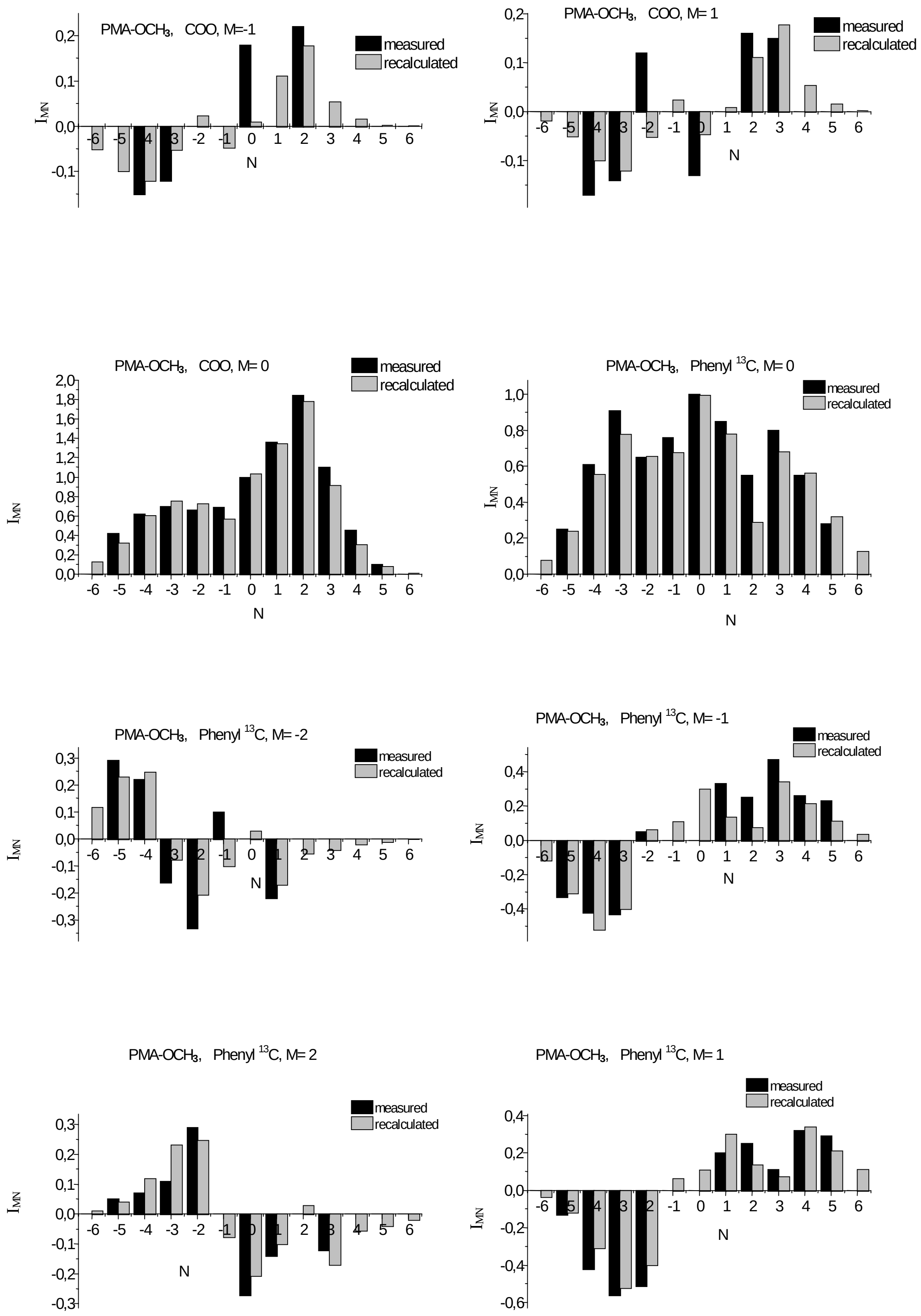

Figure 6.5 Comparison between the measured and recalculated values of the sidebands for the COO and Phenyl ^{13}C.

reproduce the spectra, or namely the sidebands $\widetilde{I_{MN}}$ from system (4.36) by using the obtained $\langle P_L \rangle$ values and the simulated I_{LMN} . The comparison between the measured $\widetilde{I_{MN}}$ and recalculated $\widetilde{I_{MN}}$ can give an idea about this. Such a graphical comparison is shown on Fig. 6.5. There is a relatively good correspondence between this values. The presence of significant deviations can be explained with the reasons like transverse anisotropy or errors in measuring the $\widetilde{I_{MN}}$ by volume integration procedure.

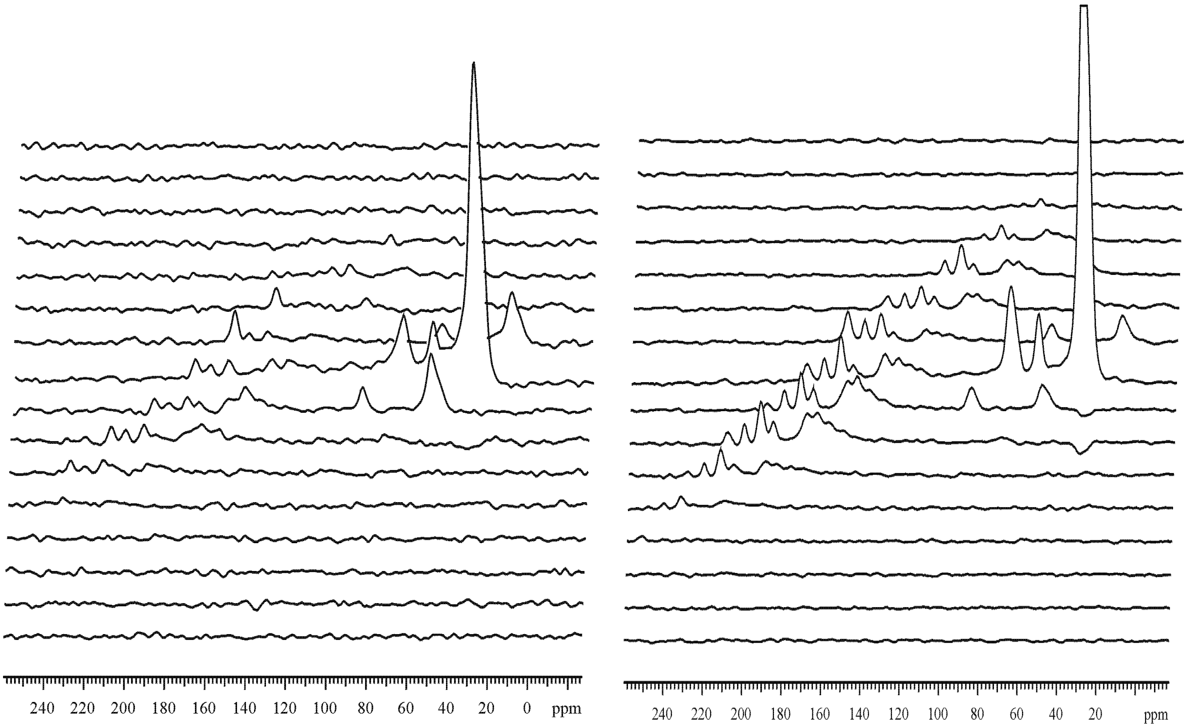

a) b)

Figure 6.6 2D PASS of oriented liquid crystal a) 6PBA13; b) 6PBA8. ω_R = 2000 Hz.

The 3D technique was applied also for studying the ODF of the 6PBAy substances but because the amount of the samples was very small in comparison to the PMA-OCH$_3$ the signal was too poor and no sidebands pattern could be obtained in a reasonable time. One possible alternative from one side for avoiding the 3D accumulation and from the other side to keep the orientation information in a sideband pattern was to apply the 2D PASS method on the oriented sample. It is so that theoretically the line intensities, which appear on the 2D spectra are always the same as those in the normal 1D MAS spectra [93] and consequently if one applies this on the oriented sample without an additional rotor synchronization the obtained sideband 2D pattern contains for each chemical specie the middle slice (M = 0), which appears in the 3D experiment or the sidebands with indexes $\widetilde{I_{0N}}$ from the Harbison-Vogt-Spiess method. Of course one has to keep in mind that in this case the information from the other slices or the lines $\widetilde{I_{\pm 1N}}$, $\widetilde{I_{\pm 2N}}$ will be lost and as it was shown in Table 6.1 the solutions for the $\langle P_L \rangle$ are very sensitive to the inaccuracy in evaluation of $\widetilde{I_{MN}}$ by volume integration procedure.

	$\langle P_2 \rangle$	$\langle P_4 \rangle$
6PBA8	-0.23	-0.17
6PBA13	0.14	-0.06

Table 6.2 Order parameters obtained by 2D PASS of oriented 6PBA8 and 6PBA13

On Fig. 6.6 the 2D PASS spectra obtained from oriented 6PBA8 and 6PBA13 are shown. The experimental conditions were as follows: ω_R = 2000 Hz, pulse width *pw* = 3.5 μs number of increments in t_1 direction *ni* = 16, number of transients for every FID *nt* = 2368, total measuring time 42 hours. The relevant $\langle P_2 \rangle$ and $\langle P_4 \rangle$ values obtained from the linear regression procedure applied over the available $\widetilde{I_{MN}}$ and corresponding simulation data I_{LMN} are presented in Table 6.2. The $\langle P_2 \rangle$ values are in similar absolute value but opposite in sign. This means that in both cases the main chain ^{13}C are not strongly ordered (as $\langle P_2 \rangle$ is much smaller than 1) and that the preferable orientation of the main chain segment is different in both cases, for one of the substances it is perpendicular to the side chain and for the other substance it is parallel to the side chain.

As there is no information available from this study about the orientation of the tensor axis relative to the segment axis we can adopt the concept from other studies [99, 51] that the ***z***-axis of the tensor of chemical shift is oriented along the local chain, or the angle ε = 0° and then (Eq. (6.9)) $\langle P_L \rangle_{CS} = \langle P_L \rangle_S$ or the main-chain part of the macromolecule for **the 6PBA8 forms more a prolate shape** while the **6PBA13 forms an oblate conformation**.

7 Conclusions

Estimation of the orientation of the main chain in liquid crystalline side chain polymers with carbon in the main chain is very difficult task. One approach for this problem is to apply ^{2}H NMR [23], which needs a special chemical treatment - labelling of the main chain with ^{2}H nuclei. Here, alternative to deuteron labelling, ^{13}C natural abundance NMR methods were successfully applied.

The following conclusions concerning the choice of the used NMR methods can be done:

- static sample (Chapter 3). The effect of the shift of the aliphatic peak by changing the angle between the director N and magnetic field $\mathbf{B_0}$ observed for the 6PBA13 substance was qualitatively interpreted as an indication of the main chain orientation parallel to the side chain (and director **N**); the absence of this effect for 6PBA8 can be explained with the perpendicular orientation of the main chain towards to side chain. Static measurements give not a quantitative result, but they show only a qualitative indication about the orientation of the main chain in the sample.

Quantitative analysis of the orientation and extraction of order parameters is not possible because of the large numbers of non-equivalent ^{13}C nuclei. This leads to the necessity of application of some MAS. The advantage of all MAS techniques is that they produce narrow lines which can be easier analyzed. However because of the big number of ^{13}C presented in the macromolecule a simple MAS spectrum is also not possible to be analysed as the sidebands overlap and can not be correctly assigned. That's why an application of some MAS 2D and 3D methods (Harbison-Vogt-Spiess [71], ORDER [84, 69] and PASS [92]) was needed. They have the benefit to spread the sidebands by their order in the one dimension and by the information for the orientation in another dimension and make the spectrum analyzable. The disadvantage of this methods is that they are very time consuming.

- For extraction of the order parameters by the linear regression procedure (4.36) elements σ_{11}, σ_{22}, σ_{33} of the chemical shift tensor σ should be measured . Chemical shift values for COO nuclei were evaluated by the

Herzfeld-Berger analysis of 2D ORDER spectrum of isotropic samples and were as follows:

for PMA-OCH$_3$ σ_{iso} = 177,7 ppm, σ_{11} = 114 ppm, σ_{22} = 149 ppm, σ_{33} = 269 ppm
for 6PBAy σ_{iso} = 168,5 ppm, σ_{11} = 97 ppm, σ_{22} = 183 ppm, σ_{33} = 220 ppm

- Data evaluation. As an alternative for former investigations [69, 71] where mostly the Gaussian fitting procedure was used, here $\langle P_L \rangle$ were calculated independently one from another by a linear regression least square fitting (See Chapter 4.7 and (4.36) for details).

The influence of some factors, like variation of the measured line intensities $\widetilde{I_{MN}}$, variation in σ_{nn} values and number of equations included on the stability of the solution $\langle P_L \rangle$ of system 4.36 was studied. Results show not so strong influence of the variation of $\widetilde{I_{MN}}$ and σ_{nn} values, but a significant in some cases influence of the number of equations included in the system. It will be better to include in the system (4.36) all the slices in which any sidebands $\widetilde{I_{MN}}$ from the nuclei of interest come.

- Solving of the system (4.36) do not directly give the order parameters, which are the aim of the study. As an intermediate step first we obtain $\langle P_2 \rangle_{CS}$, or order parameters describing ODF of the chemical shift tensor of corresponding nuclei. To get $\langle P_2 \rangle_S$ describing the orientation of the segment, the orientation of the tensor with respect to molecular frame should be known.

For COO group of PMA-OCH$_3$ polymer $\langle P_2 \rangle_S = 0.13$ was obtained. This is a very small value and it means that there is a high disorder but as the sign of $\langle P_2 \rangle_S > 0$ it can be concluded that there are more segments aligned parallel to the magnetic field and the director ***N***. It is hard to conclude something about the orientation of the main chain from this result as this group is not a part of the main chain, but it is attached to it. Part of the main chain is a quaternary ^{13}C . There is an evidence that this group is also oriented (as there are some sidebands coming from this ^{13}C) but to get $\langle P_2 \rangle_S$ from the estimated $\langle P_2 \rangle_{CS}$ is still an open question as there is no information for the orientation of the tensor with respect to the local chain.

For 6PBAy samples the estimation of $\left\langle P_2 \right\rangle_S$ for COO group, which is a part of the main chain for this substances gives the following results:

- **6PBA8**: $\left\langle P_2 \right\rangle_S = -0.23$, the negative sign is an indication of preferable orientation of the main chain perpendicular to the side chain;
- **6PBA13**: $\left\langle P_2 \right\rangle_S = 0.14$, or in opposite to the other sample here the main chain is estimated to orient parallel to the side chain despite of the high disorder.

This results confirm the indications which were obtained from the angle dependent static ^{13}C NMR measurements. Moreover these results are in agreement with suppositions done from the earlier X-ray measurements with the same substances [61].

8 Reference

1. Windle A. H., in Developments in Oriented Polymers, edited by I. M. Ward (Applied Science, London 1982), Vol. 1, pp. 1-46
2. Cifferi A., W. R. Krigbaum, R. B. Meyer, „Polymer Liquid Crystals“, Academic Press, N. Y. (1982)
3. Demus D., J. Goodby, G. W. Gray, H.-W. Spiess, V. Vill, Handbook of Liquid Crystals, Wiley-VCH (1998)
4. Advances in Polymer Science, volumes 59-61 (1984)
5. Structure and Properties of Oriented Polymers, edited by I. M. Ward (Applied science, ondon, 1975)
6. F. Brochard, J. Polym. Sci.., Polym. Phys. Ed. 17, 1367 (1979)
7. Vasilenko S., V. P. Shibaev, A. R. Khokhlov, Makromol. Chem. 186, 1951 (1985)
8. Wang X. J., M. Warner, J. Phys. A 20, 713 (1987)
9. Hardouin F., Macromol. Symp. 98, 329 (1995)
10. Noirez L., P. Keller, J. P. Cotton, Liq. Cryst. 18, 129 (1995)
11. Davidson P., A. M. Levelut, Liq. Cryst. 11, 469 (1992)
12. McBrierty V. J., and I. M. Ward, J. Phys. D 1, 1529 (1968).
13. McBrierty V. J., J. Chem. Phys. 61, 872 (1974).
14. Hentschel R., J. Schlitter, H. Sillescu and H. W. Spiess, J. Chem Phys. 68, 56 (1978).
15. Spiess H. W., “NMR in Oriented Polymers”, in Developments in Oriented Polymers, edited by I. M. Ward (applied Science, London 1982), vol. 1, p. 44.
16. Schmidt-Rohr K., H. W. Spiess, Multidimensional Solid-state NMR and Polymers, Academic Press, San Diego, 1994
17. Tang P., R. A. Santos, G. S. Harbison, Adv. Magn. Res. 13, 225 (1989)
18. Tang P., C.-L. Juang, G. S. Harbison, Science 249, 70 (1990)
19. Böffel C., H. W. Spiess, in Side Chain Liquid Crystalline Polymers, edited by C. B. McArdle (Blackie, London 1989)
20. Opella S. J., J. S. Waugh, J. Chem. Phys. 66, 4919 (1977)
21. Hempel G., A. Jacobi, W. Weissflog, M. Griebel, D. Reichert, Macromol. Chem. Phys. 200, 1608 (1999)
22. Harbison G. S., H. W. Spiess, Chem. Phys. Lett. 124, 128 (1986)
23. Böffel C., H. W. Spiess, B. Hisgen, H. Ringsdorf, H. Ohm, R. G. Kirste, Macromol. Chem. Rapid Comm. 7, 11 (1986)

24. Hardouin F., L. Noirez, P. Keller, M. Lambert, F. Moussa, G. Pepy, Mol. Cryst. Liq. Cryst. 155, 389 (1988).
25. Keller P., B. Carvalho, J. P. Cotton, M. Lambert, F. Moussa, G. Pepy, J. Physique Lett. 46, 1065 (1985)
26. Noirez L., G. Pepy, P. Keller, L. Benguigui, J. Phys. II France 1, 821 (1991)
27. Noirez L., P. Keller, J. P. Cotton, J. Phys. I France 2, 915 (1992)
28. Noirez L., P. Davidson, W. Schwarz, G. Pepy, Liq. Cryst. 16, 1081 (1994)
29. Kirste R. G., H. G. Ohm, Macromol. Chem., Rapid Commun. 6, 179 (1985).
30. Noirez L., C. Böffel, A. Daoud-Aladine, Phys. Pev. Lett. 80, 1453 (1998)
31. Pepy G., L. Noirez, P. Keller, M. Lambert, F. Moussa, J. P. Cotton, Makromol. Chem. 191, 1383 (1990)
32. Noirez L., P. Keller, P. Davidson, F. Hardouin, J. P. Cotton, J. Phys. France 49, 1993 (1988)
33. Noirez L., P. Keller, J. P. Cotton, Liq. Cryst. 18, 129 (1995)
34. Davidson P., L. Noirez, J. P. Cotton, P. Keller, Liq. Cryst. 10, 111 (1991)
35. Moussa F., J. P. Cotton , F. Hardouin, P. Keller, M. Lambert, G. Pepy, M. Mauzac, H. Pichard, J. Physique 48, 1079 (1987)
36. De Gennes P. G., Scaling Concepts in Polymer Physics (Cornell University Press)
37. Gubina T. I., S. Kize, S. G. Kostromin, R. V. Talroze, V. P. Shibaev, N. A. Plate, Liq. Cryst. 4, 197 (1989)
38. Casquilho J. P., Volino F., Mol. Cryst. Liq. Cryst. 180B, 357 (1990)
39. Davidson P., A. M. Levelut, Liq. Cryst. 11, 469 (1992)
40. Mitchell G. R., F. J. Davis, W. Guo, R. Lywinski, Polymer 32, 1347 (1991)
41. Mattoussi H., R. Ober, Macromolecules 23, 1809 (1990)
42. Mitchell G. R., M. Coulter, F. J. Davis, W. Guo, J. Phys. II, France 2, 1121 (1992)
43. Schulz G. V., Z. Phys. Chem. B 43, 379 (1939)
44. Ohm H. G., R. G. Kirste, R. C. Oberthür, Makromol. Chem. 116, 1387 (1988)
45. Portugall M., H. Ringsdorf, R. Zentel, Makromol. Chem. 183, 2311 (1982)
46. Rez W., Molec. Liq. Cryst. 155, 549 (1988)
47. Bouman W. G., W. H. de Jeu, Liq. Cryst. 16, 853 (1994)
48. Higgins J. S., K. Dogson, J. A. Semeleyn, Polymer 20, 554 (1979)
49. Mattousi H., C. Casagrande, M. Veyssie, M. A. Guedeau, H. Finkelmann, Mol. Cryst. Liq. Cryst. 144, 211 (1988)

50. Titman J. J., D.-L. Tzou, S. Feaux de Lacroix, C. Böffel, H. W. Spiess, Acta Polym. 45, 204 (1994)
51. Mehring M., “High Resolution NMR Spectroscopy in Solids”, Springer Verlag, Heidelberg 1976.
52. Hempel G., H. Schneider, Pure Appl. Chem. 54, 635 (1982)
53. Jacobi A., G. Pirwitz, W. Weissflog, Proc. SPIE Int. Soc. Opt. Eng. 3319, 249 (1998)
54. Diele S., A. Mädicke, K. Knauft, J. Neutzler, W. Weissflog, D. Demus, Liq. Cryts. 10, 47 (1991)
55. Boden N., L. D. Clark, R. J. Rishby, J. W. Emsley, G. R. Luckhurst, C. P: Stokley, Mol. Phys. 42, 565 (1981)
56. Böffel Ch., B. Hisgen, U. Pschorn, H. Ringsdorf, H. W. Spiess, Isr. J. Chem 23, 388 (1983)
57. Finkelmann, H. J. Kock, W. Gleim, G. Rehade, Makromol. Chem,, Rapid Commun. 5, 287 (1984)
58. Dubault A., R. Ober,M. Veyssie, B. Cabane, J. Phys. (Les Ulis, Fr.) 46, 1227 (1985)
59. Finkelmann H., H. Ringsdorf, J. H. Wendorff, Markomol. Chem. 179, 273 (1978)
60. Shibaev P., N. A. Plate, Y. S. Freidzon, J. Polym. Sci., Polym. Chem. Ed. 17, 1655 (1979)
61. Böhme A., PhD Thesis, Inst. Phys. Chem., Martin-Luther Universität, Halle, 1994
62. Bremser W., L. Ernst, W. Fachinger, R. Gerhards, A. Hardt, P. W. E. Lewis, “Carbon-13 NMR Spectral Data”, VCH Weinheim, 1987
63. VanderHart D. L., J. Chem. Phys., 64, 830 (1976)
64. Opella S. J., J. S. Waugh, J. Chem. Phys. 66, 4919 (1977)
65. Andrew E. R., A. Bradbury, R. G. Eades, Nature 182, 1659 (1958)
66. Lowe I. J., Phys. Rev. Lett 2, 285 (1959)
67. Maricq M. M., J. S. Waugh, J. Chem. Phys. 70, 3300 (1979)
68. Herzfeld J., A. E. Berger, J. Chem. Phys. 73, 6021 (1980)
69. Titman J. J., S. F. de Lacroix, H. W. Spiess, J. Chem. Phys. 98, 3816 (1993)
70. Abragam A., ‘The principles of Nunclear Magnetism’, Oxford Press, London, 1961
71. Harbison G. S., V. - D. Vogt, H. W. Spiess, J. Chem. Phys. 86, 1206 (1987)
72. Oliver F. W. J., in Handbook of Mathematical Functions, edited by M. A. Abramowitz and I. A. Stegun, Dover, New York, p. 363 (1965)
73. Bronstein I. N., K. A. Semendjajew, G. Musiol, H. Mühlung, Taschenbuch der Mathematik, Verlag Harri Deutsch, Thun, Frankfurt am Main (1993)

74. Zeigler R. C., R. A. Wind, G. E. Magiel, J. Magn. Res. 79, 299 (1988)
75. Kolbert A. C., H. J. M. de Groot, R. G. Griffin, J. Magn. Res. 85, 60 (1989)
76. Bax A., N. M. Szevernyi, G. E. Magiel, J. Magn. Res. 55, 494 (1983)
77. Terao T., T. Fujii, T. Onodera, A. Saika, Chem. Phys. Lett. 107, 145 (1984)
78. Yarim-Agaev Y., P. M. Tutunjan, J. S. Waugh, J. Magn. Res. 47, 51 (1981)
79. Bax A., N. M. Szevernyi, G. E. Magiel, J. Magn. Res. 51, 400 (1983)
80. Tycko R., G. Dabbagh, P. Mirau, J. Magn. Res. 85, 265 (1989)
81. Aue P., D. J. Ruben, R. G. Griffin, J. Magn. Res. 43, 472 (1981)
82. Aue P., D. J. Ruben, R. G. Griffin, J. Chem. Phys. 80, 1729 (1984)
83. Kolbert A. C., R. G. Griffin, Chem. Phys. Lett. 166, 87 (1990)
84. De Lacroix S. F., J. J. Titman, A. Hagemeyer, H. W. Spiess, J. Magn. Res. 97, 435 (1992)
85. Hagemeyer A., K. Schmidt-Rohr, H. W. Spiess, in “Advances in Magnetic Resonance”, (W. S. Warren, Ed.) 13, 85 Academic Press, San Diego, 1989
86. Dixon W. T., J. Chem. Phys. 77, 1800 (1982)
87. Dixon W. T., J. Schaefer, M. D. Sefcik, E. O. Stejskal, R. A. McKay, J. Magn. Res. 49, 341 (1982)
88. Raleigh D. P., A. C. Kolbert, R. G. Griffin, J. Magn. Res. 89, 1 (1990)
89. Hagemeyer A., D. van der Putten, H. W. Spiess, J. Magn. Res. 92, 629 (1991)
90. Levitt M. H., R. Freeman, J. Magn. Res. 33, 473 (1979)
91. Raleigh D. P., E. T. Olejniczak, R. G. Griffin, J. Chem. Phys. 89, 1333 (1988)
92. Song Zh., O. N. Antzutkin, A. Rupprecht, M. H. Levitt, Chem. Phys. Lett. 253, 349 (1996)
93. Antzutkin O. N., S. C. Shekar, M. H. Levitt, J. Magn. Res. A115, 7 (1995)
94. Solum M. S., K. W. Zilm, J. Michl, D. M. Grant, J. Phys. Chem. 87, 2940 (1983)
95. Solum M. S., J. C. Facelli, J. Michl, D. M. Grant, J. Am. Chem. Soc. 108, 6464 (1986)
96. VNMR Command and Parameters Reference, VNMR 6.1 Software, Varian Associates Inc., Printed in USA, 1997
97. Ernst R. R., G. Bodenhausen, A. Wokaun, Principles of Nuclear magnetic Resonance in One and Two dimensions, Oxford University, Oxford, (1987)
98. Edzes H. T., Polymer 24, 1425 (1983)
99. Veeman W. S., Progr. Nucl. Magn. Reson. Spectrosc. 16, 193 (1984)

Erklärung

Hiermit erkläre ich, daß die Dissertation von mir selbstständig verfaßt wurde und ich keine anderen als die angegebenen Hilfsmittel verwendet habe.

Weiterhin versichere ich, daß diese Arbeit an keiner anderen Stelle veröffentlicht wurde und erestmalig eingereicht wird.

Halle (Saale), den …………………………….   ……………………
(Albena Dimitrova)

Acknowledgments:

I would like to thank all the people who have helped me for the realisation of this thesis and in particular to:

Prof. Dr. H. Schneider	for accepting me as a Ph. D. student in the NMR group and wise leading of the study.
Dr. G. Hempel	for the excellent introduction in the field of NMR, and advising me for solving off all the problems occurred in this project.

and all other members of the NMR group of Fachbereich Physik der Martin-Luther-Universität for the pleasant atmosphere during work, Fachgruppen Saminars, as well as in the Annual SpringSeminars.

Lebenslauf

Name, Vorname:	Dimitrova, Albena
Akad. Grad:	Diplomphysiker
Geburtsdatum:	16 August 1970
Geburtsort:	Silistra, Bulgarien
Nationalität:	Bulgarisch
Familienstand:	Ledig
Schulischer Bildungsgang:	1977 – 1988 Grundschule und Gimnasium, Silistra, Bulgarien
Universitärer Bildungsgang:	Oct. 1988 – July 1993 Physikstudium im Fachbereich Physik der ‚St. Kliment Ochridski‘ Universität, Sofia, Bulgarien
Diplomarbeit:	1993 im Wissenschaftsinstitut für Mechanik und Biomechanik, bei Prof. V. Kavardzhikov zum Thema: ‚Anwendung der Speckle-Photometrie zur Registrierung und Vermessung von Verschiebungen in Grossen Objekten‘
Nov. 1993 – Oct. 1996	Wissenschaftlicher Mitarbeiterin im Institut für Physikalische Chemie der Bulgarischen Akademie der Wissenschaften; Elektrooptische Untersuchungen von Kolloiden.
Nov. 1996 – Feb. 2000	Promotionstudium im Fachbereich Physik der Martin- Luther- Universität Halle-Wittenberg; Fachgruppe Kernmagnetische Resonanz-Spektroskopie.

Halle, den

…………………..
(A. Dimitrova)